Quantum information processing in mesoscopic systems

Jose Luis Garcia Coello

A dissertation submitted in partial fulfillment

of the requirements for the degree of

Doctor of Philosophy

of the

University of London.

Department of Physics and Astronomy

University College London

November 3, 2012

I, Jose Luis Garcia Coello confirm that the work presented in this thesis is my own. Where information has been derived from other sources, I confirm that this has been indicated in the thesis.

Publications

- Large spin entangled current from a passive device.
Avinash Kolli, Simon C. Benjamin, Jose Garcia Coello, Sougato Bose, and Brendon W. Lovett. New J. Phys. **11**, 013018 (2009).*

- Spin Filtering and Entanglement Swapping through Coherent Evolution of a Single Quantum Dot.
Jose Garcia Coello, Abolfazl Bayat, Sougato Bose, John H. Jefferson, and Charles E. Creffield New J. Phys. **105**, 080502 (2010).*

- Quantum Gates Between Two Spins in a Triple Dot System with an Empty Dot.
Jose Garcia Coello and Sougato Bose. arviv.org 1104.0716v1 080502 (2010).*

- Absorption efficiency of gold nanorods determined by quantum dot fluorescence thermometry.
L. M. Maestro, P. Haro-Gonzlez, J. G. Coello, and D. Jaque. Appl. Phys. Lett. **100**, 201110 (2012);

* Publications that has been used in the thesis.

Abstract

This thesis discusses various schemes and protocols for quantum information processing in mesoscopic systems with particular focus on using the spin of a particle as the bearer of information. The first chapter introduce various aspects of the field of quantum information used in this thesis such as qubits, entanglement, its quantification, quantum logic gates and entanglement swapping. In this chapter concepts such as AKLT states, decoherence and adiabatic elimination are introduced as they will be relevant in the thesis. In chapter 2 we introduce the Quantum Dots as the solid state system that will primarily be used as the hardware for the development of Quantum Information Processing (QIP). The different properties of quantum dots depending on their size are discussed. The exchange interaction between tunnel coupled quantum dots and the background of quantum computation in quantum dots is described. The principal sources of decoherence and the measurement techniques for spin qubits are presented. In chapter 3, carbon nanowires filled with N@C60 dimers are studied to analyse the entanglement between nuclear spins. The dimer is modelled as a two coupled nuclear spin- electron spin pair with a Heisenberg interaction. The entanglement have been studied depending on the temperature and the intensity of an external magnetic field. Witnessing the entanglement, and particularly bound entanglement are discussed. In chapter 4, the way to extract a singlet from a quantum dot is explored. The system that we model will be consisting of a triple dot and analyse the best way to get the singlet out, with each electron in a separate dot. The chief motivation is to create a singlet between separate dots in a time-scale much faster than that given by spin-spin exchange interactions. In chapter 5, quantum logic gates in a triple dot system has been studied. Such gates have been widely studied in double and single quantum dots. Motivated by the advent of experimental set ups of triple dots, we have studied the natural quantum gates that came out of a triple dot system. There are still two spin quantum bits in the three dots and there is an empty intervening dot, which imparts the scheme some advantages, as well as a substantial difference from the class of schemes studied so far. In chapter 6, we model a large

square dot. As we describe in chapter 2, the properties of the large dots make them behave with some interesting properties such as hosting Wigner molecules of electrons inside. We explore the application of these structures for quantum information processing. We show here how to get singlet/triplet measurement, entanglement swapping, and how to prepare a 1D AKLT state, using the square dot as a construction block of the system. Finally in chapter 7 conclusions and further work. Here we indicate the further work that could be done with the knowledge present in this thesis and motivated by future advances in the technology.

Acknowledgements

I should have to give special gratitude to my Supervisor Prof. Sougato Bose for choosing me as his student. His enormous qualities for relations between different aspects of the fields in quantum physics. His interest and effort not only in that the development of this thesis to go ahead but also in his contribution to me for a good formation and growth as a researcher. Thanks, Sougato, for your generosity and the kindness that you have offer me your knowledge, your time, your support and your enthusiasm.

Part of my thesis has been collaborating with the material department at Oxford University, where I found enriching and friendly environment to research and discuss. First of all, I am deeply grateful to Prof. Andrew Briggs because he is very kind indeed, for his support each time that we discussed and letting me be the skipper of one of his sailing boats in Sheringham, where he was hosting one of our QIPIRC summer schools. Second, but not less important, I have to thanks very deeply to Dr. Brendon W. Lovett, Dr. Simon C. Benjamin and Dr. Avinash Kolli for their openness, interesting discussions and advice when we were developing our models of Fullerenes and Quantum Dots.

Each time that I went back to my home place in Tenerife, I have been visiting La Laguna University where I has been always welcome by my undergraduates teachers and his students being open to discuss my research and they giving me updates in theirs. I am grateful to Prof. Jose Breton, Dr. Jose P Palao Gonzlez, Dr. Santiago Brouard Martin, Dr. Javier Hernandez Rojas, Dr. Andres Mujica Fernaud,Dr Patricia Haro, Mr Eduardo Perez Gonzalez, special thanks to Mr. Alejandro Valido Flores, Mr. Luis A. Correa for organising the Christmas meeting for PhD students and giving me the opportunity to give a seminar. Special Thanks to Dr Rafael Sala Mayato and Dr Daniel Alonso Ramirez for being so helpful with all their support, references, discussions and their invitation for giving a talk in the XVI Workshop in Time in Quantum Mechanics.

In the visits that I have done during my time as a Ph.D. candidate. First I have been visiting

the Nanoscale and Quantum Photonics Lab at Stanford University, California, being grateful to Prof. Jelena Vuckovic and Arka Majumdar for explaining me their research and have interesting discussions related to experiments in Quantum Dots. Second I visited the NASA Ames Quantum Laboratory (NAQL) in California hosted by Dr. Gabriel Durkin where we discussed about Quantum Metrology, Quantum Information and Quantum Dots. Third I am really deeply greatful to Prof. Kwek Leong Chuan at Centre for Quantum Technologies (CQT) in Singapore where he hosted me and I have advices and enrichment discussions with him and also, Si-Hui Tan, Elica Kyoseva and Blas Manuel Rodriguez-Lara and Prof Vlakto Vedral.

Regarding the summer schools I have to be grateful to Num Mendez, Sheila Benitez, Marialbert Acosta and Itziar Arbesu for their kindness and hospitality in Barcelona in my way in or way out for the two Benasque Summer School in Quantum Information that I participated . With Num I have been discussing the developing and dynamics of bubbles in fluids apart from issues regarding programming languages, mathematical methods and computer science. In Benasque I was glad to enjoy my time in which apart from deep discussions regarding Quatum Information, Open systems we have football matches there with Arnau Riera Graells, Vicent Pico Perez, Thiago Rodrigues De Oliveira, Oriol Romero Isart, Justina Pytel, Prof. Ignacio Cirac, Prof. Arthur Ekert and Prof. Seth Lloyd. In the summers schools organised by the QIPIRC I have to be greatful to Prof. Andrew Briggs for his comments and advices, Prof.Andrew fisher for our discussions. Prof Charles Marcus for helping me with some experimental aspects regarding quantum dots and their experimental set-ups in his Mesoscopic Physics Lab at Harvard University. Also to enjoy and have an exceptional time there with Luca Marseglia, Andrea Cantone and Mujtaba H Zaka.

I have to give special thanks to Patricia Haro with who I discover other application for Quantum Dots in which we were able to obtain optical parameters for Gold Nanorods (GNR), working with her group at Universidad Autonoma de Madrid. It was a pleasure to work in this project with Dr. Daniel Jaque and Laura Maestro that helped me understanding the optical properties of these particles and their several applications.

With my colleagues at UCL I am consider very fortunate for sharing my time during my stay in the A5 room with Daniel Burgarth, Christopher Hadley, Abolfazl Bayat, Jose Reslen, Javier Molina, Hannu Wichterich, Tommaso Tufarelli, Alesandro Ferraro, Bobby Antonio and Tom Boness. With all of them I have several rich discussions and collaboration for developing my studies and research. Also I will like to thanks Prof. Dan Browne, Prof Tania Monteiro, Dr. Alexandra Olaya-Castro, Dr. Janet Anders for being helpful and their kindness during my time

around UCL. I am very greatful also to John H. Jefferson, Charles E. Creffield with who I understood better the properties of a Quantum Dot depending on the size and with collaboration of Abolfazl Bayat and Sougato Bose we were able to develop our spin filtering using large Quantum Dot, was a pleasure to work with them.

Very special thanks to my friends Domingo, Ismael, Emmanuel, Hector, Enrique, Jonathan, Israel, David, Fran, Carlos and Josep for a lot of nice moments and my house mates during my stay in London, Julio, Rosana, Marta, Soraya, Carmen, Tan, Rafa and Isaias, for making that I can call my house my home, special thanks to Daniela for her support in the darkness moment of my project and giving me reasons for continue. Also thanks to my Landord Andrew for his help in everything related to my house.

To my Bother Juan Pablo for his conversation and his holidays choosing always London, To my sister Elena for her loyality and never ending good moments.

To my beloved grandparents and specially my Grandmothers that passed away during my Research time. Carmen and Isabel I miss your extremly good dishes and nice smiles.

Finally this thesis is dedicated to my parents for loving me so much and their endless support. I have to thank my mother for her never ending advices and help even with the distance and to my father for his knowledge that definitely enriched me as a scientist and as a person and also his support and comments regarding science news. But having in mind that I have a wonderful parents.

Contents

List of Figures

List of Tables

Chapter 1

Introduction

In this chapter we are going to introduce some of the basic concepts and tools from quantum information science and elsewhere, that will be used in the thesis. This chapter is going to focus on more general (i.e., system independent) notions, while the next chapter, also introductory, is going to focus on the specific system of quantum dots from the angle of quantum information processing (QIP).

1.1 Qubits

Qubit is the term used for quantum two level systems or the quantum version of bits. A qubit is known to be able to exist in a state which is an arbitrary superposition $\alpha|0\rangle+\beta|1\rangle$ of two distinct states $|0\rangle$ and $|1\rangle$, where α and β are complex numbers. The importance of the notion of qubit arises from quantum computation [1]. They are the minimal dimensional systems in which information to be manipulated and exploited quantum mechanically can be encoded. When the joint state of large collections of qubits are manipulated together then quantum computation can be accomplished, which can far surpass the power of classical (i.e., "non-quantum") computers for certain classes of problems. They also have the fundamental importance of being the simplest of quantum systems and an ideal ground for illustrating the unique features of the quantum world such as measurement induced collapses, quantum entanglement and associated non-locality. Some examples of qubits which have found relevance in QIP are the two spin states $|\uparrow\rangle$ and $|\downarrow\rangle$ of an electron, the polarizations $|H\rangle$ and $|V\rangle$ of a photon and any two internal levels $|e\rangle$ and $|g\rangle$ of an atom. When a quantum system of more levels are involved in QIP, one often extends the qubit terminology to refer to them as qutrits for quantum three level systems (e.g. a spin-1 particle) or qudits for a quantum d-level system in general.

1.2 Quantum Entanglement and its Measures

Perhaps one of the most curious features of quantum mechanics is a unique form of correlations that can only exist between quantum systems. For example, consider a pair of distinct particles A and B prepared in a singlet state $|\psi^-\rangle_{AB} = \frac{1}{\sqrt{2}}(|\uparrow\rangle_A|\downarrow\rangle_B - |\downarrow\rangle_A|\uparrow\rangle_B)$ of their spins. It can be proved rigorously, using simple mathematical arguments – the so-called Bell's theorem [2], that local models describing the particles and/or the measurements on them can never reproduce the correlations inherent in the state $|\psi^-\rangle_{AB}$. In fact, to reproduce the correlations entailed by the above state, one is forced to the conclusion that the choice of the measurement basis for one of the particles somehow has an effect on the outcomes of measurements on the other particle. This goes by the name *quantum non-locality*.

In general, for a pure state (of, say, two systems A and B) to exhibit quantum non-locality, it must not be of factorizable form *i.e.*, $|\Lambda\rangle_{AB} \neq |\psi\rangle_A \otimes |\phi\rangle_B$. Such states are called *entangled*. One can generalise the notion of what is called an entangled state by defining the set of all *separable* states (of two systems A and B) as those whose states can be written as

$$\sigma_{AB} = \sum_i p_i |\psi_i\rangle\langle\psi_i|_A \otimes |\phi_i\rangle\langle\phi_i|_B. \tag{1.1}$$

Those states which *do not* fall in the set of separable states are called entangled states. Note that not all entangled states defined in the above way will exhibit quantum non-locality.

In quantum information technology, entanglement is a precious resource. For example, if an unknown state of a qubit is to be sent to a distant location, one can do this using an entangled state shared between distant parties, one qubit (say, A) of the entangled state being held by one of the parties, and the other qubit (say, B) being held by the other party, and only two bits of classical communication. This process is called teleportation, and in this process the initial state is converted to a separable state. One can thereby regard entanglement as a resource, which is *consumed* during the process of teleportation. Teleportation works best when the shared state is of the form $|\psi^-\rangle_{AB}$ (described above) or something which is obtained from this state by local unitary rotations on qubits A and B. Thereby the entanglement of these class of state is ascribed the value unity, and the unit is often called an ebit. All other states, pure and mixed, will have a lower entanglement. In view of their applications (teleportation is one example, but there is also dense coding, certain forms of quantum key distribution, as well as measurement based quantum computation), it is worthwhile to *quantify* the entanglement in any state. Usually the quantifications are motivated by the *principle* that entanglement is a resource which cannot be created by local actions by two distant parties (one holding a quantum system each) as well as

classical communication between them. Any measure which satisfies the above, and vanishes for separable states (Eq.(1.1)), is a good measure of entanglement. It is often normalized (or chosen) in such a way that it has the value unity for $|\psi^-\rangle_{AB}$. The entanglement of two higher dimensional systems (say two qudits) can be higher than unity, as local actions and classical communication may in principle create more than one copy of $|\psi^-\rangle_{AB}$ from one of them.

In this thesis, we will be using two measures of entanglement. The first one is called *concurrence* [3] and is a measure that works for arbitrary states of two qubits. To obtain it, one first takes the density matrix ρ_{AB} of two qubits and constructs from it the matrix

$$\tilde{\rho}_{AB} = \sigma_A^y \otimes \sigma_B^y \rho_{AB}^* \sigma_A^y \otimes \sigma_B^y. \tag{1.2}$$

Then one computes the square roots of the eigenvalues $\lambda_1 \geq \lambda_2 \geq \lambda_3 \geq \lambda_4$ of the matrix $\rho\tilde{\rho}$. Concurrence is given by

$$\mathcal{E}_C = \min\{0, \lambda_1 - \lambda_2 - \lambda_3 - \lambda_4\}. \tag{1.3}$$

The other measure of entanglement that we will be using in this thesis is negativity. It quantifies the entanglement of arbitrary states of two higher dimensional systems. It is motivated by the Peres-Horodecki *partial transposition* criterion [4] to check for the separability of a state. For a general state ρ_{AB} of two higher dimensional systems A and B, a partial transposition is defined as the operator $\rho_{AB}^{T_B}$, where the states of one of the systems (B in this case) has been transposed, i.e., the kets and bras have been interchanged for only Bs part of the state. Under this action, it is easy to see that the separable state σ_{AB} defined by Eq.(1.1) remains unchanged. This in turn implies that it is still a density operator for a quantum state and its eigenvalues are positive. Therefore, if for a certain state, the eigenvalues of $\rho_{AB}^{T_B}$ turn out to be negative, then this state has to be entangled. Now, the degree by which its eigenvalues are negative, have been used to frame bonafide measures of entanglement called the negativity and logarithmic negativity respectively [5, 6, 7]. If α_j are the negative eigenvalues of $\rho_{AB}^{T_B}$, then entanglement, as quantified by negativity is given by [6]

$$\mathcal{E}_N = \sum_j |\alpha_j|. \tag{1.4}$$

Sometimes we may also use the logarithmic negativity which is defined as

$$\mathcal{E}_L = \log_2(2\mathcal{E}_N + 1). \tag{1.5}$$

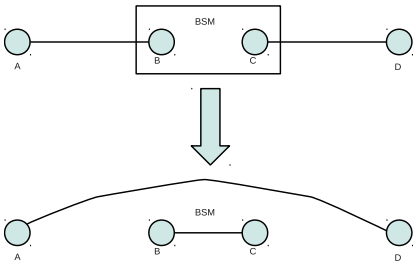

Figure 1.1: The above figure depicts the process of entanglement swapping through a Bell State Measurement (BSM) on two qubits.

1.3 Entanglement Swapping

One of the simplest intriguing manipulations that one can make on entangled states purely by measurements (actually joint measurements) is called entanglement swapping [8, 9]. For this one first has to consider a certain complete basis for measurements on two qubits, which is called the Bell basis, whose basis states are given by

$$
\begin{aligned}
|\psi^+\rangle_{AB} &= \frac{1}{\sqrt{2}}(|0\rangle_A|1\rangle_B + |1\rangle_A|0\rangle_B) \\
|\psi^-\rangle_{AB} &= \frac{1}{\sqrt{2}}(|0\rangle_A|1\rangle_B - |1\rangle_A|0\rangle_B) \\
|\phi^+\rangle_{AB} &= \frac{1}{\sqrt{2}}(|0\rangle_A|0\rangle_B + |1\rangle_A|1\rangle_B) \\
|\phi^-\rangle_{AB} &= \frac{1}{\sqrt{2}}(|0\rangle_A|0\rangle_B - |1\rangle_A|1\rangle_B),
\end{aligned} \tag{1.6}
$$

where $|0\rangle$ and $|1\rangle_A$ stand for two orthogonal qubit states such as the states $|\uparrow\rangle$ and $|\downarrow\rangle$ of a spin-1/2 particle.

Now consider the situation as depicted in Fig.1.1 where two particles A and B are entangled in a state $|\psi^+\rangle_{AB}$, and two other particles C and D are entangled in a state $|\psi^+\rangle_{CD}$. Suppose one does a measurement in the Bell basis on the qubits B and C. This is depicted in Fig.1.1 as the box with BSM (Bell State Measurement) written inside. When the outcome of the measurement is $|\psi^+\rangle_{BC}$, the state of the qubits A and D, which need not ever have directly interacted, immediately collapses to $|\psi^+\rangle_{AD}$. Similarly for the other three outcomes, i.e., outcome $|\psi^-\rangle_{BC}$ corresponds to the collapse of A and D to $|\psi^-\rangle_{AD}$ and so on. As the partners who are mutually entangled have been swapped, this process is called entanglement swapping. It is a very useful manipulation in quantum information, as it enables one to build quantum repeaters [10]. To briefly clarify this, suppose one could use various purification procedures to

create a state very close to $|\psi^+\rangle_{AB}$ over a short distance. However, the channels for transmission are so noisy that such purification procedures do not work over longer distances. Then one could make various short distance maximally entangled states and then swap the entanglement in series to establish a long distance entangled pair of particles. This long distance entangled state is then the starting point of teleportation or other quantum protocols.

1.4 Quantum Gates

A desired quantum computation generally involves an arbitrary operation in a very large Hilbert space of dimensions 2^n for n qubits. A unitary rotation on such a Hilbert space i.e., and arbitrary element of the $SU(2^n)$ group is, however, possible to be generated by means of arbitrary local unitary operations and at least one two qubit operation which entangles the qubits [11] (this is called an entangling quantum gate). These two items, therefore, can be regarded as fundamental quantum gates whose composition can result in any required quantum algorithm to run on n qubits. Operations on single qubits are often regarded as rather easy – for example, for spin qubits, as we will mostly be concerned with in this thesis, it amounts to applying an effective local magnetic field to the qubits. This may be done with the help of electrical control of spin-orbit interactions [12], or using micromagnets [13]. Therefore, usually the challenge is to design a scheme for a useful (in the sense of being "entangling") quantum gate. Indeed Chapter 5 of this thesis deals largely with the above problem in a certain setting of quantum computation with spins. Typically an interaction between two qubits is used for enabling a quantum gate between them, though quantum indistinguishability and measurements may also be used [14]. A canonical example of an entangling two qubit gate is the Controlled Z or CZ gate, given by the evolution

$$\begin{aligned} |\uparrow\rangle_A|\uparrow\rangle_B &\rightarrow |\uparrow\rangle_A|\uparrow\rangle_B \\ |\uparrow\rangle_A|\downarrow\rangle_B &\rightarrow |\uparrow\rangle_A|\downarrow\rangle_B \\ |\downarrow\rangle_A|\uparrow\rangle_B &\rightarrow |\downarrow\rangle_A|\uparrow\rangle_B \\ |\downarrow\rangle_A|\downarrow\rangle_B &\rightarrow -|\downarrow\rangle_A|\downarrow\rangle_B. \end{aligned} \tag{1.7}$$

1.5 Decoherence and Dephasing

The principal enemy of quantum information processing is decoherence. Any quantum system is inevitably coupled to an environment, and information encoded in the quantum system is gradually lost to the environment. A toy example is a qubit which starts in a state $|\psi(0)\rangle =$

$\frac{1}{\sqrt{2}}(|0\rangle + e^{i\phi}|1\rangle)$, and interacts with an environment in an initial state $|\xi\rangle$ to evolve to the joint system-environment state $|\Lambda(t)\rangle = \frac{1}{\sqrt{2}}(|0\rangle|\xi_0(t)\rangle + e^{i\phi}|1\rangle|\xi_1(t)\rangle)$, has the information about the variable ϕ in its reduced density matrix damped by a factor as follows

$$\rho(t) = \frac{1}{2}\begin{bmatrix} 1 & 2e^{i\phi}\langle\xi_1(t)|\xi_0(t)\rangle \\ 2e^{-i\phi}\langle\xi_0(t)|\xi_1(t)\rangle & 1 \end{bmatrix}.$$

We can see that if with time evolution for large times, $\langle\xi_1(t)|\xi_0(t)\rangle \to 0$, then the entire information about ϕ is lost from the qubit's state $\rho(t)$. The environment being very large, it is likely to stay at $\langle\xi_1(t)|\xi_0(t)\rangle \sim 0$ for all times exceeding a certain time-scale. The above process is called dephasing and is an example of decoherence, while the above time-scale can be called the dephasing time. More generally the state of the qubit may be disrupted in more than one way, rather than merely the loss of coherence between states of a fixed basis, for example, the proportions of $|0\rangle$ and $|1\rangle$ may begin to differ. All these effects, due to the interaction of a system with its environment, is called decoherence. The specific environments with which we deal with in this thesis, and the type of decoherence that they cause, will be described in the next chapter.

1.6 Many-body Hamiltonians

Typical systems of nature are formed with many interacting constituents. Moreover, generally the interactions between these constituents are not that controllable and, in fact, permanent (i.e., they do vary with time). Such systems are described in terms of many-body Hamiltonians. Such a Hamiltonian is generally a sum of many terms, with each term being a product of operators for two or more of the constituent systems. An example of a class of many-body systems is a spin system. A large collection of spins permanently coupled to each other make macroscopic systems such as magnets. The mutual interactions of these spins lead to ferromagnetism, antiferromagnetism or other interesting many-body phases. Often the spins are arranged in a regular lattice and coupled to each other permanently with an interaction strength decreasing with distance (as shown in Fig.1.2). A common form for the Hamiltonian for a many-body spin-system (comprising, say, spin-1/2 particles) is

$$\mathcal{H} = \sum_{ij} J_{ij}\ \vec{\sigma}_i.\vec{\sigma}_j, \tag{1.8}$$

where $\vec{\sigma}_i.\vec{\sigma}_j \equiv \sigma_i^x\sigma_j^x + \sigma_i^y\sigma_j^y + \sigma_i^z\sigma_j^z$ and $\sigma_i^x, \sigma_i^y, \sigma_i^z$ are the Pauli operators for the component of the ith spin along the x, y and z directions respectively.

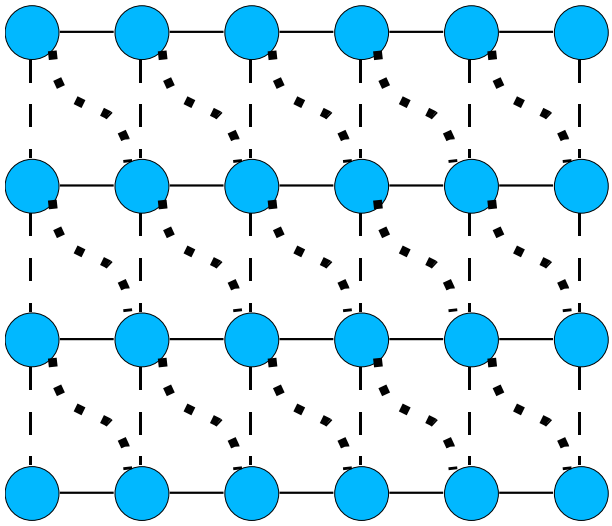

Figure 1.2: The figure shows an example of a many-body system, namely a spin system. The spins perpetually coupled to each other with an interaction strength which generally decreases with distance. The dotted lines denote weaker interactions than the solid lines.

Two many-body Hamiltonians that we actually use in parts of this thesis are the fermionic Hubbard Hamiltonian and the $t-J$ Hamiltonian. The Hubbard Hamiltonian is given by

$$\mathcal{H} = \sum_{\sigma,i} E_i \, d^{\dagger}_{i\sigma} d_{i\sigma} + \sum_{\sigma,i,j} t_{ij} (d^{\dagger}_{\mathrm{i}\sigma} d_{\mathrm{j}\sigma}) + \frac{1}{2} \sum_{i} U_i n_i (n_i - 1) + \sum_{\sigma,i,j} V_{ij} n_i n_j . \tag{1.9}$$

In the above, i, j stand for sites, $d^{\dagger}_{i\sigma}$ creates and $d_{i\sigma}$ annihilates an electron at the ith site in the spin state σ with energy E_i. Here we have assumed that the particles are created only in the lowest energy state at the site (E_i) and the higher energy levels for a single electron are so well separated that they never become involved in the problem. U_i is the Coulomb repulsion at the site i, $n_i = \sum_{\sigma} d^{\dagger}_{i\sigma} d_{i\sigma}$ in the total electron number operator of the ith site and t_{ij} and V_{ij} are tunnel and Coulomb matrix elements between different sites (generally, t_{ij} and V_{ij} are non-zero only for proximal sites and V_{ij} is often taken to be negligible in comparison to the strengths of the other terms in the Hamiltonian. While the above Hamiltonian includes both hopping (i.e., tunneling) and on-site interactions, there is another model called the $t-J$ model, where due to high values of U_i the double occupancy of sites is eliminated, and an electron interacts only with an electron on a neighbouring site by means of spin-spin interactions. The $t-J$ model is

given by the Hamiltonian

$$\mathcal{H}_{t-J} = \sum_{\sigma,i} E_i \; d^{\dagger}_{i\sigma} d_{i\sigma} + \sum_{\sigma,i,j} t_{ij} d^{\dagger}_{\mathrm{i}\sigma} d_{\mathrm{j}\sigma} + \frac{1}{2} \sum_{\sigma,i,j} J_{ij} \vec{\sigma}_i \vec{\sigma}_j. \tag{1.10}$$

1.7 Affleck-Kennedy-Lieb-Tasaki Hamiltonian and State

An interesting many-body Hamiltonian which has an exactly known ground state is called the Affleck-Kennedy-Lieb-Tasaki (AKLT) Hamiltonian [15]. Its ground states are called the AKLT states. Recently, it has been shown that one dimensional AKLT states are excellent channels for measurement based quantum communication [16], whereas two dimensional versions are excellent candidates for measurement based quantum computation [17]. For simplicity, we will restrict ourselves here to the one dimensional version, which involves spin-1 particles. The AKLT Hamiltonian is given by

$$\mathcal{H}_{\mathrm{AKLT}} = \sum_i \; \vec{S}_i . \vec{S}_{i+1} + \frac{1}{3} \sum_i (\vec{S}_i . \vec{S}_{i+1})^2, \tag{1.11}$$

where $\vec{S}_i$ are spin-1 operators for the ith spin. The above Hamiltonian can be shown to be equivalent to

$$\mathcal{H}_{\mathrm{AKLT}} = \sum_i P^{2S}_{i,i+1}, \tag{1.12}$$

where the operator $P^{2S}_{i,i+1}$ projects the ith and the $i+1$th spins to the highest spin, i.e., $2S = 2$ state. The above projector will have a zero value when the states of the two spins on neighboring sites are singlets.

Thus the ground state of the above model is constructed by first associating two fictional spins α_i and β_i with the ith site and placing the nearest neighbor spins α_{i+1} and β_i in a singlet state $|\psi^-\rangle_{\alpha_{i+1},\beta_i}$ as in Fig.1.11. Then projection operators $P^1_{\alpha_{i+1},\beta_i}$ are applied to each site (as shown by the dotted circles in Fig.1.11). The AKLT ground state is thereby given as

$$|\Psi_{\mathrm{AKLT}}\rangle = \bigotimes_j P^1_{\alpha_j,\beta_j} (\bigotimes_i |\psi^-\rangle_{\alpha_{i+1},\beta_i}), \tag{1.13}$$

where $\bigotimes_i$ denotes the tensor product. While usually the AKLT state is thought of as a ground state, any other method of producing the same in a physical implementation would be useful for the purpose of measurement based quantum communication and computation. Indeed, in this

thesis, we will discuss a method of preparing the above state through dynamics and measurements.

1.8 Thermal States

Any quantum mechanical system at thermal equilibrium is in a thermal state. If the Hamiltonian of the system is $\mathcal{H}$, then its thermal state is simply given by

$$\rho_T = \frac{e^{-\beta\mathcal{H}}}{Z}, \tag{1.14}$$

where the index T stands for the temperature of the state $\beta = 1/(K_B T)$, with K_B the Boltzmann constant and $Z = Tr(e^{-\beta\mathcal{H}})$. We introduce the thermal state here as it will be required to estimate the finite temperature entanglement in doped fullerene chains in Chapter 3.

1.9 Adiabatic Elimination

When we study problems in quantum mechanics it is common to have very large Hilbert spaces in which we study our system. As a result of the size of the Hilbert space, it is usually hard to solve the dynamics of these systems. If the energies in which we are interested in the study of the system are tiny compared to some states that we have in the hamiltonian, we can build an effective hamiltonian in a smaller/truncated Hilbert space considering that the possibility that the system evolve to the states outside this truncated Hilbert space is negligible. This procedure is called adiabatic elimination. Below we provide the step-wise algorithm for this procedure:

1. We take a basis in the full Hilbert space of the system and order this basis according to the expectation values of energies.

2. We consider the set of states of low energy and we call this set $\{|\psi_0\rangle\}$ and the set with higher energy $\{|\psi_1\rangle\}$.

3. Consider the time evolution of the whole system

$$\frac{d|\psi\rangle}{dt} = -iH|\psi\rangle. \tag{1.15}$$

Consider then the representation of the above equation

$$\frac{d\begin{pmatrix} |\psi_0\rangle \\ |\psi_1\rangle \end{pmatrix}}{dt} = -i \begin{pmatrix} H_0 & \Omega \\ \Omega^T & H_1 \end{pmatrix} \begin{pmatrix} |\psi_0\rangle \\ |\psi_1\rangle \end{pmatrix} \tag{1.16}$$

4. We make the assumption that

$$\frac{d\{|\psi_1\rangle\}}{dt} = 0. \tag{1.17}$$

This assumption is equivalent to the fact that states with high energy expectation values never take part in the dynamics (assuming the dynamics starts in the low energy sector, it continues within this sector). This implies

$$\Omega^T|\psi_0\rangle + H_1|\psi_1\rangle \ = 0 \Rightarrow |\psi_1\rangle = H_1^{-1}\Omega^T|\psi_0\rangle. \tag{1.18}$$

Thereby we can write

$$\frac{d|\psi_0\rangle}{dt} = -iH_0|\psi_0\rangle - i\Omega|\psi_1\rangle \Rightarrow \frac{d|\psi_0\rangle}{dt} = -iH_0|\psi_0\rangle - i\Omega H_1^{-1}\Omega^T|\psi_0\rangle. \tag{1.19}$$

5. By inspecting the above, one finds the effective hamiltonian to be

$$H_{eff} = H_0 + \Omega H_1^{-1}\Omega^T. \tag{1.20}$$

We shall use the above procedure in Chapter 5 of this thesis for deriving an analytically tractable effective Hamiltonian from a larger one. In that chapter we also match the analytic results obtained from the effective Hamiltonian with those obtained from a numerical solution to the full Hamiltonian.

Chapter 2

Quantum Dots for Quantum Information Processing

A quantum dot is a solid state structure in which the electronic energy levels are quantized in all the 3 spatial directions. Typically the size of the confinement is hundreds of nanometers, so that the separation between electronic energy levels, taking appropriate effective masses of electrons, can be of the order of 1 meV [18]. Because of their discrete energy level structure, such systems are often called "artificial atoms", and given a certain number of electrons, they do occupy the energy levels much like they would do in an atom. Under such confinement, the repulsive energy of two electrons can also be very important, e.g., of the order of $U \sim 10$ meV, making electron-electron interactions an important element of the physics of quantum dots. The electron-electron interactions can actually give rise to effective spin exchange interactions between electrons occupying distinct dots – this is exploited for quantum computation with quantum dots [19], as will be described later in this chapter. There are usually two broad categories of quantum dots, the "self assembled" ones (produced naturally during the growth of semiconductor structures) and the "gate-defined" ones which we will discuss in detail in the next section.

2.1 Fabrication

Gate defined dots are created from two dimensional electron gases (2DEGs) that arise at the interface of GaAs and AlGaAs layers in heterostructures grown by Molecular Beam Epitaxy (MBE) [20]. In the 2DEG, the electrons move as free particles with very long mean free paths (high mobility) in two dimensions (say, in the X-Y plane), but are completely confined in the third dimension. Metallic (Aluminium) electrodes (or gates) are deposited on top of the GaAs

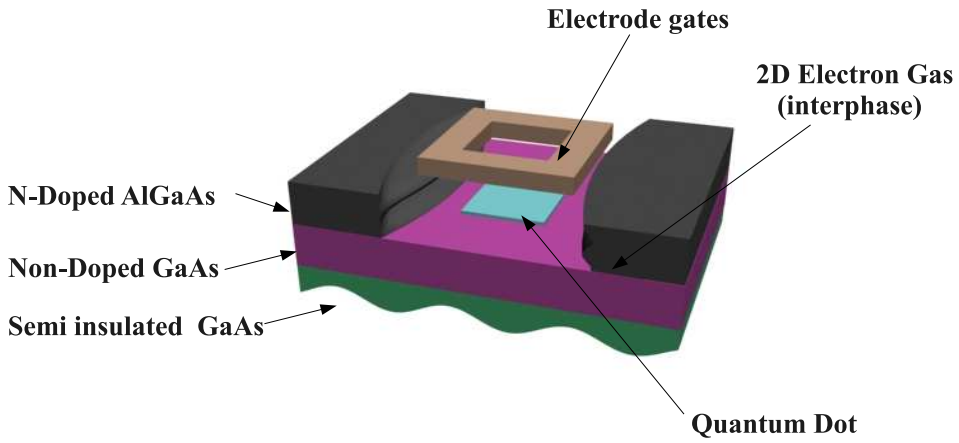

Figure 2.1: This figure depicts the three dimensional heterostructure used to generate a quantum dot. A system of three layers the top one is a N-Doped AlGaAs, below the Non-Dopped GaAs and in the bottom the Semi Insulated GaAs. In the interphase between the N-Doped AlGaAs and the Non-Doped GaAs is confined the Two-Dimensional Electron Gas (2DEG). The square shaped metal electrode at the very top generates a confined square region for electrons in the 2DEG below, which is essentially a quantum dot.

layer and these are used to apply voltages to the 2DEG to further confine the electrons in specific regions of the XY plane. Basically, an applied negative voltage to a gate depletes electrons from the region of the 2DEG directly below the gate. These then act as constrictions or potential barriers for the electrons moving in the plane of the 2DEG. When an electron is confined from all directions, this is simply a quantum dot. The type of heterostructure described above, with the position of the 2DEG and the use of electrodes to create a quantum dot in the 2DEG, are shown in Fig.2.1. In the later part of this thesis, we will be envisaging the use of electrodes to define square shaped quantum dots.

2.2 Hamiltonian for electrons in a quantum dot

As long as there is a single electron in a quantum dot, its states can be found by solving for particles in a well. The solution to that, whatever the structure of the well, there will be a set of discrete energy levels ϵ_m. In general, however, multiple electrons may occupy a quantum dot, and different numbers n_m of electrons populate the different levels. However, in this case they will also interact with each other through the Coulomb interaction. This can be especially high for smaller dots as the tight confinement brings electrons too close to each other so that they interact strongly. For very small dots, the Kinetic energy (which scales as $1/L^2$ with the dimension L of a dot – think of a free particle in a square well) dominates over the Coulomb repulsion (which scales as $1/L$) so that all the electrons have their peak densities at the centre of the wells. In this configuration, we cannot regard some pairs of electrons to be closer than the others, so that one can assume the interaction energy of each pair to be of the same value U. For a total number of $N = \sum n_m$ electrons, the Coulombic energy is thus $U\frac{N(N-1)}{2}$. In addition, the energies of all the electrons will be shifted up or down by an amount which depends on the external applied voltage $\mathcal{V}_{\text{ext}}$. The whole Hamiltonian for multiple electrons in a small quantum dot is therefore

$$H_0 = \frac{U}{2}N(N-1) - e\mathcal{V}_{\text{ext}}N + \sum_{i,m}\epsilon_m n_m \tag{2.1}$$

For larger dots, the Coulomb term both determines and depends on the positions of the electrons. This has to be determined in a self-consistent manner and will be discussed in a later section.

One of course has to solve the Schroedinger equation for finding out the quantized energy levels ϵ_m of an electron in an arbitrary quantum dot. If the density of the background 2D electron gas is ρ_{2DEG} (this also depends on the gate voltage), then the potential $V(\mathbf{R})$ is given by

$$\nabla^2 V(\mathbf{R}) = -\frac{\rho_{2DEG}(\mathbf{R})}{\varepsilon_0\varepsilon_r}, \mathbf{R} = (x, y, z). \tag{2.2}$$

In the relevant material the electron will have an effective mass m^* because of its dispersion relation in the material. Thereby solving the Schroedinger equation to be solved for the 1D and 2D cases respectively gives

$$\frac{\hbar^2}{2m^*}\nabla^2\varphi(z) + qV(Z)\varphi(z) = E_z\varphi(z), \tag{2.3}$$

and

$$\frac{\hbar^2}{2m^{*\Gamma}_{GaAs}}\nabla^2\psi_i(r) + qV_{eff\ i}(r)\psi_i(r) = E_i\psi_i(r) \tag{2.4}$$

2.3 Numerical Schroedinger Equation Method for multiple electrons in a quantum dot

Usually when there are multiple electrons and the quantum dot is relatively large, one cannot simply model the electronic interactions as the same between all pairs and the potential energy terms depend on the specific locations of the electrons. The method used in this thesis for solving the hamiltonian equation for two electrons in a quantum dot is numerical and is detailed now. The Hamiltonian is

$$H = -\frac{\hbar^2}{2m^*}[\nabla_1^2 + \nabla_2^2] + V(r_1) + V(r_2) + \frac{e^2}{4\pi\varepsilon\,|r_1 - r_2|}, \tag{2.5}$$

where the indices 1 and 2 refer to electrons 1 and 2 respectively. We consider a two dimensional array of size $\sum_i L_i \times \sum_j M_j$, where L_i and M_j are the labels of the array cells, circumscribed inside the area where one is interested to solve the Schroedinger equation. We are going to proceed to calculate for each point in the array, the kinetic energy, the potential energy and the Coulomb term of the Hamiltonian. The boundary conditions taken are going to make the probability of having an electron outside of the array equal to zero and it is forbidden to have the two electrons in the same position as then the Coulomb term will be infinite. Given the basis $|n_1, m_1, n_2, m_2\rangle$ where n_i and m_i are the electrons positions in the array. The kinetic term of a general state $\psi(n_1, m_1, n_2, m_2)$ is

$$\begin{aligned}\frac{-\hbar^2}{2m^*}\Big(&\frac{\psi(n_1-1,m_1,n_2,m_2) - 2\psi(n_1,m_1,n_2,m_2) + \psi(n_1+1,m_1,n_2,m_2)}{\delta n^2} + \\ &\frac{\psi(n_1,m_1-1,n_2,m_2) - 2\psi(n_1,m_1,n_2,m_2) + \psi(n_1,m_1+1,n_2,m_2)}{\delta m^2} + \\ &\frac{\psi(n_1,m_1,n_2-1,m_2) - 2\psi(n_1,m_1,n_2,m_2) + \psi(n_1,m_1,n_2+1,m_2)}{\delta n^2} + \\ &\frac{\psi(n_1,m_1,n_2,m_2-1) - 2\psi(n_1,m_1,n_2,m_2) + \psi(n_1,m_1+1,n_2,m_2+1)}{\delta m^2}\Big).\end{aligned} \tag{2.6}$$

When at least one of the four positions is a boundary one in the array, the term outside will be zero. The Potential $V(r_i)$ for each electron 1,2 depends on the shape and physical parameters of the quantum dots and can be parabolic, triangular, squared box with or without hardwall conditions. The Coulomb term is obtained by calculating the square of the charge of the electrons e^2 divided $4\pi\varepsilon$ times distance between each electron $\sqrt{(x_1(n_1,m_1) - x_2(n_2,m_2))^2 + (y_1(n_1,m_1) - y_2(n_2,m_2))^2}$.

After obtaining the whole hamiltonian as a $(\sum_i L_i)^2 \times (\sum_j M_j)^2$ matrix, one can proceed to numerically diagonalize it and compute the eigenstates. From the ground state, one can obtain

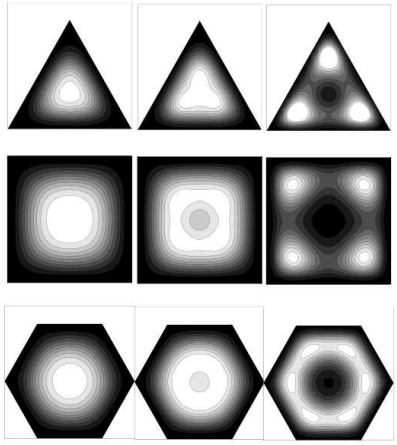

C. Creffield, W. Hausler, J. H. Jefferson, S. Sarkar, PRB 59, 10719 (1999)

Figure 2.2: Ground state charge distributions for the three types of quantum dot. Dot sizes are: (a)50 nm (b)100 nm (c)800 n . This figure has been adapted from the reference cited above.

the average probability of presence of one electron in each position of the grid by making the average of the second one in the whole array except in the same position. Using as example the solution of an squared quantum dots with hardwalls conditions one finds that depending on the size of the quantum dot there will be a prevelence of the kinetic term or the Coulomb term. For small size quantum dots, the Coulomb interaction is much smaller than the kinetic term, and the two electron ground state is similar to the one in the non-interacting ground state, with the charge distribution being peaked at the centre of the dot. The situations for large dots when the Coulomb term prevails and density distributions of electrons are peaked away from each other, are shown in Fig.2.2.

2.4 Coupled quantum dots and origin of the spin exchange interaction between them

We are now going to present how an interaction between spins can arise purely from the electrostatic interaction between two quantum dots. Two proximal quantum dots, particularly the ones in the gate defined systems as described here, can always be made to have a tunnel coupling t between them. This is described by the Hamiltonian term [21]

$$H_{\text{tunnel}} = -t\, d^{\dagger}_{A,\sigma} d_{B,\sigma} + h.c., \tag{2.7}$$

where $d^{\dagger}_{j,\sigma}$ creates an electron of spin σ in the $j = A, B$th dot. Essentially this tunnel coupling t is set by varying the voltage barrier between the quantum dots and follows the rule $t \propto e^{-\frac{\sqrt{2m(V-E)}\Delta L}{\hbar}}$, where V is the barrier height between the wells (engineered by setting the voltage), ΔL is the spatial separation between the dots and E is the energy of the electrons in the ground states of the individual quantum dots (when the interaction between them is not present). Thus two proximal quantum dots, particularly the ones in the gate defined systems as described here, can always be made to have a tunnel coupling t between them. Consider two dots with a very high $U >> E$ so that two electrons, even with the opposite spins can never sit in the same dot – energetically it will be much more favorable for them to sit in two distinct dots (with energy $2E$) than on top of each other in the same dot (with energy $E + \frac{U}{2}$).

By adiabatic elimination of the excited state of energy $E + \frac{U}{2}$, which will effectively never be occupied, the exchange interaction can be estimated to be $J \sim \frac{2t^2}{U}$. Below we outline the derivation (similar methodology will be used in Chapter 5 in the case of 3 dots). The Hamiltonian for the full system of two dots including double occupancy states, is given, in the basis

$$d^{\dagger}_{\mathrm{A}\uparrow} d^{\dagger}_{\mathrm{B}\uparrow}|0\rangle, d^{\dagger}_{\mathrm{A}\downarrow} d^{\dagger}_{\mathrm{B}\downarrow}|0\rangle, d^{\dagger}_{\mathrm{A}\uparrow} d^{\dagger}_{\mathrm{B}\downarrow}|0\rangle, d^{\dagger}_{\mathrm{A}\downarrow} d^{\dagger}_{\mathrm{B}\uparrow}|0\rangle, d^{\dagger}_{\mathrm{A}\uparrow} d^{\dagger}_{\mathrm{A}\downarrow}|0\rangle, d^{\dagger}_{\mathrm{B}\uparrow} d^{\dagger}_{\mathrm{B}\downarrow}|0\rangle, \tag{2.8}$$

$$H = \begin{pmatrix} E & 0 & 0 & 0 & 0 & 0 \\ 0 & E & 0 & 0 & 0 & 0 \\ 0 & 0 & E & 0 & -t & -t \\ 0 & 0 & 0 & E & t & t \\ 0 & 0 & -t & t & E+\frac{U}{2} & 0 \\ 0 & 0 & -t & t & 0 & E+\frac{U}{2} \end{pmatrix} \tag{2.9}$$

and now using the adiabatic elimination described in the chapter 1 in section 1.9 with

$$H_0 = \begin{pmatrix} E & 0 & 0 & 0 \\ 0 & E & 0 & 0 \\ 0 & 0 & E & 0 \\ 0 & 0 & 0 & E \end{pmatrix}, \tag{2.10}$$

$$\Omega = \begin{pmatrix} 0 & 0 \\ 0 & 0 \\ -t & -t \\ t & t \end{pmatrix}, \tag{2.11}$$

$$H_1 = \begin{pmatrix} E+\frac{U}{2} & 0 \\ 0 & E+\frac{U}{2} \end{pmatrix}, \tag{2.12}$$

and

$$\Omega^T = \begin{pmatrix} 0 & 0 & -t & t \\ 0 & 0 & -t & t \end{pmatrix}. \tag{2.13}$$

Now we set $E = \frac{2t^2}{U} << U$ because the level of energy can be arbtrarily set. We use the adiabatic elimination formula as described in section 1.9:

$$H_{eff} = H_0 + \Omega H_1^{-1} \Omega^T \tag{2.14}$$

so the effective Hamiltonian in the basis, $d^\dagger_{\mathrm{A}\uparrow} d^\dagger_{\mathrm{B}\uparrow}|0\rangle, d^\dagger_{\mathrm{A}\downarrow} d^\dagger_{\mathrm{B}\downarrow}|0\rangle, d^\dagger_{\mathrm{A}\uparrow} d^\dagger_{\mathrm{B}\downarrow}|0\rangle, d^\dagger_{\mathrm{A}\downarrow} d^\dagger_{\mathrm{B}\uparrow}|0\rangle$ will be

$$H_{eff} = \begin{pmatrix} J & 0 & 0 & 0 \\ 0 & J & 0 & 0 \\ 0 & 0 & -J & 2J \\ 0 & 0 & 2J & -J \end{pmatrix} = \tag{2.15}$$

$$J(|\uparrow\uparrow\rangle\langle\uparrow\uparrow| + |\downarrow\downarrow\rangle\langle\downarrow\downarrow| - |\uparrow\downarrow\rangle\langle\uparrow\downarrow| - |\downarrow\uparrow\rangle\langle\downarrow\uparrow|) + 2J(|\uparrow\downarrow\rangle\langle\uparrow\downarrow| + |\downarrow\uparrow\rangle\langle\downarrow\uparrow|) = \tag{2.16}$$

$$J\sigma_z \otimes \sigma_z + J(\sigma_x \otimes \sigma_x + \sigma_y \otimes \sigma_y) \Rightarrow \tag{2.17}$$

$$H_{eff} = J\vec{\sigma}\vec{\sigma} \tag{2.18}$$

Where $J = \frac{2t^2}{U}$. In the deriving of the above, we have used the identification $^{\dagger}_{\mathrm{A}\uparrow} d^{\dagger}_{\mathrm{B}\uparrow}|0\rangle = |\uparrow\uparrow\rangle$... in step 2.16, and $\sigma_x = |\uparrow\rangle\langle\downarrow| + |\downarrow\rangle\langle\uparrow|$, $\sigma_y = i(|\downarrow\rangle\langle\uparrow| - |\uparrow\rangle\langle\downarrow|)$ and $\sigma_z = (|\uparrow\rangle\langle\uparrow| - |\downarrow\rangle\langle\downarrow|)$ in step 2.17. The above interaction is equivalent to the Heisenberg exchange interaction between neighbouring spins . Our result above obtained by adiabatic elimination can also be obtained by degenerate second order perturbation theory as described in Ref.[21].

Note that here our derivation of the exchange interaction has been adapted to the case of fermionic Mott insulators as we have used a high U and a second order tunneling process. The exchange coupling $J = \frac{2t^2}{U}$ is therefore always positive, as one can see from its expression. One may thus be puzzled as to how ferromagnetism at all appears in nature if our derivation presented above is the only way one obtains an exchange interaction between the spins. In fact, the exchange interaction we have derived above is often called a super-exchange as it involves a second order process. What is often a textbook derivation of the exchange interaction can be ferromagnetic (i.e., negative J) as it involves the so called exchange integral as the energy difference between a singlet and a triplet state of two spins (J below has been defined in terms of giving the right singlet triplet difference of energy according to Eq.(2.18))

$$E_{\text{triplet}} - E_{\text{singlet}} = 4J = -\int dr_1 dr_2 \phi^*_{G,A}(r_1)\phi^*_{G,B}(r_2)\frac{e^2}{|r_1 - r_2|}\phi_{G,A}(r_2)\phi_{G,B}(r_1), \tag{2.19}$$

where $\phi_{G,A}(r)$ and $\phi_{G,B}(r)$ are ground state wavefunctions in dots A and B. As $\phi_{G,A}(r)$ and $\phi_{G,B}(r)$ are positive Gaussian wavefunctions, the integral in the above equation is always positive and thereby $J < 0$, leading to ferromagnetic coupling (triplet states – parallel spins

have lower energy). The above energy difference between the triplet and singlet automatically arises by writing the total wavefunction (spin and orbital parts) of the two electrons in the two quantum dots as antisymmetrized, computing the expectation of the Coulomb energy (in which only the orbital wavefunctions take part) in the triplet and the singlet states and taking their difference. Note that when the dots are made narrower to achieve a high U, the direct overlap of $\phi_{G,A}(r)$ and $\phi_{G,B}(r)$ severely decreases, while the term $\frac{e^2}{|r_1-r_2|}$, depending only on r_1 and r_2 remains the same. The J derived from the exchange integral above becomes vanishing. It is in this case when the second order exchange process, as derived by us, with a positive J, becomes active.

2.5 Quantum Computation with quantum dots

Qubits can be encoded in quantum dots in at least three different ways. The most fruitful in our opinion are the spin qubits in view of their large decoherence times. When surrounding nuclear spins are polarized, then the coherence time for electronic spins can be of μs time scale [22] allowing plenty of quantum operations to be performed. Before moving to the details of how quantum gates are accomplished between spin qubits, we describe the two other form of qubits in quantum dots, namely the excitonic qubits in single dots and charge qubits in double dots. The excitonic qubit states are the presence and absence of an exciton (an electron-hole excitation) in a quantum dot. Separated quantum dots can interact through the hopping of an exciton from one dot to another by the so called Föster-Dexter interaction. But an excitation also leaks outside and thereby the excitons are not outstanding qubits, though they interact at a much shorter time-scale than spin-exchange interactions. This is why there are clever schemes exploiting the best of two worlds whereby the spins are kept as qubits and converted to excitons only when a two qubit gate is desired between separated quantum dots [23]. In a double dot, whether a charge resides in the left or in the right dot of the pair is also a qubit widely considered [24]. However, their best decoherence times have been found to be of the order of 1 ns [25]. Quantum gates here, of course use very strong electrostatic interactions as opposed to the much weaker exchange interactions [26].

We will now describe the mechanism for quantum computation using spin qubits in quantum dots. One spin is confined in each quantum dot, which can be ensured by the appropriate gate voltages (this is a standard scheme these days). Fig.2.3 depicts the setup. What we essentially need is a mechanism of an *entangling* two qubit gate, as along with arbitrary local operations this forms a universal gate-set for quantum computation. At the time of a quantum

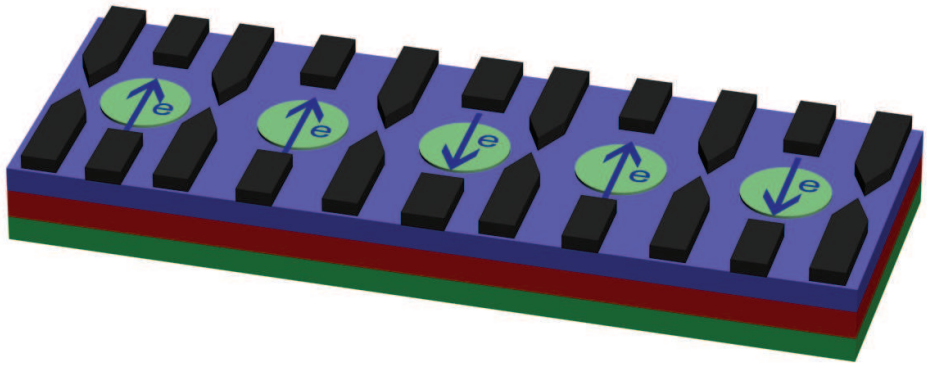

Figure 2.3: Here we represent a much larger scale of single trapped electrons in a chain of quantum dots confined in a similar way than the one explained in Fig.2.1 scaling it in a single dimension.

gate between two spin qubits, one suddenly lowers the gate barrier between two neighbouring quantum dots (the gates used to control this barrier are the ones with triangular edges in the figure) so as to suddenly increase the tunnel coupling t and thereby switch on $J \sim 2t^2/U$ for a precisely fixed interval of time. The Heisenberg exchange coupling J for the fixed interval of time gives entangling quantum gates. More precisely, the coupling switched on for an interval $\tau = \frac{\pi}{2J}$, we have the time evolution of two spins in two neighbouring dots A and B to be

$$\begin{aligned}
|\uparrow\rangle_A|\uparrow\rangle_B &\rightarrow |\uparrow\rangle_A|\uparrow\rangle_B \\
|\uparrow\rangle_A|\downarrow\rangle_B &\rightarrow \frac{1}{\sqrt{2}}(|\uparrow\rangle_A|\downarrow\rangle_B - i|\downarrow\rangle_A|\uparrow\rangle_B) \\
|\downarrow\rangle_A|\uparrow\rangle_B &\rightarrow \frac{1}{\sqrt{2}}(|\downarrow\rangle_A|\uparrow\rangle_B - i|\uparrow\rangle_A|\downarrow\rangle_B) \\
|\downarrow\rangle_A|\downarrow\rangle_B &\rightarrow |\downarrow\rangle_A|\downarrow\rangle_B.
\end{aligned} \tag{2.20}$$

The above is called an *exchange gate* and as is evident can maximally entangle two qubits in appropriate initial states. Of course, another pivotally important element in any setup is the ability to do local gates. For this reason we have, in the figure, a magnetized or high-g layer (in the high-g layer, an electron interacts more strongly with the nuclear magnetic field). At the time of a local gate on a spin qubit, the relevant electron is pushed towards this layer by gate voltages for a fixed time so that a local rotation happens to it.

2.6 Decoherence and noise of qubits in quantum dots

Spins in general may be affected by various sources of decoherence. The most relevant in the context of quantum dots are the hyperfine interactions with the nuclear spins of the material (e.g. GaAs) in which the quantum dot is fabricated. Unless a sample is such that the nuclei are spinless (for example, in isotopically pure Si^{29}), each nuclei will produce a local magnetic field which will act as a Zeeman field for an electron in its vicinity. Of course, this field falls off rapidly with distance and one only needs to take the field of the nuclei at the site of the electron into account. However, the electron itself is in a spread-out wavefunction $\psi(\mathbf{r})$ and thereby sees several nuclei that provide it with random directions of Zeeman fields. The effective Hamiltonian acting on the electron spin is therefore [18]

$$H_{\text{eff}} = \hbar\gamma_e \overrightarrow{B}_{\text{nuc}}.\overrightarrow{\sigma} \tag{2.21}$$

where $\gamma_e = g\mu_B/\hbar$ is the gyromagnetic ratio for the electron, $\overrightarrow{\sigma} = (\sigma_x, \sigma_y, \sigma_z)$ are the Pauli matrices, $\overrightarrow{B}_{\text{nuc}}$ is the effective magnetic field provided by *all* nuclei taken together. Thereby, $\overrightarrow{B}_{\text{nuc}}$ is given as

$$\overrightarrow{B}_{\text{nuc}} = v_0 \sum_{\beta} b_\beta \sum_{j} |\psi(\overrightarrow{r}_{j,\beta})|^2 I^{\beta,j}, \tag{2.22}$$

where v_0 is the volume of an unit cell, β stands for nuclear species, b_β is the effective Hyperfine field due to species β within each unit cell, j stands for the jth unit cell and $I^{\beta,j}$ for the magnitude of the nuclear spin of species β. As each nucleas points in a random direction, the total field $\overrightarrow{B}_{\text{nuc}}$ has a gaussian random distribution centred around $\overrightarrow{B}_{\text{nuc}} = 0$ with a variance $B_{\text{nuc,rms}}$ which decreases as $\frac{1}{\sqrt{N}}$ by virtue of the central limit theorem. Thus ironically enough, the larger the dot with more nuclear spins (i.e., an environment larger in size), the smaller effective random field provided by the bath! Of course, you cannot use dots too large because you want to use the single electron as a qubit with two spin levels and only one orbital level and the second orbital level comes closer the wider the dots are made. The distribution of the nuclear field is thereby given by

$$P(\overrightarrow{B}_{\text{nuc}}) = \frac{1}{(2\pi B^2_{\text{nuc,rms}})^{3/2}} \exp(-(\overrightarrow{B}_{\text{nuc}}.\overrightarrow{B}_{\text{nuc}})/2B^2_{\text{nuc,rms}}). \tag{2.23}$$

where $B_{\text{nuc,rms}} = h_1/\sqrt{N}$ is the variance of the random variable $\overrightarrow{B}_{\text{nuc}}$ with the constant h_1 being $\sim$ 4T for GaAs. There is one more important point here, namely the fact that this nuclear field fluctuates on a time-scale much higher than the dynamics of electron spins in the

dots. At low (or vanishing) external magnetic fields the fluctuations of the nuclear spin can only happen by its interaction with the electronic spin as this is much stronger than the dipolar interaction between the different nuclear spins themselves. This interaction has an effect over a microsecond time-scale whereas quantum gates between electrons happen over the time-scale of nanoseconds. Thus, over the time-scale of the gates the nuclear spins, and thereby the field $\overrightarrow{B}_{\text{nuc}}$ can effectively be regarded as frozen. This is known as the *quasistatic approximation* and greatly aids the analysis of the decoherence due to the nuclear spin bath as one can evolve different pure state trajectories corresponding to a different magnitude and orientation of $\overrightarrow{B}_{\text{nuc}}$, and later on average over these trajectories to obtain the time evolution of the system.

Another important source of decoherence that is mainly important for charge qubits are charge fluctuations in the metallic gates used to control the sample. However, spin qubits may be indirectly affected. For example, in certain types of quantum gate schemes, such as the one we present in Chapter 5, time evolution may create superpositions of states having different charge distributions though ultimately the gates are on spin qubits. Thereby it is important to consider the decoherence caused due to these fluctuators even for some schemes with spin qubits. These charge fluctuators generally cause spatial fluctuations of the voltages in a system – for example, they affect the voltage (and thereby the energy of the orbital states) randomly in different dots of a multidot system (considering small dots so that the variation of the voltage within one dot is negligible). The charge fluctuators are generally assumed to have a spectral function which is inversely proportional to their frequency ω, and are thereby regharded as producing $1/f$ noise. Spin-orbit interactions may also be important in certain materials such as GaInAs, but are generally small in GaAs quantum dots, which are the setting for most spin qubits in quantum dot experiments. In GaAs they form a much smaller correction than the Hyperfine nuclear field because the length-scale over which spin orbit interactions become important is much larger than the size of 100 nm of the quantum dots that hold the qubits.

2.7 Measurement of spin qubits

Spin of a single electron generates such a small magnetic field that it is notoriously difficult to sense spin by directly measuring the magnetic field. The charge of a single electron, on the other hand, can be easily sensed with the so called quantum point contacts (QPC) [27, 28], which is widely used these days. Therefore one can try to cleverly convert the spin alignment information to the presence or absence of a charge at some location to efficiently read it. This idea is called spin to charge conversion for readout, and we will describe two specific methods

for this. The first method is to use an energy based selection of spin orientation and is depicted in Fig.2.4. Here a lead is connected to the quantum dot holding an electronic spin in an up or a down state, where the aim is to measure the spin of the dot. Next, a Zeeman field is applied to the quantum dot so that the energies of the up and down spins become well separated. The Fermi energy of the lead is set at value lower than that of the spin down state and higher than that of the spin up state as shown in the figure. The spin up state therefore cannot tunnel out of the dot and is trapped there permanently. The spin down state, on the other hand, tunnels out eventually through the lead. Thus, a charge mesurement of the quantum dot after the tunneling time will effectively measure whether the dot's spin was initially up or down – note that this measurement destroys the spin state.

We are now going to discuss another strategy for spin measurement which can measure spin states in double dots. Particularly, it can precisely distinguish between singlets and triplets. However, it can also do a measurement of a single spin state when another spin is initialized to a reference state. This method uses a setup of an isolated double dot populated with two electrons and it take advantage of the Pauli exclusion principle. Initially the two dots are in the Coulomb blockade regime so that the (1,1) state (i.e., one electron in each dot) has far lower energy that the (0,2) state (i.e., both electrons in the same right hand dot). Suppose now the two electrons in the (1,1) state are in a singlet state S(1,1) or one of the three triplets T(1,1) and we want to distinguish between these two options. Now, to do this measurement, we raise (by electrodes) the energy of S(1,1) and T(1,1) to a higher value than the energy of S(0,2) so that energetically now tunneling is allowed for both the electrons to go to the same (second) dot. Here the phenomenon of Pauli-Blockade comes into effect as shown in Fig.2.5. Because of the Pauli exclusion principle, only the S(1,1) gets converted to S(0,2) by tunneling, but the T(1,1) state remains frozen. Therefore a charge measurement here will allow one to discriminate between a singlet and a triplet in the two dots. Here the time-scale of the spin to charge conversion is set by the tunneling time of the electron and thereby happens at a random time of the order of the tunneling time-scale. We mention this here in particular as in Chapter 6 we present a singlet-triplet discrimination strategy within a single large dot where the process of spin to charge conversion takes place at a precisely defined time because that is a coherent evolution.

Now, in presence of a nuclear bath field mostly aligned in a specific (z) direction, the nuclear field components in the x and y directions which can rotate a $J_z = 0$ triplet to a $J_z = \pm 1$ triplet are negligible (here we are referring to the (1,1) triplets). Therefore only the conversion

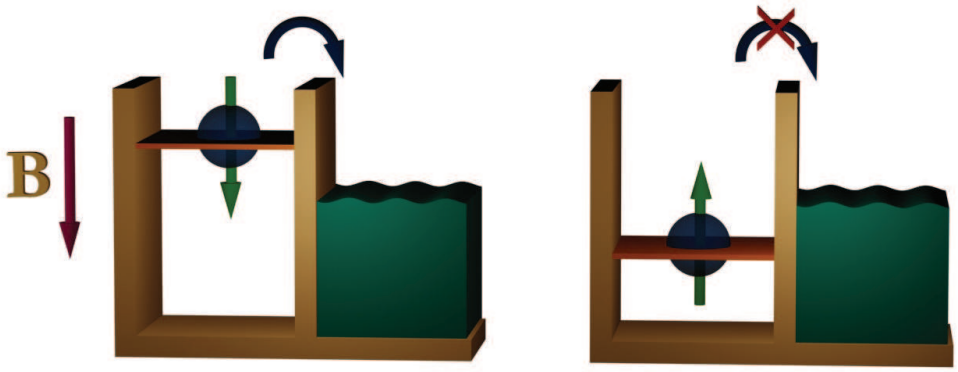

Figure 2.4: This figure depicts the energy selective conversion of spin orientation to the presence or absence of charge in a quantum dot. The quantum dot charge is then measured to measure the spin.

between $J_z = 0$ triplet and the singlet is dominant. This enables one to discriminate between an $\uparrow$ and an $\downarrow\uparrow$ in the two dots. The $\uparrow$ state will never go to the (0,2) charge configuration by tunneling due to Pauli blockade. However, the $\downarrow\uparrow$ state, being a superposition of the singlet and the triplet, will go to the (0,2) charge configuration with a probability of 0.5. However, if it does not do so in a long enough interval, and is thereby effectively projected on to the $J_z = 0$ triplet, then it is converted by the differences in the nuclear fields in the z direction in the two dots to a singlet and thereby again has a probability to tunnel. In this way the $\downarrow\uparrow$ state can eventually be converted to a (0,2) charge configuration and be detected. In this way, as single spin $\uparrow$ or $\downarrow$ in one dot can be detected if the second spin is kept in a reference state $\uparrow$.

2.8 Conclusions

In this chapter we have given a broad overview of the potential role of quantum dots in quantum information processing. Firstly, we have discussed their fabrication, with particular emphasis on the gate defined quantum dots relevant for our work. We have also introduced the hamiltonians that govern the electrons in QDs, as the spins of these electrons will be considered as qubits. After introducing different models used to describe the relevant quantum dot physics, we explain the types of quantum computation that are possible and the gates involving QD qubits that we achieve in our own work (described in subsequent chapters of this thesis). We describe the role and effects of decoherence and noise while using spin qubits in quantum dots. For example, we

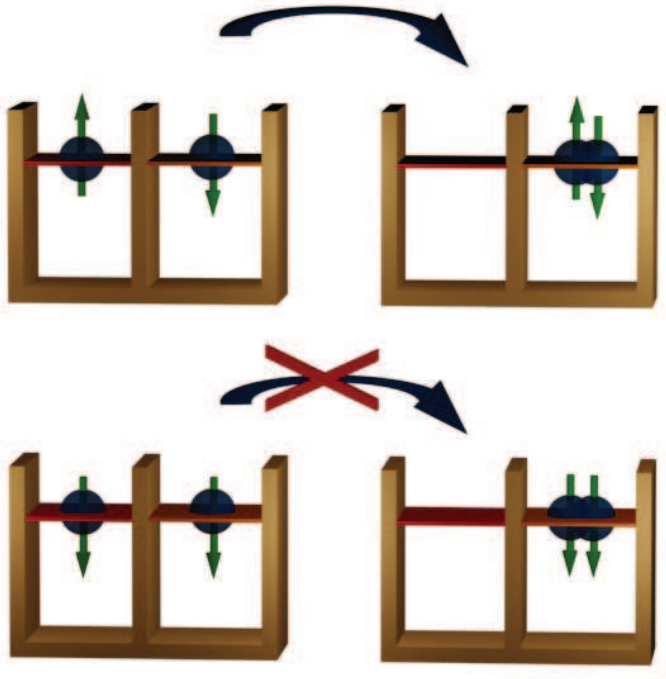

Figure 2.5: In this picture we can see how the alignment or an anti-alignament setups of initial spin directions in each site will of a double dot, allowing the tunneling for double occupancy or not in a single site due to the Pauli exclusion principle.

explain how the qubits are affected by the hyperfine interaction of the nuclei and by the noise in the voltage that defines the dots (this noise affect their tunneling and energy). We conclude the chapter with the explanation on different ways it is possible to measure a spin qubit in the QDs.

Chapter 3

Entanglement in Endohedral Fullerenes Dimers

As a new implementation of Quantum Information Processing (QIP), the possibility of endohedral fullerenes is now being explored [29, 30]. It is possible to have a chain of fullerene (C_{60}) molecules inside Carbon nano-tubes (or Wires), and moreover, it is possible to dope each fullerene molecule with a Nitrogen ^{14}N atom (this is called $^{14}N@C_{60}$). The Carbon Nano-Wire (CNW) plays the role of a scaffolding for the fullerenes, as shown in Fig.3.1(a). Each dopant contributes 3 unpaired electrons, and thereby has a spin 3/2 contributed by electrons as shown in Fig.3.1(b). These electronic spins of the doped fullerene molecules can be regarded as carriers of quantum information [29, 30]. However, each dopant inside the fullerene molecule also has a nuclear spin 1 (for a nitrogen ^{14}N dopant, as shown in Fig.3.1(b)), which have much better coherence times and thereby are a better candidate for storing the qubits, and ideal as memory qubits. The fullerene also will act as a Faraday cage so a wide part of the electromagnetic field will be neglected allowing better decoherence times. While building chain structures and their use for quantum computation is still somewhat away, at the moment, very small dimers (e.g., as shown in Fig.3.1(c)) and trimers of fullerene molecules are being prepared in the laboratory. In this context, it is sensible to study the entanglement between the different spins (nuclear and electronic) present in such a dimer structure, so that some aspect of their behaviour as bonafide "quantum" objects which can quantum mechanically correlate with each other is tested. While this is not necessarily a pre-requisite to quantum computation, it is start towards testing quantum informational quantities in endohedral fullerene systems, namely the fact that the nuclear spins in them *can* be entangled. Of course, one could entangle two nuclear spins by dynamics, say by first entangling two electronic spins and then swapping that entanglement over to

their proximal nuclei – indeed this is the standard way of using nuclei as quantum memory. However, in that case one has to induce dynamics in this system, which is a harder task than making the system relax to its ground state. This is why we examine whether we can look at the entanglement between two nuclear spins in the ground and thermal state of the combined nuclear and electronic spin system. Note that the direct dipolar interaction between two nuclear spins is extremely weak, and is negligible compared the electron-electron and electron-nuclear interactions. Thereby we take a model were the direct nuclear-nuclear interaction term is completely absent. This makes our investigation nontrivial, in the sense that we are seeking a high entanglement between systems which do not directly interact.

3.1 Hamiltonian

The nature of the interaction Hamiltonian in fullerene dimers is still not fully ascertained, and in fact the cage holding them (or the bridging atoms) may play essential roles in determining this coupling. As there is no apriori reason to have any preferred external magnetic direction, i.e., an easy axis, the most intuitive Hamiltonian to assume is

$$H = g\vec{I}_1 \cdot \vec{S}_1 + J\vec{S}_1 \cdot \vec{S}_2 + g\vec{S}_2 \cdot \vec{I}_2 \tag{3.1}$$

where g the nuclear spin–electron spin Hyperfine coupling factor, J the fullerene-fullerene coupling factor (strength) due to the electronic spins of the dopants, $\vec{I}_k$ the spin of nitrogen k and $\vec{I}_k$ the spin of the fullerene k,$\vec{S}_k$ the spin of the nitrogen, in this case k goes from 1 to 2. The magnitudes of the spins are 1 for nuclear spin $\vec{I}$ and $3/2$ for electronic spin $\vec{S}$. Additional support for the above form of Hamiltonian may be obtained from the density functional theory calculations performed in $Sc@C_{82}$ peapod structures, where it was deduced that neigbouring fullerene molecules have an antiferromagnetic *exchange* interaction [31].

3.2 Entanglement in fullerene dimers

We now proceed to investigate the entanglement between the various spins involved in a fullerene dimer system. As we have only spin-3/2 and spin-1 systems involved, and the states of any pair of spins may be a higher dimensional mixed state and the most appropriate measures to use are the negativity and the logarithmic negativity discussed in the introductory chapter. The logarithmic negativity has the advantage that for a d-dimensional maximally entangled state $\frac{1}{\sqrt{d}}(|0\rangle|0\rangle + |1\rangle|1\rangle + |2\rangle|2\rangle + ... + |d-1\rangle|d-1\rangle)$ it has the value $\log_2 d$. We are going to study the logarithmic negativity between the nuclear spins of the two Nitrogen atoms in the two

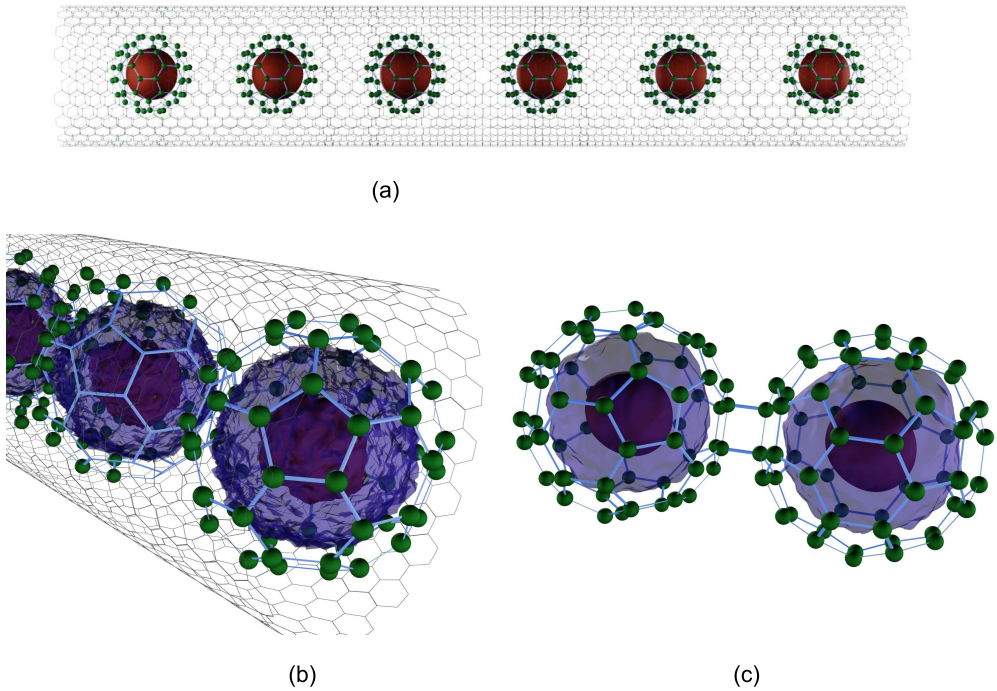

Figure 3.1: Fig.(a) shows several fullerene molecules inside a nanotube in a peapod-like arrangement. Each is doped with a Nitrogen atom as shown by red dot inside the cage in the figure. Fig.(b) shows the blow up of each doped fullerene molecule with the electron cloud of the dopant (blue colour transparent sphere) which has spin $3/2$. In the same figure, the nuclear spin of the dopant is shown by purple colour ball. Fig.(c) shows a multi-fullerene structure already being made, namely a fullerene dimer, which can already be used as a test-bed for experiments before full control over longer structures such as the peapods depicted in Fig.(a) is gained.

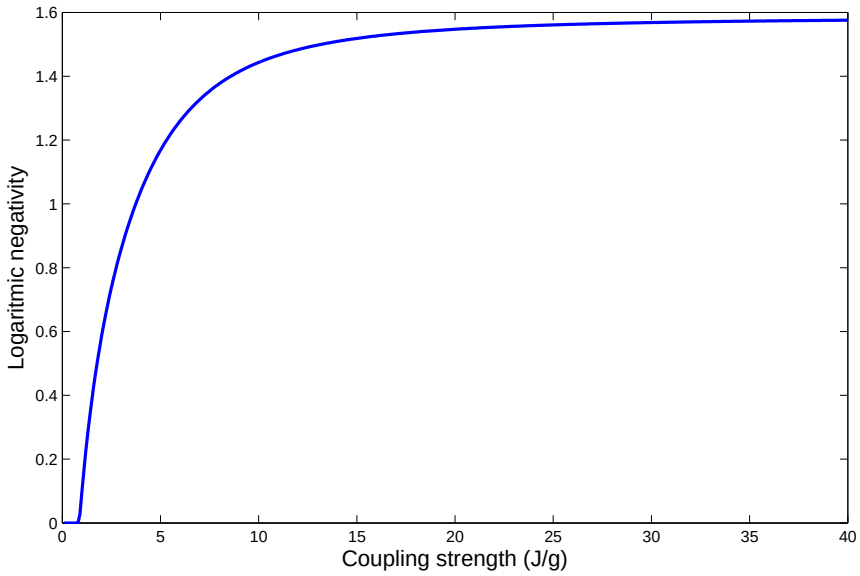

Figure 3.2: The figure shows how the ground state entanglement between the nuclei of the dopant spins of a dimer, as quantified by the logarithmic negativity, varies with the relative strength of the inter-fullerene spin-spin coupling J of the electrons and the intra-fullerene coupling g of the electronic and nuclear spins. The plot is at zero temperature.

fullerenes. As these nuclei are spin-1 systems, for them $d = 3$, and thereby the highest value of logarithmic negativity that one could possibly expect from them is $\log_2 3$ (the entanglement of the maximally entangled state of two qutrits). These nuclei are not directly interacting. Here we present a method of creating entanglement between them in a low temperature thermal state of the dimer. Moreover, ultimately, it is these nuclear spins which one would intend to use as the long memory time quantum bits (more appropriately, qutrits in this case) because of their long decoherence lifetimes. Thereby it is important to verify a bonafide quantum property displayed by them, namely the ability to be entangled. By changing the distance between the fullerene cages in the dimer, presumably by longer and longer molecular bridges, the relative strength of the nuclear-electron coupling in each fullerene (g) and the electron-electron coupling between the two fullerenes will be varied and the entanglement between the two nuclear spins, as quantified by the logarithmic negativity, will be analysed with different strengths of the couplings and in a wide range of temperatures.

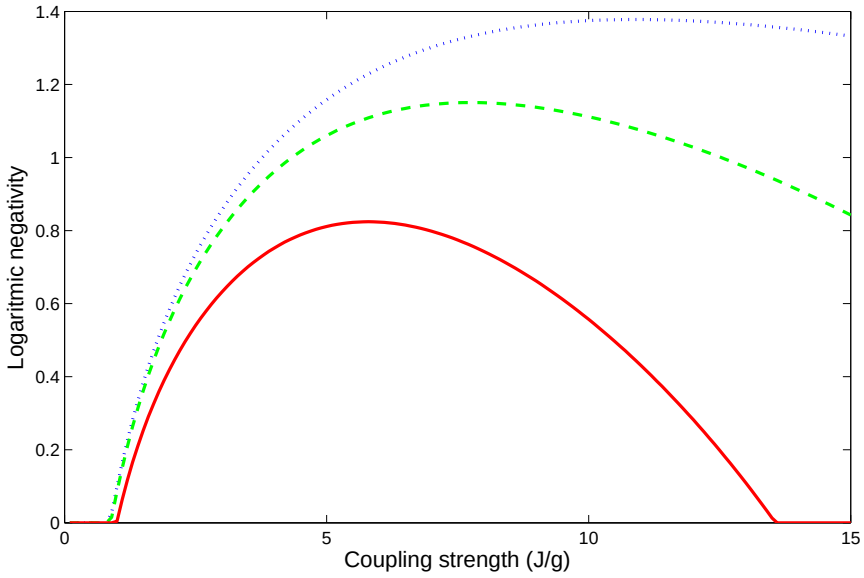

Figure 3.3: The figure shows how the entanglement between the nuclei of the dopant spins of a dimer, as quantified by the logarithmic negativity, varies with the relative strength of the inter-fullerene spin-spin coupling J of the electrons and the intra-fullerene coupling g of the electronic and nuclear spins. The plots are at a temperatures $T \sim 0.25g$ (red bold), $T \sim 0.15g$ (green dashed), $T \sim 0.08g$ (blue dotted). This figure shows that there is an optimal value for the J/g ratio at which the entanglement is maximal and that this value shifts lower J/g as the temperature is raised.

3.3 Entanglement as quantified by logarithmic negativity

As mentioned above, as the nuclear spins of our Hamiltonian (3.1) are spin-1 objects each, the negativity (and logarithmic negativity) are the only available and suitable measure that can be used to quantify their entanglement. Here we numerically diagonalized the system of 4 spins in a dimer, two spin-3/2 electronic spins and two spin-1 nuclear spins, coupled by the Hamiltonian (3.1) and obtained their ground and thermal states at low temperatures. From this the state of the two electronic spins were traced out, to obtain the reduced density matrix of the nuclear spins (we once again draw attention to the fact that the nuclear spins do not have any *direct* interaction with each other). The logarithmic negativity of the state of two nuclear spins was then calculated. The results for various values of the relevant parameters are shown in a series of figures (3.2,3.3). We see from the zero temperature case of Fig.3.2 that the entanglement remains zero till it sharply starts rising around the point $J/g \sim 1$ (more precisely, in the numerical resolution of the spacing of our points, it becomes non-zero and takes a sharp upward turn slightly above 0.9). Around $J/g \sim 9 - 10$, it starts to flatten out and reach its asymptotic value of $\log_2 3 \sim 1.585$. This proves that the nuclear qutrits go to a maximally entangled pure state at zero temperature for sufficiently large value of J/g. Clearly zero temperature is physically not possible in an experiment, so one must study the entanglement of thermal states. In finite temperatures the behaviour is as follows, there is a rise in the entanglement and afer a certain value of J/g, smaller with temperature, it will decrease until there is no entanglement. We also see that it achieves a lower value of maximum entanglement and that the peak (position of optimal J/g for highest entanglement) position shifts to lower values of J/g. These thermal state behaviour is evident from Fig.3.3.

3.4 Behaviour under the presence of an external magnetic field

It is known that the initialization of the computations can be controlled by the application of external magnetic fields. We discuss in this section how the logarithmic negativity is going to depend on the intensity of an external magnetic field of uniform magnitude in the z direction. Noting the important fact that the nuclear gyromagnetic ratio is about $\sim 10^{-5}$ times smaller than the electronic gyromagnetic ratio, the external magnetic field will effectively not be seen

by the nuclear spins (or more precisely, can always be neglected in comparison to the term coupling the magnetic field to the electronic spins), the Hamiltonian of the system will be

$$H = g\vec{I}_1 \cdot \vec{S}_1 + J\vec{S}_1 \cdot \vec{S}_2 + g\vec{S}_2 \cdot \vec{I}_2 + \sum_i^{1,2} B_{ext,z} S_{i,z}. \tag{3.2}$$

In the above, $B_{ext,z}$ is the intensity of the external magnetic field in the z direction. Firstly, it is worth pointing out that for values of $B_{ext,z}$ an order of magnitude lower than g, *no effect* is seen on the entanglement – we have therefore not plotted the entanglement for such values of $B_{ext,z}$ (the plot is identical to that of $B_{ext,z} = 0$). Fig.3.4 (b) illustrates the behaviour in an external field of high magnitude (comparable to the highest values of J/g that we take). We see interesting non-trivial behaviour here, namely the fact that the entanglement has three peaks with intermediate points were it vanishes as J/g is increased from 0 to its maximum value of $J/g \sim 30$. Peak values are lower in the presence of the magnetic field. Immediately to the left of Fig.3.4 (b), in Fig.3.4 (a) we have plotted the entanglement in absence of a magnetic field for ease of comparison. We see that while the peak of the entanglement decreases in a high magnetic field there is also a beneficial aspect of having a strong magnetic field in the sense the a high entanglement can be made to appear at a value of J/g at which there is no entanglement in the absence of a magnetic field. This gives the magnetic field as an extra handle to control the entanglement in a given region of J/g. This is nontrivial because we normally associate magnetic field with alignment and thereby the decrease of entanglement. The apperance of entanglement due to an external magnetic field where there was none it is quite interesting. We next proceed to the explanation of our results.

3.5 Discussions and Explanations

We now discuss the interpretation of our results. At zero temperature (Fig.3.2) one sees that entanglement (as quantified by the logarithmic negativity) remains low till a threshold value of the coupling after which it takes a sharp upward turn, quickly achieves an asymptotic value of about $\log_2 3$ and then stays constant. This behavior can be explained in terms of entanglement monogamy. Basically the isotropic Heisenberg interaction demands that the ground state of the system be a singlet (a state with a total spin of zero). When g dominates (i.e., is much larger than J), each of the electron-nuclear pair try to form a singlet-like maximally entangled state, but they cannot because a spin-1 and a spin-3/2 together make a spin-1/2. For any non-vanishing but small g, the effective spin-1/2 moments of these two nuclear-electronic pairs will combine to form a singlet. This state has no entanglement between the nuclear spins. When the couplings J

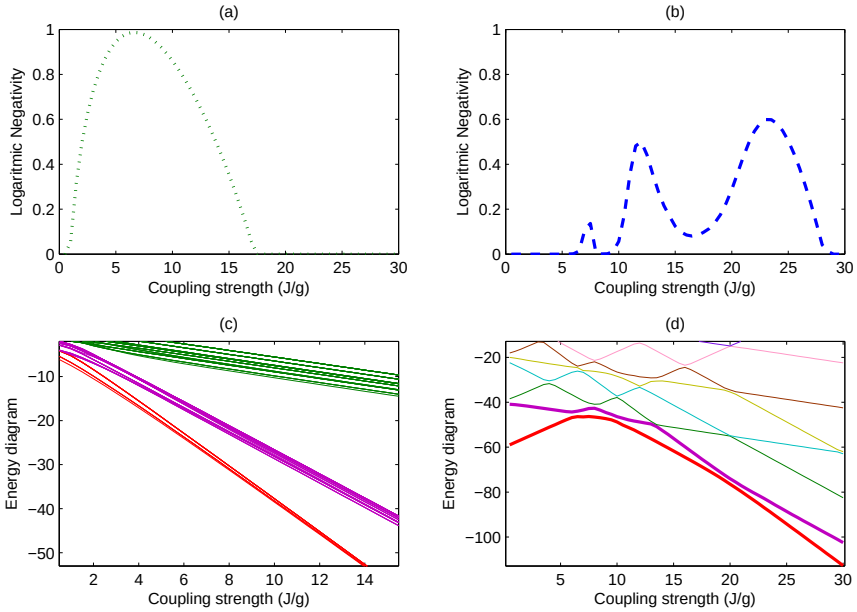

Figure 3.4: These are the plots of the behaviour of the system due to the addition of a uniform external magnetic field B and energy level plots to explain the behaviours. In figure (a) B=0, and in figure (b) B=20g, while figures (c) and (d) show the energy levels for the magnetic fields $B = 0$ and $B = 20g$ respectively. We see that a magnetic field of high enough magnitude can induce a break up of the peaks of the logarithmic negativity. The temperature for this figure is set to $T = 0.2g$.

and g are comparable, the complicated singlet state involves all the 4 spins and in general there is a low amount of entanglement between any pair of spins. However, the situation becomes simpler and interesting when the coupling between the two electronic spins (J) becomes much stronger than g. The electronic spins ($3/2$) form their own singlet and then the two nuclear spins *have to* form their own singlet with each other in order for the total 4 spin state to have a vanishing spin moment. This is a manifestation of *entanglement monogamy* in the same sense as that used in the literature of ground state long distance entanglement [32]. The central electronic spins, having used up all their entangling ability due to their entanglement with each other for large J, cannot entangle with the nuclei any more – so despite not interacting, the nuclei form a singlet with each other. For large enough J/g, the ground state is nearly a product state, of the electron-pair state and the nuclear-pair state. The nuclear-pair in this state is effectively in the state $|\psi^-_{3\times 3}\rangle = \frac{1}{\sqrt{3}}(|+1,-1\rangle - |0,0\rangle + |-1,+1\rangle)$. As J/g increases from a small value, the proportion of $|\psi^-_{3\times 3}\rangle$ in the state increases till it reaches a threshold after which the entanglement, as quantified by the logarithmic negativity becomes non-zero. After a certain large J/g, when the nuclear spins in the ground state go to the state $|\psi^-_{3\times 3}\rangle$, their logarithmic negativity reaches the maximum value of $\log_2 3$. As this always remains the ground state even when $J/g \to \infty$, we see (Fig.3.2) that the zero temperature entanglement saturates. However, as J/g increases, the gap between the states with a nuclear singlet and a nuclear triplet decreases. This is understood from the energy level diagram of Fig.3.4(c) where we can see the lowest states (red lines in colour) come closer and closer as J/g increases (they end up coinciding with each other to our degree of resolution). Thereby, for any thermal state, depending on the temperature, which populates the nuclear state with a proportion of the nuclear triplet, the mixing of the nuclear singlet and triplet causes the entanglement to degrade. Thereby there is an optimum J/g at which the entanglement is highest for each temperature. The rise of the entanglement is halted earlier for higher temperatures because of the increase in proportion of the excited states. Thus the optimum J/g value for the highest entanglement shifts to the left with temperature. The behaviour of entanglement in the thermal states has similarities with earlier investigations on two Heisenberg coupled spin-1/2 particles [33]. However, the work reported here is somewhat more counter-intuitive as the nuclear spins whose entanglement we are interested in are not directly coupled to each other.

The three peaked structure of entanglement in the presence of a strong magnetic field is more interesting and also more intricate to explain. We again appeal to an energy-level diagram (Fig.3.4(d)) in the presence of a strong magnetic field of $20g$. As the J/g is increased, we see

that there are multiple avoided crossings. The ground state for small J/g, is a non-entangled state as the magnetic field aligns the electronic spins and effectively the nuclear spins have to anti-align with them to reduce energy – resulting in a lowly entangled state. As J/g increases, we see that the energy of this state (red line in colour) increases till it has an avoided crossing with another state (purple line in colour) at $J/g \sim 7$ and changes it qualitative nature (i.e., becomes an entangled state with finite entanglement between the nuclear spins). We see that its energy separation from its next upper state continues to increase till about $J/g \sim 8$, which is the domain over which the entanglement in the thermal state grows because of increasing purity. However, the first excited state (purple line) itself undergoes an avoided crossing with a second excited state (green line) and starts coming down in energy again for J/g between 8 and 9, which causes the entanglement to decrease due to mixing. After this avoided crossing at $J/g \sim 9$, the ground state again changes its qualitative character, but is still an entangled state, at least as far as the state of the nuclear spins are concerned. The gap with the first excited state is also on the increase till $J/g \sim 12$, after which the first excited state (purple line) undergoes another avoided crossing and starts coming down, decreasing entanglement due to increasing mixedness, reaching a minimum for $J/g \sim 16 - 17$. Finally, between $J/g \sim 17 - 20$ the ground state has another avoided crossing, changes character to the state $|\psi^{-}_{3\times 3}\rangle$, which no other state can overtake as the ground state any more by increasing J/g. However, as in the case for $B_{ext} = 0$, the gap of this state from its nearest excited states decreases also with J/g making the entanglement in any thermal state eventually going to zero with increasing J/g. This explanation is not visible in Fig.3.4(d) because of the resolution in which we work (to show clearly enough those excited states in the energy level diagram which take part in all those avoided crossings that have been relevant to our explanation so far). In fact, what we have been referring to as a the ground state so far (the red line) is a group of states, with the lowest being the actual ground state. Within this group, the states come too close to each other for large J/g exactly in the same manner as the $B_{ext} = 0$ case. In a nutshell, the J/g has to compete with the B_{ext} to set up entanglement and thereby with stronger B_{ext} we need higher J/g to have entanglement. However, not only this, higher B_{ext} also create some splitting between the states to enable one to have entanglement in a thermal state at higher J/g.

3.6 Witnesses and detection

Finally some comments regarding what is required to test our findings are in order. There seems to be no alternative but to use some sort of measurements of single spins. Yet these

measurements have to be fast in comparison to all coupling strengths J and g of the system so that no time evolution occurs Let us now justify, following Ref.[36], that indeed $\langle \vec{I}_1.\vec{I}_2 \rangle$ serves to form an entanglement witness. Note the following simple algebra that for pure product states

$$\begin{aligned} |\langle \vec{I}_1.\vec{I}_2 \rangle| &= |\langle I_{1x}\rangle\langle I_{2x}\rangle + \langle I_{1y}\rangle\langle I_{2y}\rangle + \langle I_{1z}\rangle\langle I_{2z}\rangle| \\ &\leq \sqrt{\langle I_{1x}\rangle^2 + \langle I_{1y}\rangle^2 + \langle I_{1z}\rangle^2}\sqrt{\langle I_{2x}\rangle^2 + \langle I_{2y}\rangle^2 + \langle I_{2z}\rangle^2} \\ &\leq 1, \end{aligned}$$

where the penultimate line follows from the Cauchy-Schwarz inequality and the last line follows from the property of spin-1 systems (whichever direction a spin is pointing, if it is a pure spin state, one can take it arbitrarily as the $+z$ axis with $\langle I_{2z}\rangle^2 = 1$, and from symmetry $\langle I_{1y}\rangle^2$ and $\langle I_{1z}\rangle^2$ is zero). The above inequality continues to hold for any convex sum of product states and thereby for all separable states. Thus we can use $W = \max\{0, |\langle \vec{I}_1.\vec{I}_2 \rangle| - 1\}$ as an entanglement witness with any nonvanishing value of this witness signalling an entanglement in the nuclear 3×3 system. We have thereby plotted in Fig.3.5 the witnesses and logarithmic negativities in the same plot for two values of temperature. We see that for high enough J/g, there is a region at which the logarithmic negativity becomes zero, but the inseparability witness W does not. This implies that for these regions of J/g, for the 3×3 system, we have an example of what is called bound entanglement [37], which has caused a significant interest in the literature – ours is an example of a state going from a unbound to bound entangled state with the increase of effective thermal mixing (with increasing J/g).

3.7 Conclusions

In this chapter, we studied the entanglement that arises in a dimer of two fullerenes. We studied the case were the nuclear spin of a Nitrogen inside a fullerene is taken as a qubit that will effectively interact with another similar qubit in a neighbouring fullerene indirectly via the surrounding electron spins. We start modeling the system using a Heinsenberg Hamiltonian. We then study the entanglement using the logarithmic negativity. First, we start to explore the ground state entanglement between the two nuclei by tracing out the electronic spins. We find out how this depends on the ratio of coupling strengths between the nuclear-electron spin interaction and the electron-electron interaction. We find that this entanglement is larger for larger electron-electron coupling. Later we study the same entanglement in the thermal state finding that due to the decreasing gap between the energy levels, as the ratio J/g is increased, the entanglement is goes down to zero after an optimum maximum value of J/g. It is interesting that an

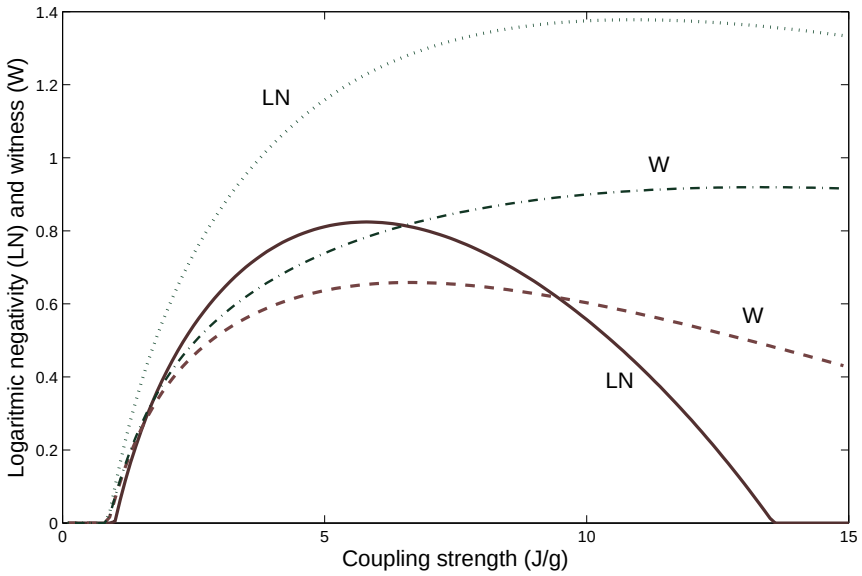

Figure 3.5: The figure depicts the value of the witness W used to detect the entangled nature of the state of the two nuclear spins, plotted in the same figure alongside the logarithmic negativity for two different temperatures. A non-zero value of the witness W that we have an inseparable state of the nuclear spins. For $T = 0.25g$ the bold brown line (with LN symbol) is the logarithmic negativity, while the dashed brown line is the corresponding entanglement witness W. For $T = 0.08g$ the dotted black line (with LN symbol) is the logarithmic negativity, while the dot-dashed black line is the corresponding entanglement witness W. This figure highlights the twin facts that while the entanglement can be detected by a simple witness, it can remain non-zero even when logarithmic negativity vanishes, thereby detecting bound entanglement between the nuclear spins.

external $\vec{B}$ changes the optimum value of J/g in which the maximum amount of entanglement is obtained. At last we compare two ways to measure the entanglement, the logarithmic negativity and a witness defined using the spins. These together allow us to identify the parameter domains where bound and free entanglement are present between the nuclei in the dimers.

Chapter 4

Coherent extraction of Singlets for Quantum Dots

As discussed in the introduction, the entanglement between distinct systems is a useful resource in quantum information processing. We have discussed earlier that spin qubits in quantum dots can be entangled by a quantum gate induced by their exchange interaction. However, the time scale for the exchange interaction to accomplish a gate is usually much longer than the tunneling time of electrons from one quantum dot to another. Thus if two quantum dots (QDs) could be entangled by a mechanism where tunneling plays a key role then this could potentially be faster. It is important to note, however, that incoherent tunneling between quantum dots will occur at random times, and that it is a problem because it is not being deterministic so will not be possible to know at what times will happen. Thereby a mechanism to entangle two quantum dots that uses *coherent tunneling* is potentially quite interesting. In this chapter, we propose a scheme in which two quantums dots are in contact with an intermediate system (a potential well) whose ground state with a filling of two electrons is a singlet (the filling can be ensured by choosing the appropriate potential). The basic idea is then that we let the 2 dot plus central intermediary well system evolve due to the tunneling Hamiltonian so that there is coherent tunneling of the electrons from the central well to the two outer dots in a deterministic time-scale set by the tunnel coupling. We would like to ensure conditions so that there is precisely one electron in each of the outer dots after a certain time due to the time evolution. Of course, there is no evolution of their joint spin state during this process, especially in the absence of nuclear spin fluctuations in the sample (this may be the case when nuclear spins in a AlGaAs/GaAs sample have been aligned by some process [22]). Thus the two electrons, one in each dot, at the end of time evolution for a certain period, will still be in a spin singlet state. This means that we have

a situation where spins in separated quantum dots are entangled in a Bell-state, while the time taken to establish this entanglement is of the order of the coherent tunneling time, rather than the much weaker exchange coupling time.

When we started on this problem, we, in effect, wanted to use as large a well size as possible to have a significant distance between the dots to which the pair of electrons in the singlet are extracted. But such a well has very closely spaced energy levels involved in the tunneling quite a few of which can be nearly resonant with the ground energy levels of the external QDs. Thereby such a model is not going to be entirely satisfactory and we decided to change the intervening medium to a another quantum dot, perhaps of dimensions slightly larger than the outer QDs to achieve better results. We will consider at least two *qualitatively* distinct protocols which are new and compare their advantages and disadvantages with some earlier suggestions for extracting singlets by spatially separating the electrons in similar setups. In one protocol, we have a 1-D chain of three QDs, with the initial state being a singlet of electrons in the middle QD (QDC) and the ground energy level of the external dots is in resonance to the ground energy level of QDC. Here we are going to study the probability of getting the singlet in the external dots with one electron in each dot. With this view in mind, we are going to imagine charge measuring apparatus being present also in the system and can herald the success of our extraction protocol when one charge is found in each outer dot. We find that, indeed, pure coherent evolution can establish a maximally entangled state between the dots. After switching on the interaction of the outer QDs with the intervening QDC, the system will evolve until we have the maximum probability of the maximally entangled singlet state in the external quantum dots. However, here we found the maximum probability to not be very high, though significant, and thereby we also considered the case where the two outer QDs to be very narrow, so that the Coulomb repulsion is very high, and we find that the probability of obtaining a maximally entangled state successfully by a similar protocol can be made very high. Moreover the charge measurement can be simplified to measuring the presence or absence of charge in QDC only and no simultaneous measurements are needed on the outer QDs as required in the case without high repulsion in the outer QDs (the high repulsion itself guarantees that there is no more than one charge in any of the outer QDs).

Another different protocol, that requires more adjustment of parameters requires breaking the left-right symmetry of the problem, as well as adjusting carefully the repulsion between electrons in two separate quantum dots. However, even this protocol is based on coherent tunneling, and thereby as fast as the previous one. We will also look at the robustness of our

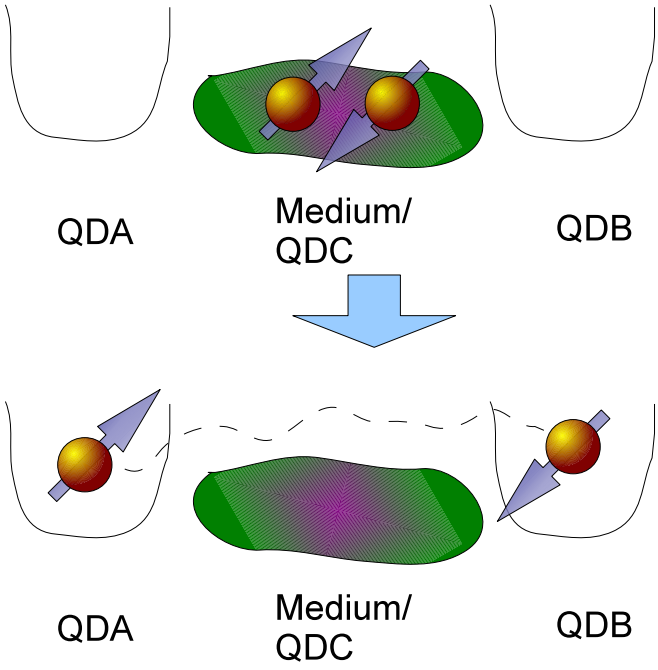

Figure 4.1: The setup considered in this chapter for the extraction of a spin entangled state in two outer dots QDA and QDB from a singlet in an intermediate dot QDC. The blue arrow denotes the coherent time evolution from the upper configuration to the lower configuration. The spin state of the electrons is unaffected (i.e., remain in the singlet) for the entire process.

suggested schemes with respect to deviations of the system from ideal settings. Before proceeding to the details of this chapter, it is worth pointing out that we worked on a *modification* of the second protocol of this chapter (the one which the left-right symmetry and requires careful parameter adjustment) with other colleagues on connecting the two dots to different leads and thereby allowing a current of entangled pairs of electrons going out of the system as long as there is another lead connected to QDC supplying it with electrons, which has been published [38] (the contribution of the lead author of that paper was in the context of the entangled currents, rather than the coherent evolution, which is the central mechanism studied in this chapter – indeed that other work, by involving the incoherent tunneling to leads, make the evolution a more complicated combination of coherent evolutions interrupted at random times by incoherent tunnelings).

4.1 Setup

Fig. 4.1 shows the scheme we have in mind. It is composed by two outer quantums dots (QDA and QDB) and an intervening medium (quantum dot QDC) which has two electrons. Tunneling between the QDA and QDB and the intervenium medium QDC allow hopping of electrons between the different QDs. Thanks to this it is possible that the two electrons are located in the external QDs in an entangled state. Our aim is to successfully establish the entanglement between the two external quantum dots with as high a probability as possible. Our initial state consists of two electrons in a singlet state in the intervening medium QDC and the QDs QDA and QDB being empty. If we assume that the Hubbard Hamiltonian governs the system, the electrons will occupy the nine different configurations available:

$$\begin{aligned}\{&d^\dagger_{\mathrm{B}\uparrow}d^\dagger_{\mathrm{B}\downarrow}|0\rangle, d^\dagger_{\mathrm{A}\uparrow}d^\dagger_{\mathrm{B}\downarrow}|0\rangle, d^\dagger_{\mathrm{C}\uparrow}d^\dagger_{\mathrm{B}\downarrow}|0\rangle, d^\dagger_{\mathrm{A}\downarrow}d^\dagger_{\mathrm{B}\uparrow}|0\rangle, d^\dagger_{\mathrm{C}\downarrow}d^\dagger_{\mathrm{B}\uparrow}|0\rangle,\\ &d^\dagger_{\mathrm{A}\uparrow}d^\dagger_{\mathrm{C}\downarrow}|0\rangle, d^\dagger_{\mathrm{A}\downarrow}d^\dagger_{\mathrm{C}\uparrow}|0\rangle, d^\dagger_{\mathrm{A}\uparrow}d^\dagger_{\mathrm{A}\downarrow}|0\rangle, d^\dagger_{\mathrm{C}\uparrow}d^\dagger_{\mathrm{C}\downarrow}|0\rangle\}\end{aligned} \tag{4.1}$$

where $d^\dagger_{i\sigma}$ creates and $d_{i\sigma}$ annihilates an electron at the ith dot in the spin state σ. The Hamiltonian can be written as

$$\begin{aligned}H = &\sum_{\sigma,i,\alpha} E_{i,\alpha} d^\dagger_{i\sigma} d_{i\sigma} + \sum_{\sigma,i,j,i\neq j} t_{ij} d^\dagger_{i\sigma} d_{j\sigma}\\ &+ \sum_i U_i n_{i\downarrow} n_{i\uparrow} + \frac{1}{2}\sum_{i,j,i\neq j} V_{ij}\varrho_i\varrho_j,\end{aligned} \tag{4.2}$$

where in the sums $i, j \in A, B, C$ and $\sigma \in \uparrow, \downarrow$, $n_{i\sigma} = d^\dagger_{i\sigma} d_{i\sigma}$, $\varrho_i = n_{i\downarrow} + n_{i\uparrow}$ and $E_{i,\alpha}$ is the αth energy level of the ith dot. In writing the above Hamiltonian, we have implicitly assumed that t_{ij} does not depend on the energy level α of the quantum dots as this assumption will be true for the regimes we will consider, namely that either (a) there is only one energy level in each quantum dot at the relevant scale of energy of our dynamics, or (b) the central wider dot has multiple closely placed energy levels while the outer ones have exactly one energy level each (the closeness of energy here makes t_{ij} very similar). The meaning of the various parameters in Eq.(4.2) is pictorially depicted in Fig.4.2. When the system evolves with this Hamiltonian for a while (starting in the initial state of a singlet in QDC, i.e., $d^\dagger_{\mathrm{C}\uparrow}d^\dagger_{\mathrm{C}\downarrow}|0\rangle$, at any instant of time, if we want to ensure that the electrons are in the external quantum dots, we will need at least two measurements of charge, one per external quantum dot. This means that we will have a charge detector in each external quantum dot. Due to fact that we are projecting charge, we are not breaking the spin entanglement. So when exactly one electron is detected in each dot, the quantum state is projected to the singlet state $|\Psi^-\rangle_{AB} = \frac{1}{\sqrt{2}}(d^\dagger_{\mathrm{A}\uparrow}d^\dagger_{\mathrm{B}\downarrow} - d^\dagger_{\mathrm{A}\downarrow}d^\dagger_{\mathrm{B}\uparrow})|0\rangle$.

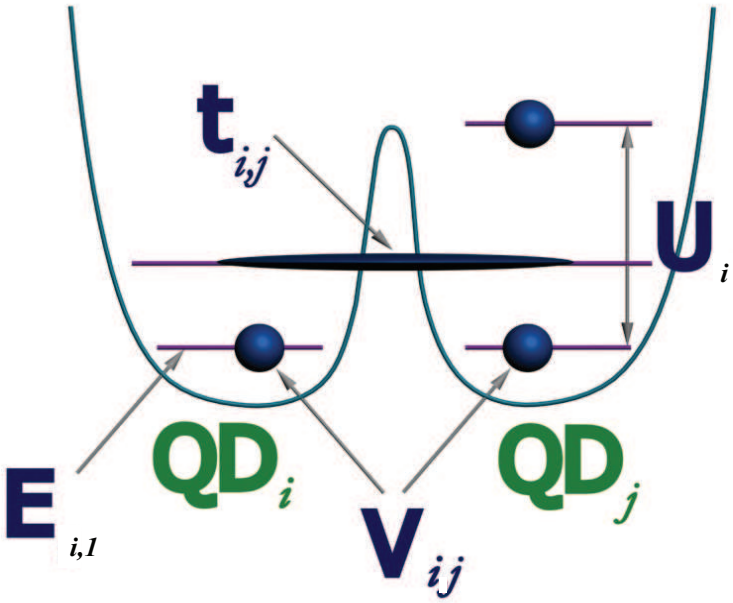

Figure 4.2: The parameters of the Hubbard model describing two tunnel coupled quantum dots.

At first, we are going to examine what happens to the simplest model that is three quantum dots with one energy level in each quantum dot. We will neglect the Coulomb blockade (i.e. assume that *all* three dots are quite large so that U_i are negligible) and assume that the energies of the quantum dots are in resonance. Thereby the conditions we set on the parameters of H in Eq.(4.2) are

$$E_A = E_B = E_C, E_N + E_M = E_{NM} N, M = A, B, C,\ U_i = 0,\ V_{ij} = 0,\ t_{ij} = t. \quad (4.3)$$

With the above parameters the Hamiltonian of the system is (in the basis of 9 states stated above):

$$H_{\text{Protocol 1}} = \begin{pmatrix} E_{BB} & -t & -t & t & t & 0 & 0 & 0 & 0 \\ -t & E_{AB} & 0 & 0 & 0 & -t & 0 & -t & 0 \\ -t & 0 & E_{CB} & 0 & 0 & 0 & t & 0 & -t \\ t & 0 & 0 & E_{AB} & 0 & 0 & -t & t & 0 \\ t & 0 & 0 & 0 & E_{CB} & t & 0 & 0 & t \\ 0 & -t & 0 & 0 & t & E_{AC} & 0 & 0 & 0 \\ 0 & 0 & t & -t & 0 & 0 & E_{AC} & 0 & 0 \\ 0 & -t & 0 & t & 0 & 0 & 0 & E_{AA} & 0 \\ 0 & 0 & -t & 0 & t & 0 & 0 & 0 & E_{CC} \end{pmatrix}.$$

Note that in the above Hamiltonian, some terms emerge as $-t$ by virtue of the commutation relations of the Fermi operators $d^\dagger_{i\sigma}$.

The time evolution of the initial state $d^\dagger_{\text{C}\uparrow} d^\dagger_{\text{C}\downarrow}|0\rangle$ under the above Hamiltonian can then be easily calculated so that, on measurement after an interval of time τ after the time evolution has started, the probability of finding a singlet in the outer dots is given by

$$P_{\text{success, Protocol 1}}(\tau) = \frac{1}{2}\sin^4\sqrt{2}t\tau. \quad (4.4)$$

We see that Eq.(4.4) implies that at regular intervals of time i.e., at $\tau = (2m+1)\frac{\pi}{\sqrt{2}t}$, where m is an integer, the probability of successfully finding two electrons, one each in A and B in a singlet state is 0.5. This probability is quite significant, however, it leaves considerable scope for improvement. Note that it is a *conditional scheme* – so that we can essentially throw away the cases when the scheme has failed and keep only those cases in which an electron was detected in each of the outer dots A and B. In these cases which are kept, the state of the electrons in the outer dots is a perfect singlet, at least in the absence of sources of spin decoherence.

We are now going to examine the possibility of improving the above probability and analyse the case in which the extenal quantum QDs have a strong repulsion. Our aim is to increase

the probability as much as possible. We are going to do that by changing some of the properties of the system. We are going to see what happens if we consider the external quantum dots being so narrow, that only one electron is allowed to stay in each QD. Finding two electrons in the external QDs can be neglected. In other words, we consider another regime of parameters in which we have a very high Coulomb repulsion in the outer quantum dots. The simple motivation is to reduce the probability of double occupancy of the outer quantum dots. This reduction of the possible state space is schematically depicted in Fig.4.3. This has the advantage that now the need of charge detection can be exclusively shifted to the central dot C. Not finding any electrons in C is equivalent to finding one each in A and B, as neither A, nor B, can be doubly occupied by virtue of the large associated energy cost. The parameter regime is given by

$$E_A = E_B = E_C = E,\ t_{ij} = t,\ U_C = 0,\ U_A = U_B = U >> E_j, t, t^2\ V_{ij} = 0. \tag{4.5}$$

In the basis

$$\begin{gathered}\{d^\dagger_{\mathrm{C}\uparrow} d^\dagger_{\mathrm{C}\downarrow}|0\rangle, d^\dagger_{\mathrm{A}\uparrow} d^\dagger_{\mathrm{C}\downarrow}|0\rangle, d^\dagger_{\mathrm{B}\uparrow} d^\dagger_{\mathrm{C}\downarrow}|0\rangle, d^\dagger_{\mathrm{A}\downarrow} d^\dagger_{\mathrm{C}\uparrow}|0\rangle, d^\dagger_{\mathrm{B}\downarrow} d^\dagger_{\mathrm{C}\uparrow}|0\rangle, \\ d^\dagger_{\mathrm{A}\uparrow} d^\dagger_{\mathrm{B}\downarrow}|0\rangle, d^\dagger_{\mathrm{A}\downarrow} d^\dagger_{\mathrm{B}\uparrow}|0\rangle, d^\dagger_{\mathrm{A}\uparrow} d^\dagger_{\mathrm{A}\downarrow}|0\rangle, d^\dagger_{\mathrm{B}\uparrow} d^\dagger_{\mathrm{B}\downarrow}|0\rangle\}\end{gathered} \tag{4.6}$$

$$H_{\text{Protocol 2}} = \left(\begin{array}{ccccccc|cc} 2E & -t & -t & t & t & 0 & 0 & 0 & 0 \\ -t & 2E & 0 & 0 & 0 & -t & 0 & -t & 0 \\ -t & 0 & 2E & 0 & 0 & 0 & t & 0 & -t \\ t & 0 & 0 & 2E & 0 & 0 & -t & t & 0 \\ t & 0 & 0 & 0 & 2E & t & 0 & 0 & t \\ 0 & -t & 0 & 0 & t & 2E & 0 & 0 & 0 \\ 0 & 0 & t & -t & 0 & 0 & 2E & 0 & 0 \\ \hline 0 & -t & 0 & t & 0 & 0 & 0 & 2E+U & 0 \\ 0 & 0 & -t & 0 & t & 0 & 0 & 0 & 2E+U \end{array}\right) \tag{4.7}$$

As $U >> E_j, t$, we can adiabatically eliminate the doubly occupied states (by the method as described in Chapter 1, Section 1.9) to have an effective 7×7 Hamiltonian given by

$$H_{\text{eff, Protocol 2}} = \begin{pmatrix} 0 & -t & -t & t & t & 0 & 0 \\ -t & \frac{t^2}{U} & 0 & -\frac{t^2}{U} & 0 & -t & 0 \\ -t & 0 & \frac{t^2}{U} & 0 & -\frac{t^2}{U} & 0 & t \\ t & -\frac{t^2}{U} & 0 & \frac{t^2}{U} & 0 & 0 & -t \\ t & 0 & -\frac{t^2}{U} & 0 & \frac{t^2}{U} & t & 0 \\ 0 & -t & 0 & 0 & t & 0 & 0 \\ 0 & 0 & t & -t & 0 & 0 & 0 \end{pmatrix} \tag{4.8}$$

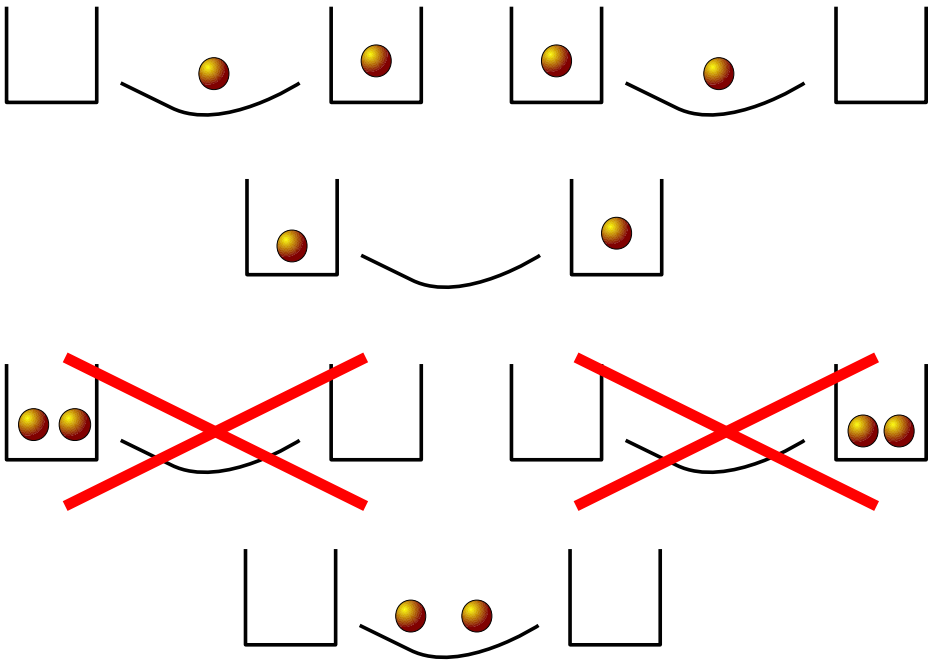

Figure 4.3: The states that get eliminated from the Hamiltonian when there is a high repulsion in the outer dots are depicted in this figure.

We will neglect the terms of $\frac{t^2}{U}$ as the U is very large compared to t^2 to obtain an analytic expression for the probability of extraction of singlets by virtue of H_{eff}. This turns out to be

$$P_{\text{success, Protocol 2}}(\tau) = \frac{8}{9}\sin^4\sqrt{\frac{3}{2}}t\tau. \tag{4.9}$$

Thus the probability of success in this case is improved to $8/9$, though the time scale to reach the highest probability is only a factor of ~ 1.15 higher, and again, this is a periodic plot. We also numerically simulate the full Hamiltonian $H_{\text{Protocol 2}}$, but this time with a finite, but high repulsion in the external quantum dots with $U \sim 10t,\ E_j = t = 1$. Results are plotted in Fig.4.4. It is easy to see that it is much better than our previous scheme (protocol 1) and the result we get is nearly the probability of 8/9, which matches with the theoretical limit obtained analytically after adiabatic elimination. Note that here it is legitimate to neglect $\frac{t^2}{U}$ though in the usual form of quantum computation this is precisely the term that plays the most important role – it is the spin exchange coupling J. Here the dynamics takes place through tunneling and thereby only t is important and the spin states do not evolve. Thereby the spin exchange J is unimportant. This highlights the difference of the scheme we are presenting with the usual quantum dot based quantum computation protocols.

It is important to study the case in which the central dot is wider (which is commensurate with our original aim of having entanglement betwee distant quantum dots A and B), how the probability of successful extraction is affected. As dots are made wider, multiple levels will become nearly resonant with the outer dots ground energy level. If we take two such levels to be nearly resonant with a gap of Δ, i.e., $E_C \pm \Delta \approx E_A, E_B$ (still considering the case of high U in the external dots) then we find that the probability is reduced. As the gap Δ vanishes, the probability in this case is maximized to the value of 0.224 in the limiting case (this means that there are two closely placed nearly resonant levels in the central dot, but only one of them is occupied with the singlet initially). Adding a further (third) level we find that the probability is 0.1047 in the limiting case when all the three levels are nearly resonant. When there are N such levels, our numerics indicate that the probability falls as $\frac{1}{N^2}$ of the original probability with exactly one resonant level. As our original motivation had been to have the entangled particles as far as possible, we want to increase the size of the intervenium medium. Analyzing it a bit further we decide to add on two wells, one in each side of the central quantum dot. Having all these dots in resonance, in addition to the high repulsion in the outer dots we obtain a maximum probability of 0.246.

We now proceed to discuss Protocol 3 which requires more adjustment of parameters – however its aim is to improve the probability further. Protocol 3 was combined with extraction

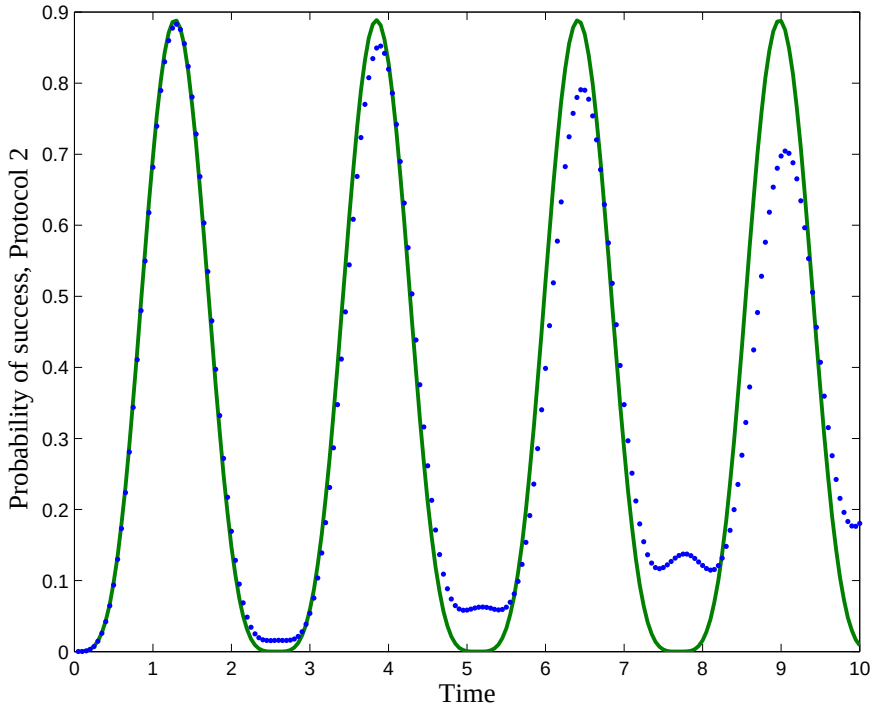

Figure 4.4: The probability of success, i.e, the probability of extracting a singlet to the outer dots of the triple dot system in our protocol 2 (when the repulsion in the outer dots is high). The solid curve shows the analytic expression under the assumption of $U >> t, E_j$, while the dotted curve plots the same numerically for $U = 10t, 10E_j$. We see that in both cases the probability of success reaches quite high $\sim \frac{8}{9}$.

on to leads to obtain a current of entangled electrons in Ref.[38] (in which both the author of this thesis and the lead author played important roles). However a delicate adjustment of parameters is required for this Protocol 3, unlike the previous protocols. We will do a completely independent presentation here as, unlike the published paper, we are not interested in the extraction to leads. We require

$$t_{CB} = t_{CA}/\sqrt{2} = t, E_A = E_B = E_C = E, t << U_C = V_{CB} = V_{AB} << V_{AC}. \quad (4.10)$$

While the above parameters seem difficult to achieve, we have depicted a configuration and size of dots in Fig.4.5 under which the above seems feasible. Basically, the central wider dot C would have the dot A close to its centre so that V_{AC} is large. Moreoever the width of the central dot and distances between the dots can be so adjusted that the electrostatic repulsions are same for the configurations of two electrons in C, one each in C and B, and one each in A and B. By the same placement, one can make the tunneling between C and A stronger than the tunneling between C and B. Under the above parameters, we equalize the energies of the two electrons being in C (energy $\sim 2E_C + U_C$) with one electron each in C and B (energy $\sim E_C + E_B + V_{CB}$) and with one electron each in A and B (energy $\sim E_A + E_B + V_{AB}$). But we prohibit the chance of an electron each to go to C and A as V_{AC} is so large (this configuration is completely off resonant with the other three configurations). Additionally important is the fact, also depicted in Fig.4.5 in terms of double arrows, is that the system cannot directly go from the configuration of two electrons in C to one each in A and B – it has to pass through the intermediate configuration of one each in C and B. Thereby the dynamics of the system can be seen from the simplified effective Hamiltonian

$$H_{\text{eff, Protocol 3}} = \begin{pmatrix} 0 & \sqrt{2}t & 0 \\ \sqrt{2}t & 0 & \sqrt{2}t \\ 0 & \sqrt{2}t & 0 \end{pmatrix}, \quad (4.11)$$

where the basis is the occupancy basis CC, CB and AB, where ij means one electron in dot i and the other electron in dot j. Note that spin states are not changed at all in our protocol, and thereby, the above is a valid way of solving for the problem – the matrix element $\sqrt{2}t$ in the upper 2×2 sector of $H_{\text{eff, Protocol 3}}$ stems from the fact that either of two electrons can tunnel to generate the configuration CB from CC. As only one electron can tunnel to go from CB to AB, there we had to explicitly choose the tunneling constant t to be larger by a factor of $\sqrt{2}$. For this 3×3 Hamiltonian, the time required the spin singlet state to be extracted to the dots A and B is then simply the time required to get to AB starting from the initial state CC. The

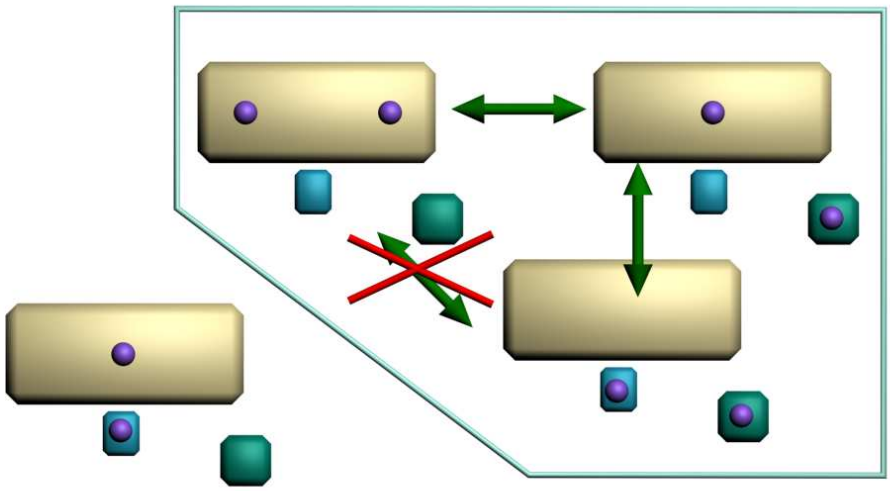

Figure 4.5: The placement and relative size of dots to obtain the parameters of Protocol 3.

probability for this to happen as a function of time τ is given by

$$P_{\text{success, Protocol 3}}(\tau) = \sin^4 t\tau. \tag{4.12}$$

As we can see from Eq.(4.12) the Probability of successful extraction now reaches unity periodically, though the time needed to reach it is larger by a factor of 1.5. Given that faster quantum operations are always desirable in view of decoherence, one cannot immediately however conclude that this protocol is better than our Protocol 2 which had a $8/9$ probability of success. To indeed check this heuristically, one can do an order of estimate check of the relevant decoherence. Firstly, the decoherence due to the nuclear spin bath is negligible in comparison to the tunnel coupling (10 GHz [18]). On the other hand the decoeherence of the charge oscillation (between dots), which is the main ingredient of our protocol, has some effect on the maximum probability achievable. Assuming that the maximum probability achievable is damped by a factor of $\exp(-\Gamma\tau)$ were Γ is the decoherence rate due to charge oscillations, and given the charge decoherences in these regimes have been known to be adequately by $\Gamma \sim 1$ GHz [24]), we can predict that the success probability of Protocol 3 of $\exp(-0.15)$ is going to exceed that of Protocol 2 of about $(8/9)\exp(-0.1)$, though both are still above 80%.

4.2 Comparison to Previous Protocols

There have been, to our knowledge, three related works on extraction of entanglement from singlets. The first one, by Yamamoto et al. [39] propose a system involving only a single quantum dot, but surrounded by and connected to three leads. One of the leads is the source of electrons and its energy level matches the average energy of the two remaining leads, which we call the output leads. Both of the output leads are located opposite to the source lead. The energy of the quantum dot is larger than the individual energy of each lead. Due to the energy matching, when the electrons cross the quantum dot they have to move across in couples, one in each output lead, generating a current of entangled electrons. The role of the quantum dot is to act both as a mediator between the source lead and the two output leads, as well as a filter between them, so that only the singlet passes through. The source merely supplies pairs of electrons to the dot. Only those in a singlet are allowed to pass through the mediating dot because of the Pauli exclusion principle (energies are so matched that only one electronic level of each dot is involved). This scheme, however, involves the adiabatic elimination of the central dot resulting in a second order process in the ratio of the tunneling t and energy of the central dot $2E_C + U$, and thus is much slower than the protocols we have presented, which have a time-scale of t. However, their difference is that they have a current in the leads, which will

also intrinsically be a stochastic process as incoherent tunneling between the leads and the dot is involved.

Another scheme, perhaps closest to our setting, has been presented by Saraga and Loss [40]. They propose a system that can create spin-entangled currents with a triple quantum dot. The three dots, as in our protocols, have a coherent process going on in them, but their protocol has leads attached to all the three dots, and thereby involves incoherent tunneling as well for the spin entangled currents and this would also affect the coherent process in the triple dot system which is now no more a closed system. However, even if one adapts their protocol to a closed system there are major differences in the parameter regime in which their protocol operates and thereby their probability of success if defined in a similar manner to us. In their scheme the central quantum dot C has an energy $2E_C + U$ in our usual notation. However, importantly, for them the parameter regime for the scheme is $2E_C + U = E_A + E_B \neq E_A + E_C \neq E_B + E_C$ so that there is a resonance between CC and AB. However, CC and AB do not have a direct matrix element between them, and the system has to pass through two intermediate off-resonant configurations CA and CB, which will, again, slow down the process to the second order in the ratio of t to the energy off-resonance. Their Hamiltonian is given by (in the dot occupancy basis CC, CA, CB, AB)

$$H_{\text{Saraga-Loss}} = \begin{pmatrix} 2E_C + U & \sqrt{2}t_{CA} & \sqrt{2}t_{CB} & 0 \\ \sqrt{2}t_{CA} & E_C + E_A & 0 & t_{CB} \\ \sqrt{2}t_{CB} & 0 & E_C + E_B & t_{CA} \\ 0 & t_{CB} & t_{CA} & E_A + E_B \end{pmatrix}. \tag{4.13}$$

It is not easy to obtain an analytic expression for the probability of success (as defined before by us) and thereby we optimize over the parameters keeping them constrained as noted above. The probability of success at optimal parameters (shortest time to peak, combined with the highest probability, which turned out to be realized for $U \sim 1, E_C = U/2$) is plotted in Fig.4.6. For the convenience of the reader our protocols 2 and 3 are plotted on the same plot. We find that the Saraga-Loss protocol achieves at best a probability of success amounting to ~ 0.45, which is much lower than those of the protocols we presented here.

4.3 Conclusions

In this chapter we have achieved an important task, namely the preparation of an entangled state of two electrons on a time-scale much faster than the exchange coupling J. If one were to use the usual quantum dot based quantum computation schemes, such as that of Loss and

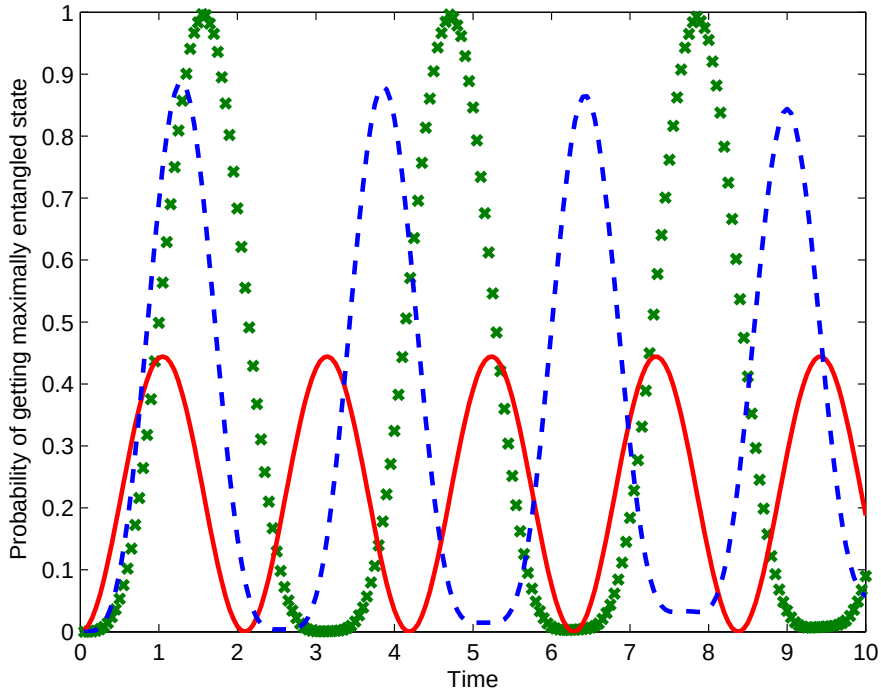

Figure 4.6: This plot compares the performance of our protocols 2 and 3 with the protocol of Saraga and Loss for the extraction of spin entangled states. The continuous (red) plot shows the probability of obtaining the singlet state in the outer dots for the Saraga-Loss protocol against time, while the dashed (blue) and starred (green) plots show the corresponding probability for our protocols 2 and 3 respectively. We see that while the peak in the Saraga-Loss protocol may be achieved slightly earlier depending on the appropriate adjustment of parameters, our protocols achieve much higher probabilities.

DiVincenzo, quantum gates, and hence entanglement can be generated only on a time-scale of J. Here we simply use tunneling to prepare the desired entangled state at a time-scale set by the tunnel coupling t. Note the singlet inside the central dot, which is our starting resource, is assume to be prepared by equilibration of the central dot to its lowest (ground) state. While this process will take its due time, depending on the relaxation time-scale of the dot, we do not worry too much about that at this stage as this process leads to a robust initialization. It is only for operations to generate entanglement between distinct dots containing distinct qubits that we want to reduce the time so that decoherence has less time to act. It is true that our method hits a bottleneck for further processing once the singlets are there. To do universal quantum computation it does not suffice to have an ensemble of pairs of entangled particles only. Further operations have to be done between them. For example, entangling two spins, one from each singlet coherently (i.e., through a unitary evolution), will be needed if one is to generate entangled resources needed for measurement based quantum computation. To this end, we aim to study in the future where such processes are also possible on a time-scale set by the tunnel, rather than the exchange couplings. An idea will be to use the tunnel coupling to bring two electrons coherently to the *same* quantum dot inside which the intra-dot exchange coupling between spins is much stronger than the interdot coupling.

Chapter 5

Quantum Gates in Triple Dots with Empty middle Dot

5.1 Introduction

Quantum Dots (QDs) are regarded as a good system for the storage and manipulation of Quantum Information (QI). In these systems, the qubit could be encoded, for example, in the spin of an electron [18, 19, 41, 42, 43, 44] or the electronic charge distribution [45] or even the presence/absence of excitons [23]. Spin qubits are particularly important because of their long decoherence times. The earliest proposals advocated the use of the spin of a single electron in a quantum dot as a qubit with quantum gates being realized by tuning the tunnel coupling between two quantum dots [19]. On the other hand, some early experiments [41] and recent proposals [43] have focussed on qubits encoded on two spins in double dot systems, where the control parameter is the energy mismatch between the quantum dots. This is motivated by the fact that the energy mismatch between dots can be simple to control, for example, through source-drain bias [46] or local electrostatic gates [41]. It would thus be interesting to have a protocol where one requires only the above control (namely the energy mismatch between dots) and is yet able to use a single spin as a qubit. In this paper, we propose such a protocol using a linear triple dot system where qubits (individual electronic spins) are placed in the outer dots with the central dot being kept unfilled. An alternative motivation for our work stems from the fact that various triple dot systems are now being fabricated and their charge stability diagram with small numbers of electrons is being studied [47, 48]. However, most experiments in quantum information context (with the exception of Ref.[48]) have so far been limited exclusively to double dot systems. It would thereby be very timely to have a scheme such as ours, which

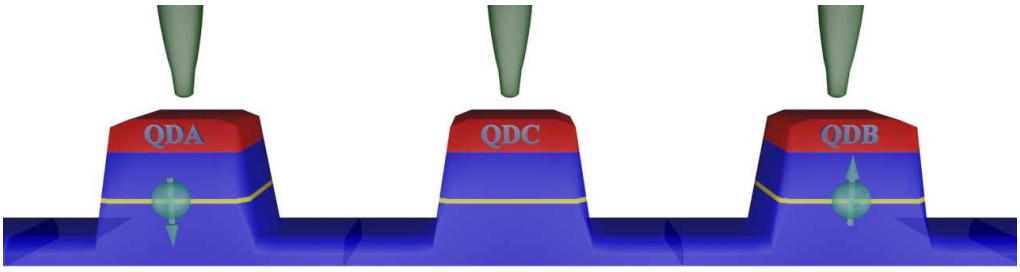

Figure 5.1: The above figure depicts the triple dot system where we investigate the possibility of quantum gates. There are two spins in the outer dots which behave as qubits, while the central dot is empty both before and after the quantum gates. QDA, QDC and QDB in the figure stand for quantum dots A, C and B respectively, while separate electrodes controlling the voltages of each dot are also shown in the figure.

enhances the scope of quantum gate related experiments to triple dot systems. Of course, the most straightforward generalization of the schemes in double dots [19] would be to have three spin qubits in three quantum dots i.e., the filling of the quantum dots being $(1, 1, 1)$. Another possibility is to have a spin in the central dot as a *mediator* for an effective coupling between the outer dots, a configuration which has recently been studied in the molecular context [49]. Another possibility with a $(1, 1, 1)$ filling is to encode a single qubit in three dots [50], which has been explored in a very recent experiment [48]. Here we find out that a lower filling configuration, namely a $(1, 0, 1)$ filling, also provides a system for two qubit quantum gates with the qubits being in the outer dots. The $(1, 0, 1)$ filling prevents one from reducing the problem to one of distinguishable spins (labeled by their sites) interacting through exchange interactions as in the existing schemes for quantum gates with spin qubits. Thus both the tunneling of electrons from one site to another, and careful second quantized treatment are important in the current problem and make it interesting.

5.2 Setup

Our setup consists of 3 quantum dots (QDs) in a row, with the voltage applied to the central one being controllable by some electrode, as shown in Fig.5.1. We label the outer dots of the chain as dot A and dot B, while we label the central dot as dot C. We will assume that the

Mott-Hubbard Hamiltonian describes the system well (for example, see Refs.[51]), whereby the relevant Hamiltonian is

$$\mathcal{H} = \sum_{\sigma,i} E_i \; d^\dagger_{i\sigma} d_{i\sigma} + \sum_{\sigma} t_{\rm AC}(d^\dagger_{{\rm A}\sigma} d_{{\rm C}\sigma} + d^\dagger_{{\rm C}\sigma} d_{{\rm A}\sigma})$$
$$+ \sum_{\sigma} t_{\rm CB}(d^\dagger_{{\rm C}\sigma} d_{{\rm B}\sigma} + d^\dagger_{{\rm B}\sigma} d_{{\rm C}\sigma}) + \frac{1}{2}\sum_i U_i n_i(n_i - 1). \tag{5.1}$$

In the above, i stands for A, B and C, $d^\dagger_{i\sigma}$ creates and $d_{i\sigma}$ annihilates an electron at the ith dot in the spin state σ with energy E_i. Here we have assumed that the particles are created only in the lowest energy state at the site (E_i) and the higher energy levels for a single electron are so well separated that they never become involved in the problem. U_i is the Coulomb repulsion in the QD i, $n_i = \sum_\sigma d^\dagger_{i\sigma} d_{i\sigma}$ in the total electron number operator of the ith dot and $t_{\rm AC}$ and $t_{\rm CB}$ are tunnel matrix elements between dots. Here we have assumed that another term, often present in Hubbard models for dot arrays, namely the inter-dot electrostatic interaction is zero. Moreover, we have assumed that there exists no tunneling between the non-neighboring dots, namely A and B. This should be a good approximation in serial triple dot systems [47] as A and B have a high separation. Some relevant experimental values for E_i, U_i, $t_{\rm AC}$ and $t_{\rm CB}$ from recent experiments are given in the table 1 of Ref.[18], which will provide our guide for exploring feasibility issues. The dots at the two ends (i.e., QD A and QD B) are each assumed to be filled up by a single electron as shown in Fig.5.1. These two electronic spins will be the two qubits in our problem. As these qubits are identified by their sites, they can be referred to as qubit A and qubit B respectively. Of course, we should be able to control when we want to enact a quantum gate between the aforementioned qubits, and for those intervals of time when we do not want any gates, nothing should happen to the qubits (the state of the qubits, whatever they are, should remain intact). To ensure this, one has to ensure that the qubits stably remain in a $(1, 0, 1)$ filling as shown in Fig.5.1 and do not hop into QD C during this non-processing stage. This is achieved by choosing an appropriate set of voltages applied to the triple dot system and there are quite a few experimental examples by now in which the $(1, 0, 1)$ filling has already been realized. Typically, if the Hamiltonian $\mathcal{H}$ of Eq.(5.1) is valid with $t_{\rm AC} \approx t_{\rm CB} = t$, then one has to set the voltage applied to QD C to a lower value and the voltages of QDs A and B to a higher equal value. Also we have to work with systems with $t << |E_{\rm C} - E_{\rm A}|, |E_{\rm C} - E_{\rm B}|$ so that hopping is severely suppressed. In this "non-processing" mode of our system, the evolution effectively freezes. When one intends to accomplish a quantum gate, one rapidly sets $E_{\rm C} = E_{\rm A} = E_{\rm B}$ and a time evolution starts (this is true as long as the Hamiltonian $\mathcal{H}$ with $t_{\rm AC} \approx t_{\rm CB} = t$ is a good approximation of the triple dot system in consideration; in different experimental realizations,

the Hamiltonian may deviate differently from this, and then, for the processing mode, one has to apply that voltage which ensures the electrostatic energy of the configurations $(1,0,1),(1,1,0)$ and $(0,1,1)$ to be equal. We will show that a two qubit "entangling" quantum gate can be obtained between the qubits by virtue of this evolution through Hamiltonian $\mathcal{H}$. Though during the time evolution, the electrons can hop into the otherwise empty QD C, and indeed this is necessary for their spins to interact, at the end of a fixed period of evolution, one electron is back in each of QD A and QD B. We will assume that single qubit gates on the spins in the outer dots can be trivially implemented by using local fields, so that we are going to concentrate only on the demonstration of a two qubit entangling gate. The demonstration of the two qubit entangling gate is at the heart of demonstrating the viability of a system for universal quantum computation.

5.3 The two qubit gate

The specific gate that we will demonstrate as enactable between the spins in the outer dots by means of their evolution through the Hamiltonian $\mathcal{H}$ is given by the following evolution of the computational basis states $|\uparrow\rangle$ (up spin along any axis, say z, standing for the logical state $|0\rangle$) and $|\downarrow\rangle$ (down spin along any axis, say z standing for the logical state $|1\rangle$):

$$\begin{aligned}
|\uparrow\rangle_A|\uparrow\rangle_B &\rightarrow |\uparrow\rangle_A|\uparrow\rangle_B \\
|\uparrow\rangle_A|\downarrow\rangle_B &\rightarrow e^{i\frac{\pi}{4}}\frac{1}{\sqrt{2}}(|\uparrow\rangle_A|\downarrow\rangle_B - i|\downarrow\rangle_A|\uparrow\rangle_B) \\
|\downarrow\rangle_A|\uparrow\rangle_B &\rightarrow e^{i\frac{\pi}{4}}\frac{1}{\sqrt{2}}(|\downarrow\rangle_A|\uparrow\rangle_B - i|\uparrow\rangle_A|\downarrow\rangle_B) \\
|\downarrow\rangle_A|\downarrow\rangle_B &\rightarrow |\downarrow\rangle_A|\downarrow\rangle_B. \qquad (5.2)
\end{aligned}$$

Note that the above gate is manifestly an entangling quantum gate as it takes the initial states $|\uparrow\rangle_A|\downarrow\rangle_B$ and $|\downarrow\rangle_A|\uparrow\rangle_B$ to entangled states. Thus the above gate suffices, in conjunction with local unitary operations on qubits A and B, for universal quantum computation [52].

Before proceeding further, we have to briefly clarify the notation that we will use. The gate presented above is in the usual notation of states of multiple qubits, where all the qubits are distinguishable and each qubit has its own distinct label. However, this distinctive labels (namely, qubit A and qubit B) are true only in the "non-processing" phase, i.e., before and after the time evolution by H. The two electrons may loose their site labels (namely A and B) during the evolution and thereby a fully second quantized treatment which automatically takes account of the indistinguishability of the electrons is necessary. So, as basis states for writing

down the Hamiltonian of the system, we shall use the states $d^\dagger_{i\sigma} d^\dagger_{j\sigma'}|0\rangle$ with $i, j = \mathrm{A}, \mathrm{B}, \mathrm{C}$ and $\sigma, \sigma' = \uparrow, \downarrow$, where $|0\rangle$ is the state with all three dots empty, and evaluate the matrix elements of the Hamiltonian H in this basis.

Let us point out that the total spin component along any axis is conserved by H. Choosing an axis to be the z axis, for example, and remembering our $(1, 0, 1)$ initial filling, the problem becomes three independent problems for the total z component of the spin in the three sites S_z being $+1$ ($\sum_i d^\dagger_{i\uparrow} d_{i\uparrow} = 2$), 0 ($\sum_i d^\dagger_{i\uparrow} d_{i\uparrow} = 1$) or -1 ($\sum_i d^\dagger_{i\uparrow} d_{i\uparrow} = 0$). In the $S_z = +1$ sector, a complete basis comprises three states $d^\dagger_{\mathrm{A}\uparrow} d^\dagger_{\mathrm{C}\uparrow}|0\rangle, d^\dagger_{\mathrm{A}\uparrow} d^\dagger_{\mathrm{B}\uparrow}|0\rangle$ and $d^\dagger_{\mathrm{C}\uparrow} d^\dagger_{\mathrm{B}\uparrow}|0\rangle$, in which the 3×3 Hamiltonian is simply

$$H_{S_z=+1} = \begin{pmatrix} 0 & t & t \\ t & 0 & 0 \\ t & 0 & 0 \end{pmatrix}$$

From the above Hamiltonian it is easy to see that if the system starts in the two qubit state $|\uparrow\rangle_A|\uparrow\rangle_B$ (which actually means the state $d^\dagger_{\mathrm{A}\uparrow} d^\dagger_{\mathrm{B}\uparrow}|0\rangle$), then at times $\tau_m = m\frac{2\pi}{\sqrt{2}t}$, where m is an integer, the system comes back to its original state without any phase factor. Thereby, if we halt the evolution at any of these instances of time (by suddenly setting the voltages to the non-processing mode), we will have the $|\uparrow\rangle_A|\uparrow\rangle_B \rightarrow |\uparrow\rangle_A|\uparrow\rangle_B$ part of the quantum gate in Eq.(5.2) satisfied. Exactly the same result holds for the $|\downarrow\rangle_A|\downarrow\rangle_B \rightarrow |\downarrow\rangle_A|\downarrow\rangle_B$ part of the quantum gate, which evolves in the $S_z = -1$ sector with an identical Hamiltonian matrix. Therefore it remains to check whether there exist any values of m for which the remainder of the quantum gate of Eq.(5.2) happens at τ_m. For that we have to look at the Hamiltonian in the $S_z = 0$ sector.

5.4 The evolution in the $S_z = 0$ sector and demonstration of the gate

In the $S_z = 0$ sector a complete basis is made of the 9 states $d^\dagger_{\mathrm{A}\uparrow} d^\dagger_{\mathrm{C}\downarrow}|0\rangle, d^\dagger_{\mathrm{A}\downarrow} d^\dagger_{\mathrm{C}\uparrow}|0\rangle, d^\dagger_{\mathrm{C}\uparrow} d^\dagger_{\mathrm{B}\downarrow}|0\rangle, d^\dagger_{\mathrm{C}\downarrow} d^\dagger_{\mathrm{B}\uparrow}|0\rangle$, $d^\dagger_{\mathrm{A}\uparrow} d^\dagger_{\mathrm{B}\downarrow}|0\rangle, d^\dagger_{\mathrm{A}\downarrow} d^\dagger_{\mathrm{B}\uparrow}|0\rangle, d^\dagger_{\mathrm{A}\uparrow} d^\dagger_{\mathrm{A}\downarrow}|0\rangle, d^\dagger_{\mathrm{B}\uparrow} d^\dagger_{\mathrm{B}\downarrow}|0\rangle, d^\dagger_{\mathrm{C}\uparrow} d^\dagger_{\mathrm{C}\downarrow}|0\rangle$. The 9×9 Hamiltonian matrix in this basis is not reproduced here for brevity, but it is important to note that here some elements such as $\langle 0|d_{\mathrm{A}\uparrow} d_{\mathrm{C}\downarrow} \mathcal{H} d^\dagger_{\mathrm{A}\uparrow} d^\dagger_{\mathrm{A}\downarrow}|0\rangle$ are t, while others such as $\langle 0|d_{\mathrm{A}\downarrow} d_{\mathrm{C}\uparrow} \mathcal{H} d^\dagger_{\mathrm{A}\uparrow} d^\dagger_{\mathrm{A}\downarrow}|0\rangle$ are $-t$. This sign difference is important and cannot be obtained without proper second quantized treatment. Now assuming $U >> t$, one can adiabatically eliminate the double occupancy states $d^\dagger_{\mathrm{A}\uparrow} d^\dagger_{\mathrm{A}\downarrow}|0\rangle, d^\dagger_{\mathrm{B}\uparrow} d^\dagger_{\mathrm{B}\downarrow}|0\rangle, d^\dagger_{\mathrm{C}\uparrow} d^\dagger_{\mathrm{C}\downarrow}|0\rangle$ to obtain the effective Hamiltonian

$$\mathcal{H}_{eff} = \begin{pmatrix} -2J & 2J & -J & J & t & 0 \\ 2J & -2J & J & -J & 0 & t \\ -J & J & -2J & 2J & t & 0 \\ J & -J & 2J & -2J & 0 & t \\ t & 0 & t & 0 & 0 & 0 \\ 0 & t & 0 & t & 0 & 0 \end{pmatrix}$$

with $J = t^2/U$. The above effective Hamiltonian is that of a 3-site $t-J$ model, with parameter t for hopping and parameter J for a spin-spin interaction *only* when the spins are in neighboring sites. We define $\eta^{\pm} = -(3J \pm \sqrt{9J^2 + 2t^2})$ and $\xi^{\pm} = \sqrt{2 + (\eta^{\pm})^2/t^2}$, in terms of which, the eigenvalues of H_{eff} are $\{0, -2J, -\sqrt{2}t, \sqrt{2}t, \eta^+, \eta^-\}$, while its eigenvectors are:

$$\begin{aligned}
|v_1\rangle &= \{\frac{1}{2}, \frac{1}{2}, -\frac{1}{2}, -\frac{1}{2}, 0, 0\} \\
|v_2\rangle &= \{-\frac{1}{2}, \frac{1}{2}, \frac{1}{2}, -\frac{1}{2}, 0, 0\} \\
|v_3\rangle &= \{-\frac{1}{2\sqrt{2}}, -\frac{1}{2\sqrt{2}}, -\frac{1}{2\sqrt{2}}, -\frac{1}{2\sqrt{2}}, \frac{1}{2}, \frac{1}{2}\} \\
|v_4\rangle &= \{\frac{1}{2\sqrt{2}}, \frac{1}{2\sqrt{2}}, \frac{1}{2\sqrt{2}}, \frac{1}{2\sqrt{2}}, \frac{1}{2}, \frac{1}{2}\} \\
|v_5\rangle &= \{\frac{\eta^+}{2t\xi^+}, -\frac{\eta^+}{2t\xi^+}, \frac{\eta^+}{2t\xi^+}, -\frac{\eta^+}{2t\xi^+}, -\frac{1}{\xi^+}, +\frac{1}{\xi^+}\} \\
|v_6\rangle &= \{\frac{\eta^-}{2t\xi^-}, -\frac{\eta^-}{2t\xi^-}, \frac{\eta^-}{2t\xi^-}, -\frac{\eta^-}{2t\xi^-}, \frac{1}{\xi^-}, -\frac{1}{\xi^-}\}
\end{aligned} \tag{5.3}$$

We want to show that the initial state $|\uparrow\rangle_A|\downarrow\rangle_B$ of qubits A and B evolves to $e^{i\pi/4}\frac{1}{\sqrt{2}}(|\uparrow\rangle_A|\downarrow\rangle_B - i|\downarrow\rangle_A|\uparrow\rangle_B)$ at a certain time under the action of the Hamiltonian $\mathcal{H}_{eff}$. Moreover this time must be coincident or approximately coincident with $\tau_m = m\frac{2\pi}{\sqrt{2}t}$ (discussed in the previous section) for some m, so that the gate of Eq.(5.2) is accomplished at the time τ_m. The initial state $|\uparrow\rangle_A|\downarrow\rangle_B$, or more accurately the second quantized state $d^\dagger_{\mathrm{A}\uparrow} d^\dagger_{\mathrm{B}\downarrow}|0\rangle$, evolves with time τ as:

$$\begin{aligned}
|\psi_{A\uparrow,B\downarrow}(\tau)\rangle &= \frac{1}{2}\{e^{i\sqrt{2}t\tau}|v_3\rangle + e^{-i\sqrt{2}t\tau}|v_4\rangle\} \\
&- \frac{e^{-i\eta^+\tau}}{\xi^+}|v_5\rangle + \frac{e^{-i\eta^-\tau}}{\xi^-}|v_6\rangle
\end{aligned} \tag{5.4}$$

If we now once more invoke $U >> t$ to neglect terms of $O(t/U)$, we can simplify the modulus squared overlap of $|\psi_{A\uparrow,B\downarrow}(\tau)\rangle$ with the target state $e^{i\pi/4}\frac{1}{\sqrt{2}}(|\uparrow\rangle_A|\downarrow\rangle_B - i|\downarrow\rangle_A|\uparrow\rangle_B)$ to the

analytic expression

$$\begin{aligned} & \frac{\cos^2\sqrt{2}t\tau}{8}[\{1+\sqrt{2}\cos(3J\tau-\frac{\pi}{4})\}^2 \\ + \quad & \{1-\sqrt{2}\cos(3J\tau+\frac{\pi}{4})\}^2]. \end{aligned} \tag{5.5}$$

Notice that there are two distinct frequencies in the above expression, namely the higher frequency $\sqrt{2}t$, which is due to the tunneling, and the much lower frequency $3J$, which is due to the spin-spin interactions. Also note that, as expected, the modulus squared overlap with the target state is 0.5 at time $\tau = 0$. However, most important to note is that at times $\tau_n^{'} = (2n+1)\pi/6J$ with n being an integer, the modulus squared overlap is unity implying that at these instances, the initial state $|\uparrow\rangle_A|\downarrow\rangle_B$ of qubits A and B has fully evolved to the entangled state $e^{i\frac{\pi}{4}}\frac{1}{\sqrt{2}}(|\uparrow\rangle_A|\downarrow\rangle_B - i|\downarrow\rangle_A|\uparrow\rangle_B)$. By following identical steps as above, one can prove that at times $\tau_n^{'}$ the initial state $|\downarrow\rangle_A|\uparrow\rangle_B$ of qubits A and B evolves to $e^{i\frac{\pi}{4}}\frac{1}{\sqrt{2}}(|\downarrow\rangle_A|\uparrow\rangle_B - i|\uparrow\rangle_A|\downarrow\rangle_B)$. As $2\pi/\sqrt{2}t << \pi/6J$, for any $\tau_n^{'}$ there will exist several values of m for which τ_m is close to $\tau_n^{'}$. Thus one can always choose some m and n so that $\tau_m \approx \tau_n^{'}$ and at this particular time the quantum gate of Eq.(5.2) is accomplished. Ideally we would like to choose the shortest possible time to accomplish the quantum gate to minimize the effects of decoherence. The earliest opportunity is at time $\tau_0^{'}$ as this is the earliest time the second and third lines of the gate of Eq.(5.2) is accomplished. Depending on the strength of the tunnel coupling t, nearly always it is possible to find a m such that $\tau_m \approx \tau_0^{'}$ so that the quantum gate of Eq.(5.2) is accomplished at $\tau_0^{'}$. To convince the readers about this, we take explicit values of parameters in scaled units. First we set the energy scale of about 10μeV, which is a realistic typical scale of t [18, 53, 39] to unity. In these units, we take $t = \sqrt{2}$ and $U = 20$ so that $U >> t$ is valid and yet $J \sim 0.1$ is not too small. Such ratios of U/t are available realistic [53, 39]), and plot some relevant curves in Fig.5.2.

It is clear from the figure that the modulus squared overlaps of the $|\uparrow\rangle_A|\uparrow\rangle_B$ state with itself and the $|\uparrow\rangle_A|\downarrow\rangle_B$ with $\frac{1}{\sqrt{2}}(|\uparrow\rangle_A|\downarrow\rangle_B - i|\downarrow\rangle_A|\uparrow\rangle_B)$, both achieve values indistinguishable from unity at time $\tau_0^{'}$. Further note that if one could always tune the two free parameters t and U, to ensure that $\tau_0^{'} \approx \tau_m$ holds for some m. Fig.5.2 also presents a plot for the evolution of $|\uparrow\rangle_A|\downarrow\rangle_B$ to $\frac{1}{\sqrt{2}}(|\uparrow\rangle_A|\downarrow\rangle_B - i|\downarrow\rangle_A|\uparrow\rangle_B)$ from exact numerical diagonalization of Eq.(5.1) to show that the approximations (adiabatic elimination) leading to the expression of Eq.(5.5) is valid. However, to verify the quantum gate, one also needs to verify the phases outside the brackets on the right hand sides of the second and third lines of Eq.(5.2). We temporarily postpone this, and will verify these through additional plots that we make in the next section where

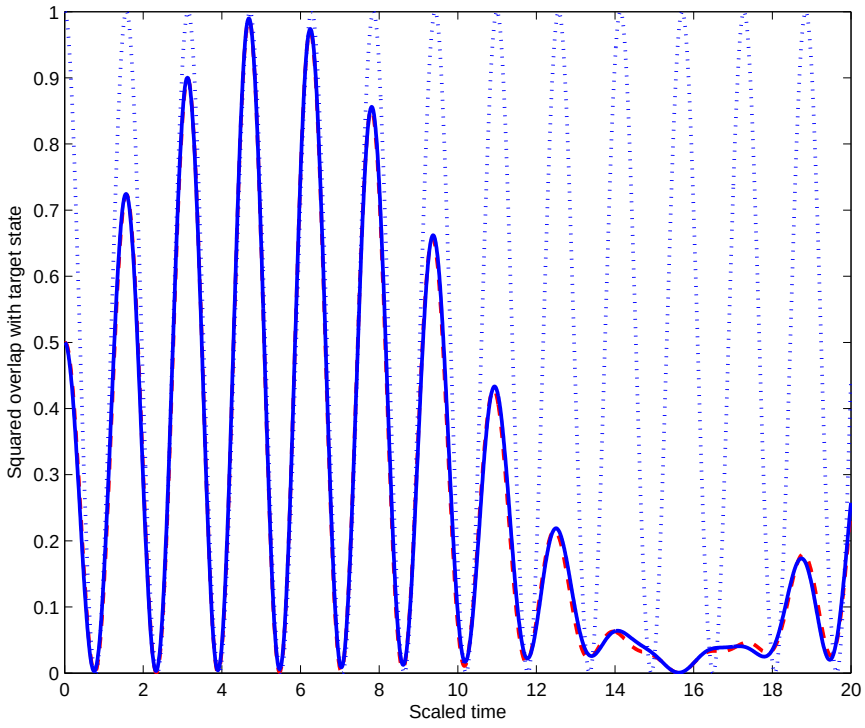

Figure 5.2: Plots to demonstrate the occurrence of an entangling quantum gate at a certain instant of time between the spins A and B. The dotted line is the modulus squared overlap of $|\uparrow\rangle_A|\uparrow\rangle_B$ with the state it evolves to as a function of time after the gating Hamiltonian is switched on. Both the solid and the dashed lines show the modulus squared overlap of $\frac{1}{\sqrt{2}}(|\uparrow\rangle_A|\downarrow\rangle_B - i|\downarrow\rangle_A|\uparrow\rangle_B)$ with the state to which $|\uparrow\rangle_A|\downarrow\rangle_B$ evolves as a function of time after the gating Hamiltonian is switched on. The solid line is from our analytic expression of Eq.(5.5), while the dashed line from numerics without approximations. The parameters used in the plot are $t = \sqrt{2}$ and $U = 20$ in scaled units where the energy scale 10μeV is set to unity (one unit of the scaled time is about 0.1ns.)

we treat decoherence.

5.5 Role of noise and decoherence

Now that we have demonstrated the possibility of an entangling gate between the spin qubits in our triple dot setting, we proceed to investigate how this gate is affected by various sources of decoherence. During the fleetingly small time window of gate operation (about a nanosecond) transient charge superpositions will exist, and thereby the gate will be subject to some charge decoherence despite operating between spin qubits. Note that this is *not unique* to our setting, but, in fact, also automatically present when one intends to implement two qubit gates with singlet-triplet qubits defined in double dots. There the singlet and the triplet have to go to distinct charge configurations to enable gates between two double-dot qubits [43]. As such decoherence is only during the gate operation, one can suppress it effectively by making the gate faster (i.e., J stronger). In our case, during storage of the qubits, though, only spin decoherence, primarily due to the hyperfine interaction with nuclear spins, will be present.

We first model the effect of charge decoherence numerically. As the temperature is lowered enough so that the effect of phonons is eliminated (this assumption is met in current quantum dot experiments), decoherence due to spin-orbit interactions is suppressed. The $1/f$ noise generated in the triple dot device due to the fluctuations in the background charge is then the predominant source of decoherence. We will phenomenologically fix the amplitude of this noise to set a charge decoherence time-scale of about 1 ns (coherent charge oscillations have been observed till about 2 ns [25] and even much higher have been reported in non-gated devices [54]). Setting the amplitude in this phenomenological way also has the advantage that it models charge decoherence of the best observed strengths irrespective of its cause (for example, some phonons may still be present). We have numerically generated a $1/f$ noise and used a distinct value of the noise in each time step. The numerical program that generates the noise guarantees that it has $1/f$ noise spectrum. We have also taken the tunneling t to change with the mismatch of the dot energies – we have taken t to vary with the energy mismatch with a narrow gaussian profile of width 0.01 (this profile of t has been taken only for this phenomenological decoherence estimation and not elsewhere in the paper). We then vary the average strength of the fluctuations till we get about a nanosecond time-scale of decay of the oscillations of the state $|\uparrow\rangle_A|\uparrow\rangle_B$ during the gate, which are essentially purely charge oscillations. This is plotted in Fig.5.3. We now take the *same* strength of noise for the evolution of $|\uparrow\rangle_A|\downarrow\rangle_B$ under the gate and numerically plot (in Fig.5.3) the probability of it to evolve to its ideal target state $e^{i\frac{\pi}{4}}\frac{1}{\sqrt{2}}(|\uparrow\rangle_A|\downarrow\rangle_B - i|\downarrow\rangle_A|\uparrow\rangle_B)$.

From the plot one can see that the effect of charge decoherence is not significant (the probability of the gate driving the initial states to their right targets is higher than 0.95 for both states). This has happened because we have chosen parameters carefully enough to get a J which can give a gate faster than the currently known charge decoherence rates.

An additional form of decoherence that will be active is the nuclear baths in the quantum dots, which induce decoherence of the spin states. It is known that the orientations of the nuclear spins evolve at a much slower time-scale in comparison to the dynamics of the electrons (time-scales of $1/t$ and $1/J$) in quantum dot systems [18] so that during one operation of our gate we may effectively regard the nuclear bath to provide a random but fixed (frozen in time) field. This is known as the quasistatic approximation [18]. The effect of decoherence is then due to different constant fields in various runs of the gate (a distinct random direction and magnitude in each of the quantum dots for each run of the gate). Following the parameters given in Ref.[18], we have modeled the dynamics using a magnetic field of about an order of magnitude less than the tunneling t in a random direction. The direction is chosen completely at random, while the magnitude is chosen from a Gaussian distribution given as $P(B) = \frac{1}{(2\pi B_{\rm nuc}^2)^{3/2}} \exp{(-B^2/2B_{\rm nuc}^2)}$. Here one cannot really use restricted spaces any more and the full Hilbert space of the problem is involved as the nuclear magnetic field connects these spaces. Thereby we tackle this part of the problem numerically in the full Hilbert space consisting of the $S_z = 0, \pm 1$ sectors by exact diagonalization of $\mathcal{H}$ with the addition of a random magnetic field term in each dot and using a charge decoherence of the same strength as before. The results are plotted in Fig.5.4 and show that the probability of successful occurrence of the quantum gate (Eq.(5.2)) remains higher than 0.9 for $B_{\rm nuc} \sim 0.1$ in our units, which is comparable to its experimental values [18]. In principle, though, this decoherence can be eliminated to a large degree by polarizing the background nuclear spins [22] so that one can have quantum gates with fidelity only restricted by charge decoherence in a fleetingly small time window of gate operation. Even this latter decoherence should decrease with technology, and have already been reported to have very low values in non-gated devices [54]. Alternatively it is known that quantum dot-like experiments can be performed also with *neutral* fermionic atoms in optical lattices [55] where charge decoherence is inactive.

Now we return to the issue of verifying all features of the gate of Eq.(5.2) through appropriate plots. To verify all features of a quantum gate, one really (ideally) needs to find the closeness of the completely positive map realized in presence of decoherence with the unitary operation corresponding to the gate i.e., the gate fidelity. However, we are going to use, for simplicity, a

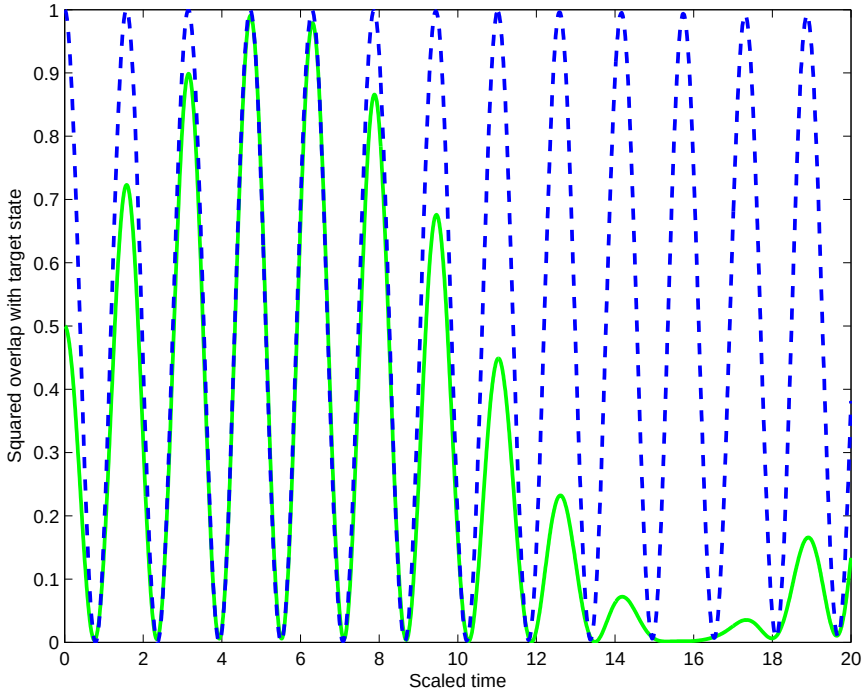

Figure 5.3: The figure shows the effect of charge decoherence on the quantum gate of our protocol. We induce a charge decoherence time-scale of about 1 ns (about 10 units of our scaled time) by appropriately tuning a $1/f$ noise. The time evolution of the modulus squared overlap of an initial $|\uparrow\rangle_A|\uparrow\rangle_B$ state under this noise with itself (dashed curve) shows the purely charge based decoherence effect. Keeping the parameters of the charge noise the same, we have also plotted the modulus squared overlap of the state $\frac{1}{\sqrt{2}}(|\uparrow\rangle_A|\downarrow\rangle_B - i|\downarrow\rangle_A|\uparrow\rangle_B)$ with the state to which $|\uparrow\rangle_A|\downarrow\rangle_B$ evolves as a function of time after the gating Hamiltonian is switched on (solid curve).

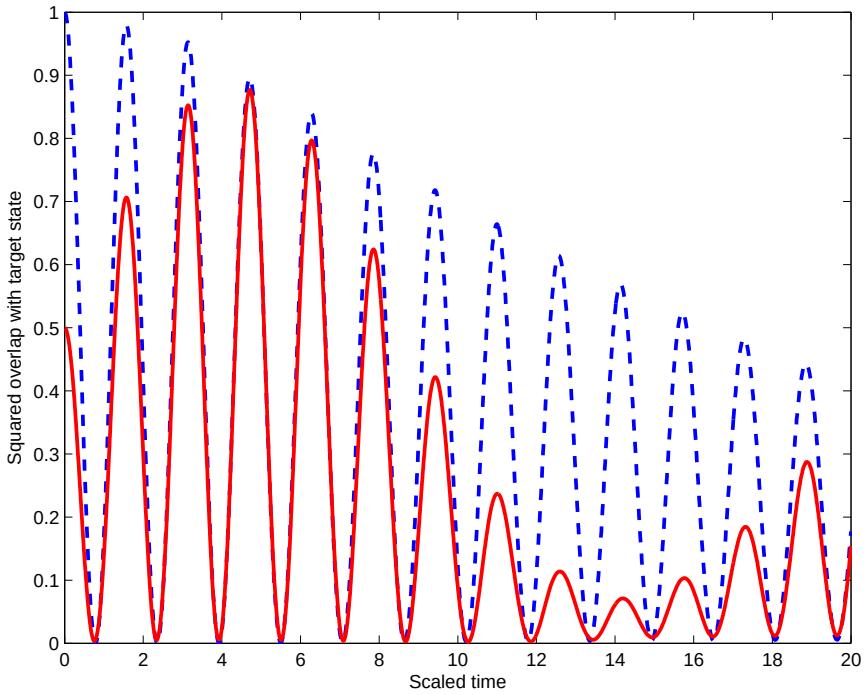

Figure 5.4: This plot shows the combined effect of both hyperfine interactions and charge decoherence on the quantum gate proposed by us. Charge noise is set so as to have a charge decoherence time-scale of about 1 ns, while the strength of the random nuclear field causing the spin decoherence is set to the realistic value of $B_{\rm nuc} \sim 0.1$ in scaled units (with 10μeV taken as unity). The time evolution of the modulus squared overlap of an initial $|\uparrow\rangle_A|\uparrow\rangle_B$ state under this noise with itself is shown as the dashed curve, while the modulus squared overlap of the state $\frac{1}{\sqrt{2}}(|\uparrow\rangle_A|\downarrow\rangle_B - i|\downarrow\rangle_A|\uparrow\rangle_B)$ with the state to which $|\uparrow\rangle_A|\downarrow\rangle_B$ evolves as a function of time after the gating Hamiltonian is switched on is shown as the solid curve.

poor man's way of verifying the gate, which we think suffices as a witness of the reliability of the gate. Once the fidelity of the computational basis states going to the ideal ones are verified, what is left to verify is the error in the relative phases between the computational basis states due to the decoherence. We thus need to verify that the phases outside the second and third lines of Eq.(5.2), and particularly, how it gets affected by decoherence. One way to examine this is to use $\frac{1}{\sqrt{2}}(|\uparrow\rangle_A|\uparrow\rangle_B + |\uparrow\rangle_A|\uparrow\rangle_B)$ as an initial state and verify how close it evolves to the ideal state (i.e., state under no decoherence) $\frac{1}{\sqrt{2}}|\uparrow\rangle_A|\uparrow\rangle_B + \frac{e^{i\pi/4}}{2\sqrt{2}}(|\uparrow\rangle_A|\downarrow\rangle_B - i|\downarrow\rangle_A|\uparrow\rangle_B)$ at time $\tau_0^{'}$. This is demonstrated under only charge decoherence and both charge and hyperfine interaction induced decoherences in Fig.5.5.

5.6 Gates in a high decoherence regime

Suppose one has a very high charge decoherence (so that coherence stays, say, for only 0.1 ns) then one can still use our triple-dot setup for a gate by stopping at the very first peak of the oscillation of the $|\uparrow\rangle_A|\uparrow\rangle_B$ state, i.e., at a time $\tau_1 = 2\pi/t \sim 0.1$ ns. The resulting quantum gate is however different and obtained by replacing the right hand sides of the second and third rows of Eq.(5.2)(in the $t >> J$ limit) by $e^{i3J\tau/2}(\cos 3J\tau/2|\uparrow\rangle_A|\downarrow\rangle_B - i\sin 3J\tau/2|\downarrow\rangle_A|\uparrow\rangle_B)$ and $e^{i3J\tau/2}(\cos 3J\tau/2|\downarrow\rangle_A|\uparrow\rangle_B - i\sin 3J\tau/2|\uparrow\rangle_A|\downarrow\rangle_B)$ respectively. This has a lower entangling power, but is nonetheless an entangling gate, still useful for universal quantum computation. One merely has to halt the Hamiltonian at an earlier time (before decoherence has become too prominent) to get the gate and repeat the gate a few times to get a maximally entangling gate such as a CNOT from it. In Fig.5.6, we have plotted the overlap of the ideal target state $e^{i3J\tau/2}(\cos 3J\tau/2|\uparrow\rangle_A|\downarrow\rangle_B - i\sin 3J\tau/2|\downarrow\rangle_A|\uparrow\rangle_B)$ when one starts from the state $|\uparrow\rangle_A|\downarrow\rangle_B$ and has an evolution under the presence of both mechanisms of decoherence.

5.7 Discussions

The primary achievement in this chapter is to show that using triple dot systems, one can encode two single spin qubits and have an entangling quantum gate between them merely by tuning the voltage of the central dot (or voltage mis-alignment between the dots). This eases the restriction of having to tune the tunnel coupling t on a fast time-scale, which might be difficult [43] or even impossible to tune in some setups of permanently built dots. One can scale this scheme to several qubits by using a one dimensional array in a $ABABAB...ABA$ scenario with the A sites having single qubits and the B sites being empty in the non-operative state of the system. Whenever a quantum gate between two qubits is required, we tune the voltage of only the B

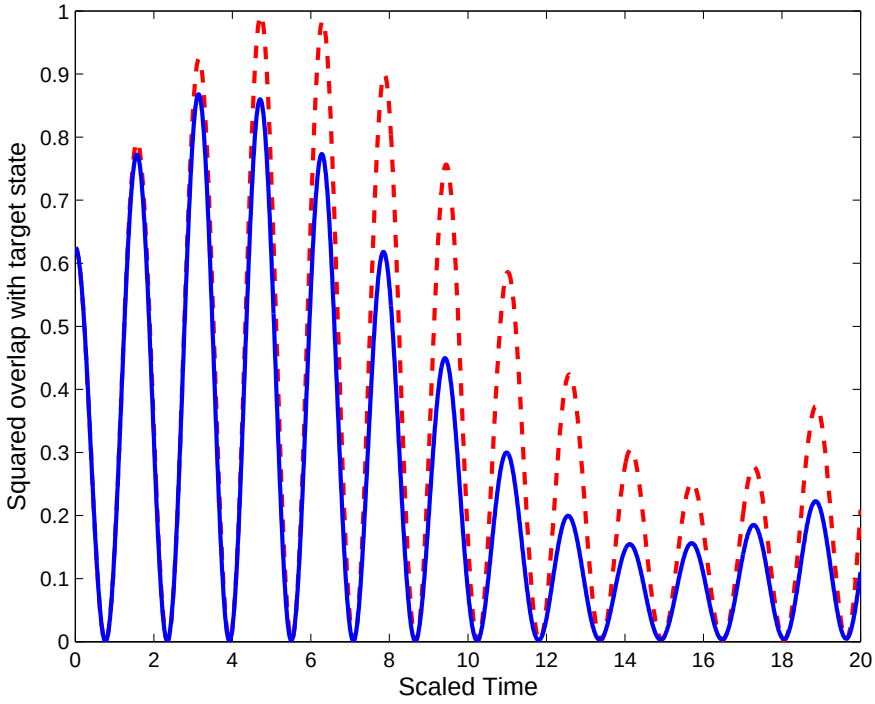

Figure 5.5: This plot shows the effects of decoherence on an initial state $\frac{1}{\sqrt{2}}(|\uparrow\rangle_A|\uparrow\rangle_B + |\uparrow\rangle_A|\downarrow\rangle_B)$. It plots the evolution of the squared overlap of this state with is intended target state at the end of the gate, namely $\frac{1}{\sqrt{2}}|\uparrow\rangle_A|\uparrow\rangle_B + \frac{e^{i\pi/4}}{2\sqrt{2}}(|\uparrow\rangle_A|\downarrow\rangle_B - i|\downarrow\rangle_A|\uparrow\rangle_B)$. The dashed curve shows the evolution when only charge decoherence is present, while solid curve presents the evolution when both the charge as well as hyperfine induced decoherences are present. Charge noise is set so as to have a charge decoherence time-scale of about 1 ns, while the strength of the random nuclear field causing the spin decoherence is set to the realistic value of $B_{\text{nuc}} \sim 0.1$ in scaled units (with 10μeV taken as unity).

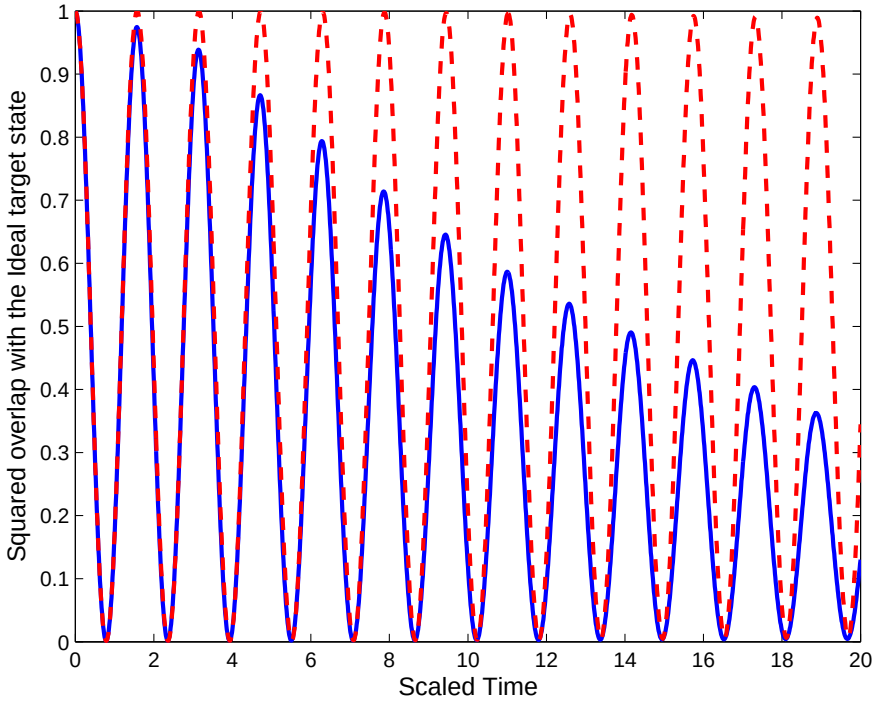

Figure 5.6: This plot shows the effects of decoherence on an initial state $|\uparrow\rangle_A|\downarrow\rangle_B$. It plots the evolution of the squared overlap of this state, under both mechanisms of decoherence, with the state that it evolves to at any time τ under ideal conditions (i.e., $t << U$ and no decoherence), namely $e^{i3J\tau/2}(\cos 3J\tau/2|\uparrow\rangle_A|\downarrow\rangle_B - i\sin 3J\tau/2|\downarrow\rangle_A|\uparrow\rangle_B)$. The dashed curve shows the evolution when only charge decoherence is present, while solid curve presents the evolution when both the charge as well as hyperfine induced decoherences are present. Charge noise is set so as to have a charge decoherence time-scale of about 1 ns, while the strength of the random nuclear field causing the spin decoherence is set to the realistic value of $B_{\text{nuc}} \sim 0.1$ in scaled units (with 10μeV taken as unity).

site between the qubits to enable a gate between them. We have shown that the gate works with high enough fidelities for a variety of input states for achievable values of charge and spin decoherence rates. For stronger charge decoherence, one can halt the unitary evolution at earlier pertinent times and still get an entangling gate, albeit with lower power.

Chapter 6

Singlet-Triplet Filtering in Square Dots

6.1 Introduction

Realizing quantum information and computation tasks in solid state physics, particularly quantum dots, has attracted a lot of interest in recent years. Electron spins in QDs are promising candidates for physical implementation of a qubit [19] due to their long coherence time [18]. Initialization, manipulation, and readout of electron spins have already been demonstrated [42, 41] and ideas exist for quantum gates based on single qubits encoded in two QDs [56]. As it is timely for "proof of principle" demonstrations of multi-qubit processes, it would be highly desirable to establish a coherent two qubit process in a *single* quantum dot.

the quantum dot whereas the triplets are frozen at their initial locations. By initializing the system in an unentangled superposition state we are then able to project onto a singlet or triplet state simply by a charge measurement to detect whether or not the charge has moved during the evolution. We use this property to propose some quantum information applications such as entanglement swapping and generating the Affleck-Kennedy-Lieb-Tasaki (AKLT) state, which is a resource for measurement-based quantum computation [59].

Recently, a dissipative method for singlet-triplet measurement has been implemented in the lab [41]. In this method a double QD is prepared with one electron in each QD, and after lowering the barrier one of the electrons will hop to the other QD provided that they are in a singlet state. As the singlet state is produced by a dissipative decay, there is *no set time* at which the electron will hop and the timescale for dissipative relaxation is usually longer than coherent evolution in the same range of energy. On the other hand in our coherent mechanism time is known and since evolution is faster decoherence has less effect on final achievements. Moreover, in our approach we are able to go beyond the singlet-triplet measurement to realize

some quantum computation tasks such as: entanglement swapping, teleportation and generating an AKLT-like state.

here we propose a mechanism for singlet-triplet measurement based on the coherent dynamics of two electrons in a large square quantum dot followed by a single charge detection . This is due to a sufficiently large energy separation between the low-lying eigenstates and higher-lying ones which allows us to construct an effective Hamiltonian. This effective Hamiltonian leaves the triplets unchanged while the singlets rotate around the quantum dot during the evolution. It means that spin part of the wave function controls the charge mobility and we have used this property to filter singlet-triplet states from each other. We also go beyond the singlet-triplet measurement to propose some quantum information applications such as entanglement swapping and generating the Affleck-Kennedy-Lieb-Tasaki (AKLT) state which is a resource for measurement base quantum computation [59].

From a practical perspective a large square QD is easier to fabricate than a small one and will also be modeled more accurately by our effective Hamiltonian, since the energy gap between the ground manifold and the lowest excited states increases rapidly with dot size, making the ground manifold increasingly isolated. On the other hand, as the absolute sizes of the singlet-triplet splitting in the ground manifold fall exponentially with dot size, large QDs have slower operation times and are more susceptible to errors. There is thus a trade-off between these factors, favoring QDs of intermediate size. Our simulations show that for square QDs of $L = 200-800$ nm our effective Hamiltonian is sufficiently accurate, and operates at frequencies within the range achieved in recent current experiments [25].

6.2 Effective Hamiltonian

We consider a system of two electrons held in a square semiconductor Quantum Dot (QD) with a hard-wall boundary, which can be realized in experiment by gating a two-dimensional electron gas (2DEG) at a heterojunction interface. The spectrum, and in particular, the structure of the low-lying eigenstates of this system, are determined by the competition between the kinetic energy of the electrons and the Coulomb repulsion between them. This can be governed simply by controlling the size of the dot, since the kinetic energy scales as $\sim 1/L^2$ while the Coulomb energy varies as $\sim 1/L$. In small QDs the kinetic term is thus the dominant component of the Hamiltonian. Consequently the ground-state will resemble that of non-interacting particles, with a charge density that is peaked in the center of the dot. Conversely in large dots, when the Coulomb interaction dominates, the energy of the system is minimized by the electrons local-

izing in space to minimize the electrostatic interaction energy. In analogy to the concept of the Wigner crystal state in bulk two-dimensional systems [60] these highly-correlated quasicrystalline states are termed "Wigner molecules". Thus simply by altering the size of the dot we are able to continuously tune the system from weak to strong interactions.

Assuming an effective mass m^* for the electrons the square QD is modeled by:

$$H = -\frac{\hbar^2}{2m^*}\left[\nabla_1^2 + \nabla_2^2\right] + V(\mathbf{r}_1) + V(\mathbf{r}_2) + \frac{e^2}{4\pi\varepsilon|\mathbf{r}_1 - \mathbf{r}_2|} \tag{6.1}$$

where $V(\mathbf{r})$ is the two-dimensional confining potential which. We choose to be hard-wall with precisely square symmetry, though the results to follow are not qualitatively changed under deviations from a perfect square, as we discuss later. The last term in Eq. (6.1) represents the coulomb repulsion between the two electrons, screened by the dielectric constant. In the strongly-correlated regime, in which the size of the square is large compared with the Bohr radius (~ 10nm in GaAs), eigenstates of this simple Hamiltonian are extremely demanding to obtain exactly. We show in Fig. 6.1(a) the low-lying energy spectrum of a GaAs QD with side-length 800 nm, obtained by diagonalising the full two-electron Schrodinger equation. We see that two degenerate triplets ($|n\rangle$, $n = 3, 4, ..., 8$) sit approximately (but not precisely) midway between two singlets ($|S_{1(2)}\rangle$), while all these 8 states are separated from the next multiplet of eigenstates by a relatively large gap. The charge distribution for the ground-state $|S_1\rangle$ is shown in Fig. 6.1(b), and clearly shows how the charge density strongly peaks near the corners of the QD. One can better appreciate the form of the states by defining linear combinations of the two singlets

$$|1\rangle = (|S_1\rangle + |S_2\rangle)/\sqrt{2} = |\Phi_1^S\rangle|\psi^-\rangle \tag{6.2}$$

$$|2\rangle = (|S_1\rangle - |S_2\rangle)/\sqrt{2} = |\Phi_2^S\rangle|\psi^-\rangle, \tag{6.3}$$

where $|\psi^-\rangle = (|\uparrow\downarrow\rangle - |\downarrow\uparrow\rangle)/\sqrt{2}$ is the singlet spinor, and $|\Phi_{1(2)}^S\rangle$ is the symmetric spatial component of the two-electron wave function. In Fig. 6.1(c) and 6.1(d) we plot the charge distribution of these states, clearly showing how they are localized at diagonally-opposite corners of the QD. For the triplets we adopt a similar labeling scheme

$$|3\rangle = |\Phi_1^A\rangle|\psi^+\rangle, |4\rangle = |\Phi_2^A\rangle|\psi^+\rangle, |5\rangle = |\Phi_1^A\rangle|\uparrow\uparrow\rangle, \tag{6.4}$$

$$|6\rangle = |\Phi_2^A\rangle|\uparrow\uparrow, |7\rangle = |\Phi_1^A\rangle|\downarrow\downarrow\rangle, |8\rangle = |\Phi_2^A\rangle|\downarrow\downarrow\rangle, \tag{6.5}$$

where $|\psi^+\rangle = (|\uparrow\downarrow\rangle + |\downarrow\uparrow\rangle)/\sqrt{2}$, and $|\Phi_1^A\rangle$ ($|\Phi_2^A\rangle$) is the anti-symmetric charge distribution, which resembles that of the states $|1\rangle$ and $|2\rangle$, being peaked at the same sites ac (bd). Note that

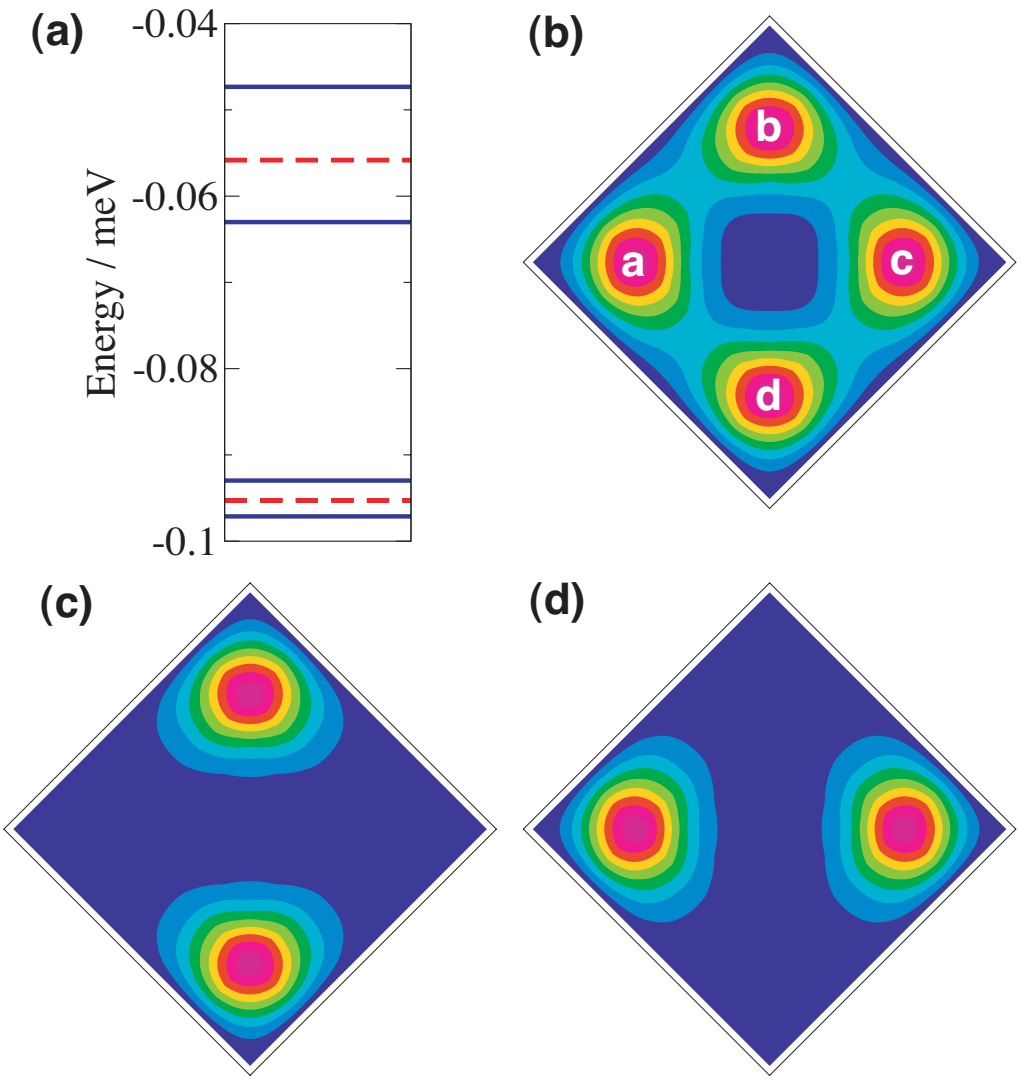

Figure 6.1: (Color online) Eigensystem of a GaAs dot with a side-length of $L = 800$ nm, obtained by exact diagonalization of the effective-mass Hamiltonian (Eq. 6.1). (a) The lowest two multiplets of states; singlets are shown with solid (blue) lines, triplets with dashed (red) lines. We consider only the dynamics of the lowest multiplet, consisting of two singlets ($|S_1\rangle$ and $|S_2\rangle$) with two degenerate triplets lying between them. (b) Charge distribution of the ground-state, showing the formation of a Wigner molecule, with peaks labeled $abcd$ near the dot corners. (c) Charge distribution of the symmetrized singlet state $|1\rangle = (|S_1\rangle + |S_2\rangle)/\sqrt{2}$, localized about bd. (d) Charge distribution of the antisymmetrised singlet state $|2\rangle$, localized about ac.

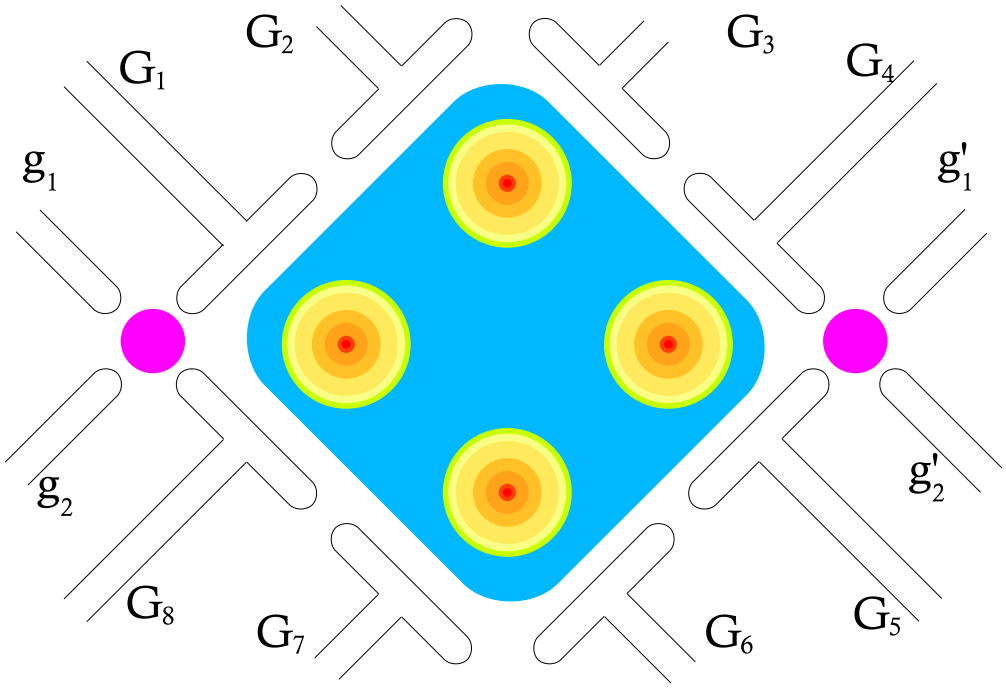

Figure 6.2: Gate structure for a large QD (central shaded square), connected to two smaller QDs (pink circles) at opposite corners.

while the triplets $|n\rangle$ ($n = 3, 4, ..., 8$) are eigenvectors of H, the singlets $|1\rangle$ and $|2\rangle$ are not. We can immediately write down an effective Hamiltonian for the low-lying energy eigenstates

$$H_{\text{eff}} = -\Delta_1 |S_1\rangle\langle S_1| + \Delta_2 |S_2\rangle\langle S_2| + E_0 \sum_{n=3}^{8} |n\rangle\langle n|, \tag{6.6}$$

where E_0 is the energy of the two degenerate triplets, and Δ_1 (Δ_2) is the energy separation between the triplets and $|S_1\rangle$ ($|S_2\rangle$). By restricting ourselves to the ground manifold, and using the sum rule $\sum_{n=1}^{8} |n\rangle\langle n| = I$, the effective Hamiltonian may be written in the charge-spin form

$$H_{\text{eff}} = E_0 I - \Delta(|1\rangle\langle 2| + |2\rangle\langle 1|) + J\left(\mathbf{s}_1 \cdot \mathbf{s}_2 - 1/4\right), \tag{6.7}$$

where $J = (\Delta_2 - \Delta_1)/2$ and $\Delta = (\Delta_1 + \Delta_2)/2$.

This form has the following simple physical interpretation. Coulomb repulsion pushes the electrons to opposite corners on a diagonal giving two charge states $|1\rangle$ and $|2\rangle$ for each combination of spin. Whilst in the corners the spins of these electrons have an effective anti-ferromagnetic Heisenberg exchange interaction with exchange constant J and they may tunnel

from one charge state to the other with amplitude Δ. Charge-spin Hamiltonians of this form may also be derived approximately starting with a lattice model in which electrons are confined to one-electron states occupying the four corners, with only one state for each corner. The one-electron states may be constructed using a broken-symmetry Hartree approximation and writing the hamiltonian Eq.(6.1) in this localized basis leads directly to an extended Hubbard model which may be mapped onto the charge-spin model Eq. (6.7) [61]. However, whilst this approximation gives an appealing interpretation in terms of localized (Heitler-London) one-electron states, it is unnecessary and would give errors in the energy parameters J and Δ compared with the exact solutions, for which the orbital base states are themselves correlated.

6.3 Dynamics

We now consider the time evolution of two electrons which are injected into the square dot such that one is located near corner a and the other near corner c (as labeled in Fig. 6.1(b)). This could be achieved in principle using surface gates as shown schematically in Fig. 6.2. Initially there is an electron localized in each of the small dots adjacent to the large dots. These electrons are then transferred to the large dot by lowering barriers using gates G_1, G_8 and G_4, G_5 and subsequently restoring them to their previous potentials after electron transfer has completed. If both electrons have the same spin, ie total $S_z = \pm 1$, then this spin will not subsequently change with time under coherent evolution of the Hamiltonian (6.7) and the two electrons will therefore remain close to their parent corners, within a spin coherence time. However, if the two injected electrons are of opposite spin (occurring with probability 1/2) then the state after injection will be an equal superposition of a singlet state and an $S_z = 0$ triplet state, which *w*ill subsequently change with time. To be specific, let us consider the state in which a spin-up electron is injected at corner a and a spin-down electron at corner c. We may approximate this state initially by

$$\begin{aligned} |\psi(0)\rangle &= \frac{|1\rangle + |3\rangle}{\sqrt{2}} \\ &= \frac{|\Phi_1^S\rangle + |\Phi_1^A\rangle}{\sqrt{2}} |\uparrow\downarrow\rangle - \frac{|\Phi_1^S\rangle - |\Phi_1^A\rangle}{\sqrt{2}} |\downarrow\uparrow\rangle. \end{aligned} \tag{6.8}$$

Note that both components correspond to spin-up at a and spin down at c since $\Phi_1^S + \Phi_1^A \sim 0$ except when $\mathbf{r}_1 \sim \mathbf{r}_a, \mathbf{r}_2 \sim \mathbf{r}_c$ and $\Phi_1^S - \Phi_1^A \sim 0$ except when $\mathbf{r}_1 \sim \mathbf{r}_c, \mathbf{r}_2 \sim \mathbf{r}_a$. Hence this state is unentangled.Under the Hamiltonian (6.7), the time-evolution of $|\psi(0)\rangle$ can be determined analytically as

$$|\psi(\tau)\rangle = \frac{e^{-iE_0\tau}}{\sqrt{2}} \left[e^{iJ\tau} \left(\cos(\Delta t)|1\rangle + i \sin(\Delta t)|2\rangle \right) + |3\rangle \right], \tag{6.9}$$

choosing units with $\hbar = 1$ and where τ is the time in which the initial state evolves under the action of $H_{\rm eff}$. We see directly from this equation that at time $\tau^* = \pi/2\Delta$, for which $\sin(\tau^*\Delta) = 1$, we have a superposition of the two states $|2\rangle$ and $|3\rangle$ with the same probability of finding either of them. The importance of this superposition is that at time τ^*, a simple single charge detection at *any corner* (let us say b) will project $\psi(\tau^*)$ into a singlet (with the electrons in corners b and d) or a triplet (with electrons remaining in corners a and c). Hence, if an electron is detected at corner b (with probability of $1/2$), then we know that the system is projected into the singlet, for which the electrons will oscillate between corners bd and ac. Conversely, if an electron is not detected at b, then the system must have been projected into the triplet state. Thus a single charge measurement will project onto a singlet or a triplet state with perfect probability. Furthermore, this measurement *ipso facto* induces full entanglement for the singlet case and the $S_z = 0$ triplet.

The probability of detecting the singlet state at time t, starting in the $S_z = 0$ subspace, is $P_2 = |\langle 2|\psi(\tau)\rangle|^2 = \frac{1}{2}\sin^2\Delta\tau$. Thus P_2 oscillates harmonically with maximum probability 1/2 but independent of the exchange, J, which simply induces a phase factor in the singlet component of the wave function. This independence of J implies that our method of 'filtering' the singlet by measurement

$$P_{\psi(0)} = |\langle\psi(0)|\psi(\tau)\rangle|^2 = \frac{1 + \cos^2\Delta\tau + 2\cos J\tau\cos\Delta\tau}{4} \tag{6.10}$$

which shows that only for special cases (e.g. $J = 0$) does the system return to its starting state.

6.4 Applications

The ability to make singlet-triplet measurements paves the way to implement some quantum computation tasks such as entanglement swapping, or equivalently, teleportation. To achieve these we generate two singlet pairs outside a square dot as shown in Fig. 6.3(a). These pairs may be generated via surface gates in a similar fashion to those shown in Fig. 6.2 in which electrons are transferred from the surrounding 2DEG reservoir. The singlets are formed simply by cooling the system [41]. We then push one electron from each singlet pair to hop to the big square QD as shown in Fig. 6.3(b). We now have two electrons in the corners a and c in the square QD and after time τ^* we measure the charge at one corner. With probability of $1/4$, the state of the electrons in the square QD collapses to a singlet at sites bd. In this case two external electrons in the small QDs get entangled as another singlet as shown in Fig. 6.3(c). This process is called *entanglement swapping* (or the *teleportation* of entanglement) and generates

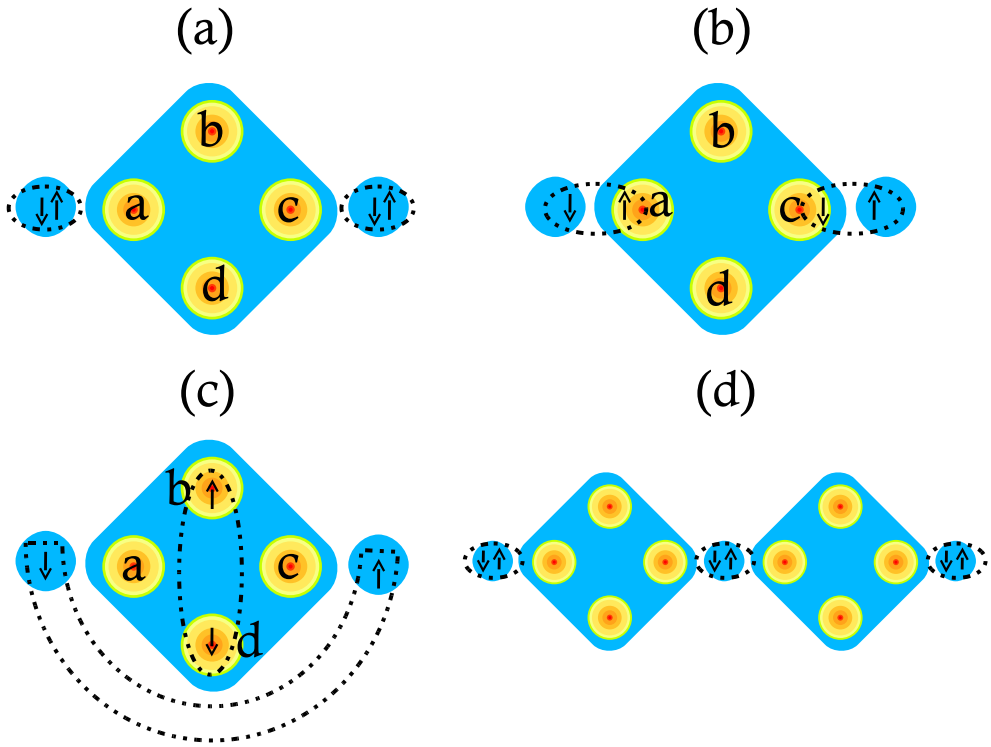

Figure 6.3: (Color online) (a) two small QDs, with a singlet pair in each, beside a large square QD (dashed lines denote entanglement); (b) One electron from each singlet is pushed into the square QD; (c) Entanglement swapping; (d) Scaling up the system to an array of QDs.

long-range entanglement between distant particles. This scheme can be scaled up through a geometry shown in Fig. 6.3(d) where a series of empty square dots are arranged between some small dots containing electron singlet pairs. By pushing one electron from each small dot to its neighboring square QD, one makes all small dots empty except the two which terminate the array, where they are holding one electron each. Dynamical singlet-triplet measurement on all the square QDs generates a singlet between the electrons held in the terminating small dots when the result of all measurements is singlet. The probability of having this is $(1/4)^N$, where N is the number of square QDs.

Surprisingly, When the result of measurement in Fig. 6.3(b) is a triplet, rather than a singlet, we can generate the so-called AKLT state [15]. Originally this was introduced as the ground state of the AKLT Hamiltonian [15], which models the interaction of a series of spin-1 particles with two spin-1/2 particles at the boundaries of a chain. The AKLT ground state can be generated by again starting with a series of spin-1/2 singlets in small QDs but this time, projecting two particles of neighboring singlets into a triplet to represent their spin-1 nature. This occurs with probability $3/4$ when the result of the measurement in Fig. 6.3(b) is a triplet. This can also be scaled up with the geometry shown in Fig. 6.3(d), with probability of success is $(3/4)^N$that all square QD states will be in a triplet state. The AKLT state can be used as resource for ground-code measurement-based quantum computation [59].

6.5 Gate Errors

The above results for the time-development of the initial state are exact, requiring only the energy parameters J and Δ, which may be obtained directly for the eigenenergies of the ground-manifold of the effective-mass Hamiltonian Eq.(6.1). However, these results are somewhat contrived in that the starting state lies precisely within the Hilbert space of the ground-manifold and must therefore remain within this ground-manifold under time evolution. In any realistic situation these conditions will not be met and in particular the starting state will deviate from the idealized form, Eq. (6.8). It will contain small admixtures of the other base states in the ground-manifold and excited singlet states. These admixtures will increase with decreasing dot size but should still give small errors for $L > 10a_B$, say. We may derive expressions for the fidelity starting with a more realistic state, $|\widetilde{\psi}(0)\rangle$. This could be produced, for example, by applying a positive potential to gates located near the sites a and c. In the numerical calculations, this was modeled by dividing the square dot into four quadrants and applying a constant positive potential to the two diagonally opposite quadrants that contain the corners a and c. In this scheme setting

the gating potential to 0.1 V yields values for the overlap $\langle\widetilde{\psi}(0)|\psi(0)\rangle$ of 0.80, 0.940, and 0.97 for QDs of $L = 200$ nm, 800 nm and 1200 nm respectively, which are reasonably close to unity, and could be enhanced further by using more elaborate gating potentials. We may derive an expression for the fidelity with this more realistic initial state by expanding $|\widetilde{\psi}(0)\rangle$ in terms of $|\psi(0)\rangle$, $(|1\rangle - |3\rangle)\sqrt{2}$ and the remaining eigenstates of the full effective-mass Hamiltonian. After time evolution and projection onto $|2\rangle$ we obtain

$$P_2^e = |\langle 2|\widetilde{\psi}(\tau)\rangle|^2 = (\alpha \sin \Delta\tau)^2 - 2\alpha\beta \sin J\tau \sin \Delta\tau + \beta^2 \tag{6.11}$$

where $\alpha = \langle 1|\widetilde{\psi}(0)\rangle$ and $\beta = \langle 2|\widetilde{\psi}(0)\rangle$. Note that P_2^e is *independent of excited states*, and since $|\alpha|^2 \sim 1/2$, $|\beta|^2 \sim 0$, it is robust to gate errors. This is illustrated in Table I where we see only small deviations from the ideal P_2, even for the smallest dot of $L = 100$nm, the main effect being a suppression of the maxima and enhancement of the minima.

6.6 Charge measurement

For simplicity we have so far assumed that charge detection may be made on a timescale much less than the coherent charge evolution time τ^*. Typical values of τ^*, however, being of the order of nanoseconds for our parameters (see Table I) are challenging to measure directly in experiment. For practical implementation, we propose a similar scheme to Ref. [25], which is able to achieve an acceptable time resolution. At the moment of measurement we restore the quadrant gate-potentials (used previously to initialize the system) to freeze the dynamics of the electrons. A strong charge measurement at one of the corners of the QD can then be made to project the state into a singlet or triplet.

6.7 Charge dephasing

Charge dephasing reduces the coherence between $|1\rangle$ and $|2\rangle$ in Eq. (6.9), but since our measurement projects onto these states anyway, it does not fundamentally affect our scheme. By damping the sinusoidal oscillations between $|1\rangle$ and $|2\rangle$, charge dephasing only reduces $P_2(\tau^*) = |\langle 2|\psi(\tau^*)\rangle|^2$ such that in the extreme case of very strong decoherence it goes to $1/4$. In this case if $|2\rangle$ is detected successfully the scheme is completed as before, giving entanglement swapping. Otherwise, we end up with a superposition of $|1\rangle$ and $|3\rangle$, as in the initial state, which again undergoes damped oscillations. By repeating this process one can reliably (with exponential improvement according to number of trials) discriminate between singlets and triplets in the initial state. However, due to our fast dynamics this extreme case is very unlikely. As

L (nm)	Δ (meV)	J (meV)	$\|\alpha\|^2$	$\|\beta\|^2$	$E_{hf}(\mu eV)$
100	0.814	-0.243	0.441	5.23×10^{-2}	1.74
200	0.145	-4.363×10^{-2}	0.445	3.63×10^{-5}	7.76×10^{-1}
400	2.11×10^{-2}	-5.05×10^{-3}	0.420	1.21×10^{-3}	3.88×10^{-1}
800	2.08×10^{-3}	-2.20×10^{-4}	0.453	2.78×10^{-4}	1.94×10^{-1}
1600	9.34×10^{-5}	-1.66×10^{-6}	0.490	6.02×10^{-6}	9.69×10^{-2}

Table 6.1: Physical parameters for a GaAs QD. $|\alpha|^2$ and $|\beta|^2$ (Eq. (6.11)) are the projection of the initial state onto the singlet states $|1\rangle$ and $|2\rangle$ by applying a gating potential of 0.1 V.

an example, for $L = 400$ nm we have $\tau^* = 0.2$ ns, which is safely below the dephasing time $T_2 \sim 1 - 2$ ns in a system with comparable size [25].

6.8 Hyperfine Interaction

The most destructive effect, according the decoherence, in the spin qubit QD system is due to the interaction with nuclear spins [62]. This is called "hyperfine" interaction which is determined by substituting the effect of the nuclei with an effective magnetic field $\overrightarrow{B}$ coupled to the electron spin as follows

$$H_h = \hbar\gamma_e \overrightarrow{B}.\overrightarrow{\sigma} \tag{6.12}$$

where $\gamma_e = g\mu_B/\hbar$ and $\overrightarrow{\sigma} = (\sigma_x, \sigma_y, \sigma_z)$ are the Pauli matrices. $\overrightarrow{B}$ have a gaussian random distribution given by

$$P(\overrightarrow{B}) = \frac{1}{(2\pi B_{nuc}^2)^{3/2}} exp(-(\overrightarrow{B}.\overrightarrow{B})/2B_{nuc}^2). \tag{6.13}$$

where B_{nuc} is the variance of the random variable $\overrightarrow{B}$. Due to the fact that the dynamics of the electrons are much faster than the nuclei, we can consider the quasi-static approximation which fixes the nuclei's effect for the evolution of each electrons. So when we generate initial state of the system as $|\psi(0)\rangle$ the hyperfine interaction causes all triplets evolve as well as the singlet state. Due to the random nature of the magnetic field we can just study the average dynamics of the system when it evolves under $H_t = H + H_h$. So for each random vector $\overrightarrow{B}$ we compute the following quantities which are overlap of the $|\psi(\tau)\rangle$ and singlet or triplet at sites ac and bd

$$P_1 = \langle|1|\psi(\tau)\rangle|^2\rangle, \quad P_2 = \langle|\langle 2|\psi(\tau)\rangle|^2\rangle, \tag{6.14}$$

$$P_3 = \langle|\langle 3|\psi(\tau)\rangle|^2\rangle, \quad P_4 = \langle|\langle 4|\psi(\tau)\rangle|^2\rangle, \tag{6.15}$$

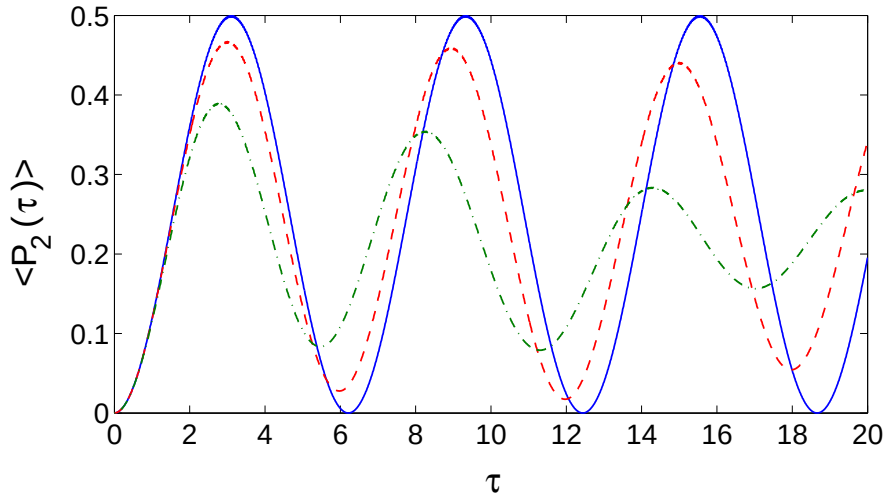

Figure 6.4: ((Color online) Hyperfine interaction effect for $U = 25$ mev, $V = 3$ mev and $b = 50\mu$ ev. In the figure $\hbar\gamma_e B_{nuc} = 0$ (solid blue line), $\hbar\gamma_e B_{nuc} = 0.1b$ (dashed red line) and $\hbar\gamma_e B_{nuc} = 0.2b$ (dotted-dashed green line). The probability $P_2(\tau)$ of finding the singlet in the sites bd as a function of time.

where $< ... >$ means average over all possible values of $\overrightarrow{B}$ which we compute it numerically by averaging over 1000 different randomly chosen values for $\overrightarrow{B}$. Results are shown in Fig. 6.4 for different values of B_{nuc} and typical values for the parameters of the Hamiltonian. In Fig. 6.4 we have plotted the probability of finding a singlet in site bd. As this figure shows clearly, while the probability of finding the singlet in sites bd decreases by increasing the noise. Furthermore this figure clearly show the decoherence effect in their damping oscillations.

Here we pause to point out to the advantage of using this proposal for doing singlet-triplet measurement than the one proposed in [41]. First of all in our dynamical strategy when we put electrons in the square QD we do not need any extra control like applying a voltage or etc to the system while the dissipative scheme [41] relies on time dependent controlled voltage gates. Secondly, dissipative scheme is always a probabilistic strategy which is not always successful while in our proposal since we do not use a dissipative phenomena and it is based on the non-equilibrium dynamics the result of the singlet-triplet measurement is deterministic. The third benefit of our scheme from a practical point of view is providing an easier manipulation of the QD. This comes from the fact that in our scheme we need a big square dot which is much easier to implement in the lab.

6.9 Conclusions

We showed that the dynamics of a pair of electrons in a large square quantum dot can be used to perform singlet-triplet spin measurement using just a single charge detection. Opposed to the previous schemes, this is a deterministic process which does not require any extra control during the process. This leads us to conclude that this strategy is less complex to be realized in the laboratory with current technology. The AKLT ground state, which has been proposed already for quantum computation, can be obtained in our system. It is also possible to do teleportation and entanglement swap through the natural dynamics of the electron pairs. Furthermore, evolution of the system is faster than the dephasing time T_2 imposed by hyperfine interaction into the system. Also our analytic results, found for the perturbative regime, is valid for a wide range of system parameters particularly it is in a very good agreement for typical experimental values of the Hamiltonian parameters.

Chapter 7

Conclusions

In this thesis, we have discussed the possibilities to obtain entangled spins and perform some quantum information processing protocols in two types of nanostructures. Primarily the studies have been couched in terms of electron spins in quantum dots, with one study on nuclear and electronic spins of Nitrogen atoms inside fullerene dimers in nanotubes. Most of the studies have attempted to look beyond the standard setups and protocols popular in literature. For example, in quantum dot based quantum computing, usually one considers one electron per dot encoding a qubit in its spin degree of freedom. Usually Coulomb blockade regime is invoked so that the chance of two electrons per dot is suppressed. We have gone beyond this in two quite different directions. One setup in which there is an empty dot (Chapter 5), offers certain advantages in terms of control, initialization and measurements, namely that no tunnel barrier now needs to be controlled and simply gate voltages on individual dots suffice as the control parameters. However, as now the electrons cannot be identified through which dot they belong to throughout the dynamics, it becomes important to keep track of the fermionic statistics of the electrons while writing down the Hamiltonian matrices – there are some terms with t and some with $-t$, where t is the tunnel coupling. So obtaining a quantum gate here is nontrivial (not easy to speculate beforehand that it will indeed be possible as *both* spin and orbital degrees of freedom are involved) and we are fortunate to find that such a gate indeed happens at a specified time. In another setup (Chapter 6), we consider multi-electron logic inside a *single* quantum dot, which is also quite different from the conventional approach.

Most of the presented ideas open up many questions for further studies, though we have not been able to consider all those within the scope of this thesis. Here we just note down

these further possibilities as an idea bank for the future continuation of the strands of work in this thesis. For example, in Chapter 4 we have shown that a singlet can be created on distinct dots on the fast time-scale dictated by tunneling, rather than by exchange. As most quantum gate ideas are exchange based, and thereby happen over the much slower time scale of an exchange coupling, it remains an important question as to what other relevant processing can be accomplished apart from singlet generation, on a time-scale faster than the exchange. For example, after extraction, what can one use these fast generated singlets for? An interesting idea would be to let one spin each from two distinct singlets interact in a single dot remembering that the single dot exchange couplings are much stronger than the exchange coupling between two distinct dots. Again, being able to use coherent tunneling to put two electrons in separate dots to a single dot at a predetermined time might prove advantageous here. In that type of setting, by welding one member from distinct singlets together (here by welding we mean making a maximally entangling gate), it will be possible to generate cluster states for measurement based quantum computing if some separate local operations on all the electron spins are also done. Indeed, in the question we have examined in chapter 5 with an empty dot, one could alternatively think of using coherent tunneling to put the two outer electrons together in the central dot in order to have a quantum gate whose time-scale is dictated by tunneling and the strong exchange in the single central dot, rather than by the weak exchange between distinct dots. As we used all the three dots in the Coulomb blockade regime, our gate in that chapter has a time-scale of entanglement generation still set by the weak interdot exchange coupling J, though tunneling t also plays an important role. One therefore has to consider variants of the setup of Chapter 5 in order to check whether quantum information processing with spin qubits, but entirely dictated by tunneling (and perhaps the Coulomb interaction in a single dot giving a intra-dot exchange) is at all possible. In a very similar context, it is worthwhile to consider whether the square dots considered in Chapter 6 can act as the "welders" mentioned above. In that chapter, Δ is a tunneling time-scale, albeit inside a single dot, and between distinct two electron states. Clearly, if two electrons (from say, two distinct singlets, but now well separated singlets in the sense of Chapter 4) in distinct states coherently tunnel into two opposite vertices (their simultaneous tunneling in is, of course, a different calculation) of a square dot, then the fact that their singlet combination oscillates, while the triplet remains frozen, could perhaps be exploited for an entangling quantum gate.

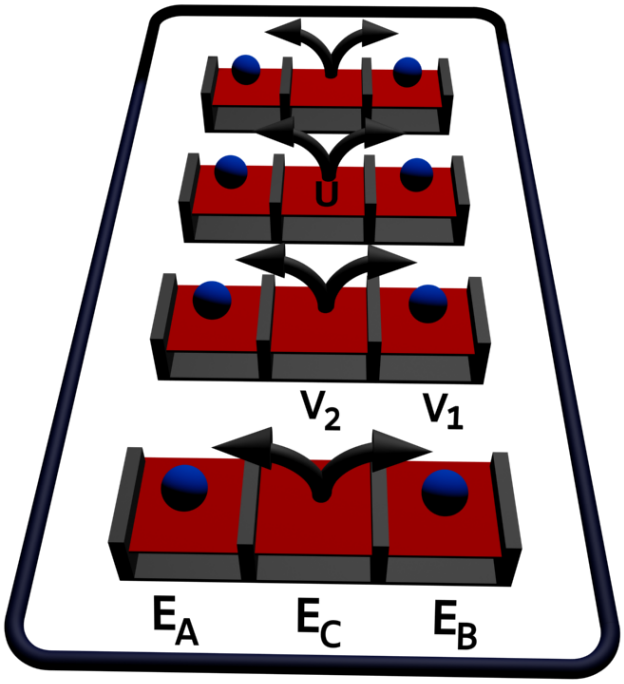

Figure 7.1: The figure shows the correlated extraction of several singlets in parallel from a line of central dots by matching the energy of the initial and the final configurations.

An interesting question immediately stemming as an extension to Chapter 4 is whether a correlated tunneling of electrons can extract multiple parallel singlets from multiple dots as illustrated in Fig.7.1. This may have the advantage that measuring just one charge state, namely that of a single central dot in one of the parallel copies suffices to ensure that singlets in all the parallel copies have been extracted. It might also have the advantage if the extraction has to be followed by certain other protocols such as entanglement purification and repeaters in an automated way subject to all copies being extracted. The criterion for coherent extraction of multiple singlets at a precisely known time (i.e., resonance between the unextracted and extracted states) is $2nE_C + nU + (n-1)V_2 = nE_A + nE_B + 2(n-1)V_1$, where E_A, E_B, E_C and U have their standard meanings as defined earlier in the thesis, V_2 is the interdot interaction with 2 electrons in each dot, V_1 is the interdot interaction with 1 electron in each dot and n is the number of parallel channels of singlet extraction. We assume here that interdot interaction is solely between neighbouring qubits. With so many independent parameters, one should be able to meet such type of criterion for some values of n. However, V_2 has to be calculated for given dots and there are two major obstacles otherwise to the efficiency of such a multiple extraction process. In our single singlet extraction protocol, t connects configurations of same energy and the extraction is completed after the system goes from CC through two intermediate states of the same energy CA and CB before ending up in AB. Therefore time-scale of the process is still t. Here we will have many intermediate configurations (corresponding to extractions in single dots) and thereby the time-scale can become slower – this is the price we pay if we demand correlated (simultaneous) extraction.

Another interesting area emerging from the contents of thsi thesis is whether one can do interesting quantum measurements or gates with multiple electrons in polygonal dots. An example is shown in Fig.7.2, where it might be worth considering whether 4-spin singlets and triplets can be distinguished from the time evolution of the charge distribution, generalizing the case we studied in Chapter 6. It is possible that the time evolution for a fixed period also leads to useful quantum gates between the four spins. We have to wait a time till the charge configurations are back to their original form irrespective of whether we started from a singlet, a triplet or even spin-2 state (possible for 4 electrons) and then check whether appropriate relative phases for useful quantum gates have appeared. Of course, this has similarities with the quantum gate with an empty dot of Chapter 5 in the sense that there are sites with empty charge

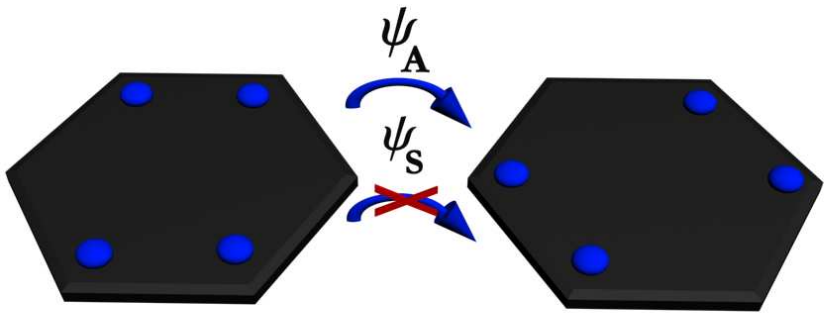

Figure 7.2: The figure shows the oscillation of four electron states in a hexagonal dot. It is possible that any 4 electron spin singlets ψ_A with symmetric spatial wavefunction will oscillate, while any 4 electron spin triplets ψ_S with an antisymmetric spatial wavefunction will remain frozen. In this way the total spin zero space may be projected out.

distribution and the dynamics of charge distribution will cause some decoherence. It is possible that the spin-2 and the triplet will not have different time evolutions as they are both symmetric spin states and thereby will have the same antisymmetric charge state.

In continuation with Chapter 3, it is worthwhile to look at quantum gates induced between nuclear spin qubits due to interaction of electronic spins. The idea is to have a strong enough magnetic field to effectively decouple the electronic and the nuclear spin qubits when the nuclear spins are being used as a memory. One has to probably operate the system near $J/g \sim 5$ (or similar, depending of the physical system) where our results show that in the presence of a magnetic field the nuclear spins can effectively be initialized in a product state by cooling. Local gates can then initialize each nuclear spin to arbitrary pure states. On the other hand, for such J/g, in the absence of a magnetic field the nuclear spins are highly entangled in their ground state.This latter fact provides the hope to dynamically generate entanglement between the nuclear spins when the magnetic field is suddenly switched off. However, we have simply assumed local gates on the nuclear spins in the above discussion and to implement them probably requires other ideas.

Chapter 8

Bibliography

Bibliography

[1] M. A. Nielsen and I. L. Chuang, *Quantum Computation and Quantum Information* (Cambridge, 2000).

[2] J. S. Bell, Physics **1**, 195 (1964); J. F. Clauser, M.A. Horne, A. Shimony and R. A. Holt, Phys. Rev. Lett. **23**, 880 (1969).

[3] W. K. Wootters, Phys. Rev. Lett. **80**, 2245 (1998).

[4] A. Peres, Phys. Rev. Lett. **77**, 1413 (1996); M. Horodecki, P. Horodecki, and R. Horodecki, Phys. Lett. A 223, 1 (1996).

[5] J. Eisert, Ph.D. thesis, University of Potsdam, 2001.

[6] G. Vidal and R. F. Werner, Phys. Rev. A **65**, 32314 (2002).

[7] M. B. Plenio, Phys. Rev. Lett. **95**, 090503 (2005).

[8] M. Zukowski, A. Zeilinger, M. A. Horne, and A. K. Ekert, Phys. Rev. Lett. **71**, 4287 (1993).

[9] S. Bose, V. Vedral and P. L. Knight, Phys. Rev. A **57**, 822 (1998).

[10] H.-J. Briegel, W. Dür, J. I. Cirac, and P. Zoller, Phys. Rev. Lett. **81**, 5932 (1998).

[11] M. J. Bremner, C. M. Dawson, J. L. Dodd, A. Gilchrist, A. W. Harrow, D. Mortimer, M. A. Nielsen, T. J. Osborne, Phys. Rev. Lett. **89**, 247902 (2002).

[12] K.C. Nowack, F.H.L. Koppens, Yu.V. Nazarov and L.M.K. Vandersypen, Science **318**, 1430 (2007).

[13] E. A. Laird, C. Barthel, E. I. Rashba, C. M. Marcus, M. P. Hanson, A. C. Gossard, Semicond. Sci. Tech. **24**, 064004 (2009).

[14] E. Knill, R. Laflamme and G. J. Milburn, Nature **409**, 46 (2001).

[15] I. Affleck, T. Kennedy, E. H. Lieb, and H. Tasaki, Phys. Rev. Lett. **59**, 799 (1987); Commun. Math. Phys. **115**, 477 (1988).

[16] Gavin K. Brennen, Akimasa Miyake, Phys. Rev. Lett. **101**, 010502 (2008).

[17] Tzu-Chieh Wei, Ian Affleck, Robert Raussendorf, Phys.Rev.Lett **106**, 070501 (2011).

[18] J. M. Taylor, J. R. Petta, A. C. Johnson, A. Yacoby, C. M. Marcus, M. D. Lukin, Phys. Rev. B **76**, 035315 (2007).

[19] D. Loss and D. P. DiVincenzo, Phys. Rev. A **57**, 120 (1998).

[20] U. Meirav, M. Heiblum and F. Stern, Appl. Phys. Lett. **52**, 11 (1988).

[21] A. B. Kuklov and B. V. Svistunov, Phys. Rev. Lett. **90**, 100401 (2003).

[22] D. Reilly et al., Science **321**: 817-821 (2008)

[23] G. Ortner *et. al*, Phys. Rev. Lett. **94**, 157401 (2005).

[24] T. Fujisawa,T. Hayashi, H. D. Cheong,Y. H. Jeong, Y. Hirayama, Physica E. **21**, 2-4, 1046-1052.

[25] G. Shinkai, T. Hayashi, T. Ota and T. Fujisawa, Phys. Rev. Lett. **103**, 056802 (2009).

[26] H. W. Liu, T. Fujisawa, T. Hayashi, and Y. Hirayama, Phys. Rev. B **72**, 161305 (2005).

[27] H. van Houten and C.W.J. Beenakker, Physics Today **49** (7):22-27 (1996).

[28] J.M. Elzerman et al., Physical Review B **67** 161308 (2003).

[29] S. C. Benjamin, A. Ardavan, G. A. D. Briggs *et. al.*, J. Phys: Cond. Mat. **18**, S867 (2006).

[30] M. Feng and J. Twamley, Phys. Rev. A **70**, 030303 (2004).

[31] Ling Ge, Barbara Montanari, John H. Jefferson, David G. Pettifor, Nicholas M. Harrison, and G. Andrew D. Briggs, Phys. Rev. B **77**, 235416 (2008).

[32] L. Campos Venuti, C. Degli Esposti Boschi and M. Roncaglia, Phys. Rev. Lett. **96**, 247206 (2006); L. Campos Venuti, S. M. Giampaolo, F. Illuminati, P. Zanardi, Phys. Rev. A **76**, 052328 (2007).

[33] M. C. Arnesen, S. Bose and V. Vedral, Phys. Rev. Lett. **87**, 017901 (2001).

[34] D. Kaszlikowski, P. Gnacinski, M. Zukowski, W. Miklaszewski and A. Zeilinger, Phys. Rev. Lett. **85**, 4418 (2000).

[35] R. A. Bertlmann, K. Durstberger, B. C. Hiesmayr and P. Krammer, Phys. Rev. A **72**, 052331 (2005).

[36] C. Brukner and V. Vedral, arXiv:quant-ph/0406040v1 (2004).

[37] M. Horodecki, P. Horodecki and R. Horodecki, Phys. Rev. Lett. **80**, 52395242 (1998).

[38] Avinash Kolli, Simon C. Benjamin, Jose Garcia Coello, Sougato Bose, and Brendon W. Lovett. New J. Phys. **11**, 013018 (2009).

[39] T. Byrnes, N. Y. Kim, K. Kusudo and Y. Yamamoto, Phys. Rev. B **78**, 075320 (2008).

[40] D. S. Saraga and D. Loss Phys. Rev. Lett. **90**, 166803 (2003).

[41] J. R. Petta et al., Science **309**, 2180 (2005).

[42] R. Hanson et al., Phys. Rev. Lett. **94**, 196802 (2005).

[43] R. Hanson and G. Burkard, Phys. Rev. Lett. **98**, 050502 (2007).

[44] H.-A. Engel, L.P. Kouwenhoven, D. Loss and C.M. Marcus, Quantum Information Processing **3**, 115 (2004).

[45] J. H. Jefferson, M. Fearn, D. L. J. Tipton and T. P. Spiller, Phys. Rev. A **66**, 042328 (2002).

[46] C. Flindt, A. S. Sorensen, M. D. Lukin and J. M. Taylor, Phys. Rev. Lett. **98**, 240501 (2007).

[47] D. Schroer et. al., Phys. Rev. B **76**, 075306 (2007); G. Yamahata et. al., Solid-State Electronics **53**, 779 (2009); M. Pierre et. al. Appl. Phys. Lett. **95**, 242107 (2009).

[48] E. A. Laird *at. al.*, Phys. Rev. B **82**, 075403 (2010).

[49] J. Lehmann, A. Gaita-Arin, E. Coronado and D. Loss, Nature Nanotech. **2**, 312 (2007).

[50] D. P. DiVincenzo, D. Bacon, J. Kempe, G. Burkard and K. B. Whaley, Nature **408**, 339 (2000).

[51] C.A. Stafford and S. Das Sarma, Phys. Rev. Lett. **72**, 3590 (1994); R. Kotlyar, C.A. Stafford and S. Das Sarma, Phys. Rev. B **58**, R1746 (1998); C.A. Stafford, R. Kotlyar and S. Das Sarma, Phys. Rev. B **58**, 7091 (1998); M.R. Wegewijs and Y.V. Nazarov, Phys. Rev. B **60**, 14318 (1999).

[52] M. J. Bremner *et. al.* Phys. Rev. Lett. **89**, 247902 (2002).

[53] L. Gaudreau *et. al.* Phys. Rev. Lett. **97**, 036807 (2006).

[54] J. Gorman, D. G. Hasko and D. A. Williams, Phys. Rev. Lett. **95**, 090502 (2005).

[55] S. Trotzky *et. al.*, Science **319**, 295 (2008).

[56] R. Hanson and G. Burkard, Phys. Rev. Lett. **98**, 050502 (2007).

[57] C. H. Bennett, *et al.*, Phys. Rev. Lett. **70**, 1895 (1993).

[58] M. Zukowski, A. Zeilinger, M. A. Horne, A. K. Ekert, Phys. Rev. Lett. **71**, 4287 (1993).

[59] G. Brennen and A. Miyake, Phys. Rev. Lett. **101**, 010502 (2008).

[60] E.P. Wigner, Phys. Rev. **46**, 1002 (1934).

[61] C.E. Creffield, W. Hausler, J.H. Jefferson, and0 S. Sarkar, Phys. Rev. B **59**, 10719 (1999).

[62] I. A. Merkulov, A. L. Efros and M. Rosen, Phys. Rev. B **65**, 205309 (2002); D. Paget, G. Lampel, B. Sapoval and V. Safarov, Phys. Rev. B **15**, 5780 (1977).